

Studies of Dihadron Electroproduction in DIS with Longitudinally Polarized Hydrogen and Deuterium Targets

(A CLAS12 Run Group C Proposal)

H. Avakian^{a,1}, A. Courtoy², C. Dilks^{a,b,3}, T. Hayward⁴, M. Mirazita⁵, O. Soto^{a,5} and A. Vossen^{3,1}

¹*Thomas Jefferson National Accelerator Facility, Newport News, Virginia 23606*

²*Instituto de Física, Universidad Nacional Autónoma de México, 01000 Ciudad de México, Mexico*

³*Duke University, Durham, North Carolina 27708*

⁴*College of William and Mary, Williamsburg, Virginia 23187*

⁵*INFN, Laboratori Nazionali di Frascati, 00044 Frascati, Italy*

We propose a comprehensive program to measure dihadron correlations produced in SIDIS to investigate novel aspects of non-perturbative QCD in proton structure and hadronization. Compared to the well-explored single-hadrons observables, dihadron production has an additional degree of freedom which allows for targeted access to quark-gluon correlations in the proton, transverse-momentum dependent parton distributions (TMDs), and previously unexplored spin-orbit correlations in hadronization via the framework of dihadron fragmentation functions (DiFFs). The experiment is proposed to be a part of Run Group C, using the upgraded CLAS12 detector with an 11 GeV highly-polarized electron beam scattering off a longitudinally polarized target, effectively composed of either hydrogen or deuterium in solid ammonia (NH₃ or ND₃). The CLAS12 detector provides a unique opportunity for this physics program due to its large acceptance, which allows for the simultaneous detection of the scattered electron and dihadron. Target spin asymmetries in dihadrons, as well as double spin asymmetries, are sensitive to spin-orbit correlations in hadronization, as well as TMDs and collinear twist-3 parton distributions; these measurements combined with recent beam spin asymmetries measurements at CLAS12 allow for a cleaner interpretation of their constraints on distribution and fragmentation functions. A comparison of these asymmetries from the hydrogen target to those from the deuterium target is sensitive to the flavor dependence of these distributions. Moreover, the detection of target fragments will allow for the extension of the program into the target fragmentation region (TFR). An analysis of correlations between a hadron produced in the TFR with a hadron in the current fragmentation region (CFR) is sensitive to the fracture functions, which encode the probability of finding a parton in a nucleon fragmenting into a particular hadron. A wide range of fracture functions is accessible in target spin, beam spin, and double spin asymmetries of this class of dihadrons. The large acceptance at CLAS12 provides a unique opportunity for several dihadron correlation measurements, and a polarized target extends the program, broadening our overall understanding of the nucleon and the dynamics of its constituents.

^a Co-spokesperson

^b Contact: dilks@jlab.org

Contents

35

36	I. Introduction	3
37	II. Collinear Dihadron production in the current fragmentation region at twist3	4
38	A. Introduction	4
39	B. Observables	5
40	C. Partial-wave analysis	8
41	D. Flavor structure	8
42	E. Cross sections	9
43	F. Parametrization of the DiFF H_1^\lessgtr	10
44	G. Collinear twist-3 parton distribution functions $e(x)$ and $h_L(x)$	11
45	III. Novel spin-orbit correlations in hadronization in TMD DiFFs	16
46	A. Access to the helicity DiFF	16
47	B. Transverse Momentum Dependent DiFFs	18
48	IV. Correlations in hadron production in the current and target fragmentation region	20
49	A. SIDIS in the TFR	20
50	B. The Double SIDIS (DSIDIS) process	21
51	1. DSIDIS cross section and asymmetries	21
52	2. Integrated cross sections	23
53	V. Experimental details	25
54	A. CLAS12	25
55	B. CLAS12 Particle Identification	25
56	C. The polarized target	25
57	D. The data set and analysis	26
58	1. Event Selection Criteria	28
59	2. Asymmetry Measurement	29
60	VI. Expected results	31
61	A. Existing data on target spin and double spin asymmetries	31
62	B. Preliminary CLAS12 dihadron beam spin asymmetries	32
63	C. Statistical projections for this proposal	34
64	D. Systematic Uncertainty	41
65	VII. Summary and Request	42
66	A. Depolarization Factors	44
67	B. Convolutions	44
68	C. Simulation	45
69	References	49

I. Introduction

In recent years, measurements of azimuthal moments of polarized hadronic cross sections in hard processes have emerged as a powerful tool to probe the nucleon structure. Many experiments worldwide are currently trying to pin down various effects related to the nucleon structure through semi-inclusive deep-inelastic scattering. In fact, learning about the partonic structure of the nucleon and other fundamental aspects of QCD revealed in the strongly coupled system that is the nucleon as well as in hadronization is at the core of the physics program that motivated the 12 GeV upgrade as well as the future EIC. Azimuthal distributions of final state particles in semi-inclusive deep inelastic scattering, in particular, are sensitive to the orbital motion of quarks and play an important role in the study of transverse momentum distributions (TMDs) of quarks in the nucleon and spin orbit correlations in hadronization. For an overview see Refs. [1, 2].

This proposal aims at extracting Twist-3 distribution functions $e(x)$ and $h_L(x)$ from longitudinal spin asymmetries. The functions $e(x)$ and $h_L(x)$, together with the better known twist-2 functions $f_1(x), g_1(x)$ and $h_1(x)$ as well as the twist-3 function $g_T(x)$ completely describe the nucleon structure in a collinear picture up to twist-3. Experimental evidence suggests that they are of sizable magnitude and observables are of similar size as for leading twist quantities at JLab kinematics [3, 4]. They have strong connections to TMDs but contain additional information about non-perturbative QCD dynamics inside the nucleon. Details of this part of the proposal are described in Sec. II.

Longitudinal spin asymmetries are also sensitive to dihadron fragmentation functions, in particular to the helicity-dependent fragmentation function G_1^\perp . Measuring target spin asymmetries, in addition to beam spin asymmetries, will help constrain G_1^\perp . Furthermore, spin asymmetries are sensitive to the partial wave expansion of the dihadron fragmentation functions, which can shed light on correlations between fragmenting quark polarization and the final state angular momentum of the dihadron.

Another aim of this proposal is to explore correlations between the current and target fragmentation regions to access fracture functions. Recent theoretical work [5] highlighted that the knowledge of these functions is essential to understand particle production over a large part of the kinematical phase space covered by the JLab DIS experiments. The related measurements are discussed further in Sec. IV.

Lastly, we note that this proposal is in large part an update of [6], a PAC38 proposal. This proposal was deferred in favor of higher priority measurements for the first 5 years of 12 GeV operations, but now it is time to revisit the possibility of the proposed measurements. We propose that these measurements take place during Run Group C, in parallel with approved experiments, which include [7–10].

II. Collinear Dihadron production in the current fragmentation region at twist3

A. Introduction

Recent theoretical progress on Twist-3 TMDs, clarifying the connection to TMDs as well as elucidating their connection to quark-gluon correlations [11], led to renewed interests in these quantities. At Twist-3, and before integration over transverse momentum, there are 16 distribution functions (see Tab. I) for different combinations of target (rows in Tab. I) and quark (columns in Tab. I) polarizations. Only three functions survive integration over transverse momentum (collinear functions): e , h_L and g_T . Together with the twist-2 PDFs (f_1 , g_1 , h_1), they give a detailed picture of the nucleon in longitudinal momentum space. The main goal of the present proposal is to access the functions e and h_L .

Higher twist (HT) functions are of interest for several reasons. Most importantly they offer insights into the physics of the largely unexplored quark-gluon correlations which provide direct and unique insights into the dynamics inside hadrons, see, e.g., [12]. They describe multiparton distributions corresponding to the interference of higher Fock components in the hadron wave functions, and as such have no probabilistic partonic interpretations, yet they offer fascinating doorways to studying the structure of the nucleon. The x^2 -moment¹ of the HT function $e(x)$ describes the average transverse color force acting on a transversely polarized quark, in an unpolarized nucleon [13]. The x^2 moment of $h_L(x)$ vanishes, but the higher-order x^3 moment describes the average longitudinal gradient of the transverse force that acts on a transversely polarized quark; the sign of this gradient will help to study correlations between the nucleon spin and its color magnetic field [14].

HT contributions are also indispensable to correctly extract twist-2 parts from data. Although suppressed with respect to twist-2 observables by $1/Q$, twist-3 observables are not small in the kinematics of fixed target experiments. This is illustrated by the fact that the single-hadron twist-3 asymmetry $A_{UL}^{\sin \phi}$ is a large and cleanly seen effect, while the twist-2 asymmetry $A_{UL}^{\sin 2\phi}$ is small and compatible with zero in the kinematics of HERMES, JLab, and COMPASS [15–19].

N/q	U	L	T
U	f^\perp	g^\perp	h, e
L	f_L^\perp	g_L^\perp	h_L, e_L
T	f_T, f_T^\perp	g_T, g_T^\perp	$h_T, e_T, h_T^\perp, e_T^\perp$

TABLE I. Twist-3 transverse momentum dependent distribution functions. The U,L,T correspond to unpolarized, longitudinally polarized and transversely polarized nucleons (rows) and quarks (columns)

The theoretical description of twist-3 observables is challenging in single-hadron SIDIS. Although lots of effort was devoted to their study [20–34], these observables are still not understood. Partially, this has to do with the problem of formulating a TMD-factorization at twist-3 level [35, 36].

An important process which can provide complementary information on twist-3 TMDs is the dihadron production in SIDIS described by interference functions [37–43]. In fact, the measurement of single-spin asymmetries with a longitudinally polarized target or beam is sensitive in particular to the twist-3 chiral-odd distribution functions e and h_L , in combination with the chiral-odd interference fragmentation function H_1^ζ [41]; the twist-3 distribution functions are collinear and survive integration over the quark transverse momentum. Dihadron production becomes a unique tool to study the higher twist effects appearing as $\sin \phi$ modulations in target or beam spin dependent azimuthal moments of the SIDIS cross section. The interference fragmentation function H_1^ζ has been used to obtain information on the transversity parton distribution function [44].

One of the main sources of systematic uncertainties is the contribution from target fragmentation, which is of its own interest and will be also studied in the proposed measurement. It was shown that the leading order azimuthal asymmetries in the case where one of the hadrons is produced in the target fragmentation region provide access to polarized TMD Fracture Functions, which are conditional probabilities to produce

¹ in particular, the moment of the pure twist-3 part of the distribution

a hadron h in TFR when hard scattering occurs on a quark q from the target nucleon N [45, 46]. For these processes for longitudinally polarized lepton scattering, the cross section depends on initial quark longitudinal polarization even if one does not measure the final quark polarization already in leading order.

The JLab 12-GeV upgrade will provide the unique combination of wide kinematic coverage, high beam intensity (luminosity), high energy, high polarization, and advanced detection capabilities necessary to study the transverse momentum and spin correlations in dihadron production in double-polarized semi-inclusive processes both in the target and current fragmentation regions.

B. Observables

We consider the process

$$\ell(l) + N(P) \rightarrow \ell(l') + h_1(P_1) + h_2(P_2) + X, \quad (1)$$

where h_1 and h_2 denote the produced hadrons, ℓ the beam lepton and N the nucleon target. The four-momenta are given in parentheses.

In the one-photon exchange approximation and neglecting the lepton mass, the cross section for two-particle inclusive DIS, integrated over the transverse momentum of the produced pair, can be written in the following way [47]:

$$\begin{aligned} \frac{d\sigma}{dx dy d\psi dz_h d\phi_{R\perp} dM_h d\cos\theta} &= \frac{\alpha^2}{xy Q^2} \left(1 + \frac{\gamma^2}{2x} \right) \\ &\times \left\{ A(x, y) F_{UU,T} + B(x, y) F_{UU,L} + \frac{1}{2} V(x, y) \cos\phi_{R\perp} F_{UU}^{\cos\phi_{R\perp}} + B(x, y) \cos(2\phi_{R\perp}) F_{UU}^{\cos 2\phi_{R\perp}} \right. \\ &+ \lambda_e \frac{1}{2} W(x, y) \sin\phi_{R\perp} F_{LU}^{\sin\phi_{R\perp}} \\ &+ S_L \left[\frac{1}{2} V(x, y) \sin\phi_{R\perp} F_{UL}^{\sin\phi_{R\perp}} + B(x, y) \sin(2\phi_{R\perp}) F_{UL}^{\sin 2\phi_{R\perp}} \right] \\ &+ S_L \lambda_e \left[C(x, y) 2 F_{LL} + \frac{1}{2} V(x, y) \cos\phi_{R\perp} F_{LL}^{\cos\phi_{R\perp}} \right] \\ &+ |\mathbf{S}_\perp| \left[\sin(\phi_{R\perp} - \phi_S) \left(A(x, y) F_{UT,T}^{\sin(\phi_{R\perp} - \phi_S)} + B(x, y) F_{UT,L}^{\sin(\phi_{R\perp} - \phi_S)} \right) \right. \\ &+ B(x, y) \sin(\phi_{R\perp} + \phi_S) F_{UT}^{\sin(\phi_{R\perp} + \phi_S)} + B(x, y) \sin(3\phi_{R\perp} - \phi_S) F_{UT}^{\sin(3\phi_{R\perp} - \phi_S)} \\ &+ \frac{1}{2} V(x, y) \sin\phi_S F_{UT}^{\sin\phi_S} + \frac{1}{2} V(x, y) \sin(2\phi_{R\perp} - \phi_S) F_{UT}^{\sin(2\phi_{R\perp} - \phi_S)} \left. \right] \\ &+ |\mathbf{S}_\perp| \lambda_e \left[C(x, y) \cos(\phi_{R\perp} - \phi_S) 2 F_{LT}^{\cos(\phi_{R\perp} - \phi_S)} + \frac{1}{2} V(x, y) \cos\phi_S F_{LT}^{\cos\phi_S} \right. \\ &+ \frac{1}{2} V(x, y) \cos(2\phi_{R\perp} - \phi_S) F_{LT}^{\cos(2\phi_{R\perp} - \phi_S)} \left. \right] \Big\}, \quad (2) \end{aligned}$$

where α is the fine structure constant, λ_e is the beam polarization, \mathbf{S} is the target polarization, with longitudinal component S_L and transverse component $|\mathbf{S}_\perp|$. The functions A, B, C, V, W are kinematic depolarization factors (see Appendix A), dependent on the the ratio ε of longitudinal and transverse photon flux [48]:

$$\varepsilon = \frac{1 - y - \frac{1}{4}\gamma^2 y^2}{1 - y + \frac{1}{2}y^2 + \frac{1}{4}\gamma^2 y^2}. \quad (3)$$

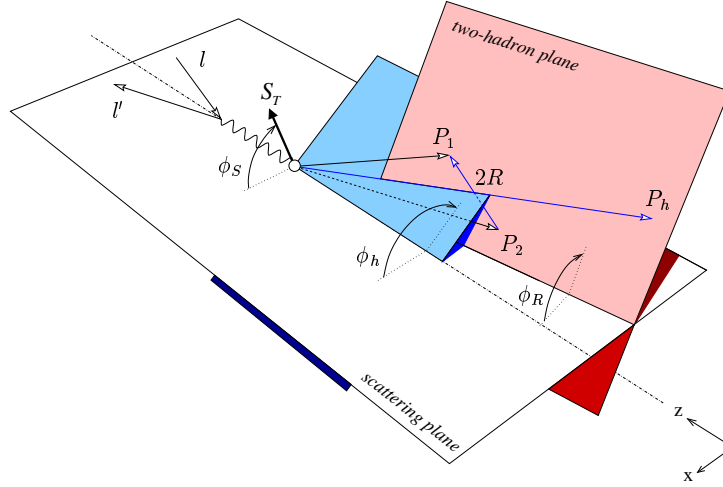


FIG. 1. Definitions of azimuthal angles ϕ_h , ϕ_R , and ϕ_S . The white plane is the lepton scattering plane, the red plane is the plane spanned by the virtual photon and the dihadron total momentum, and the blue plane contains the hadron momenta. From [40].

Following the Trento conventions [49] all relevant angles are defined on figure 1 [40].² The final hadrons' invariant mass M_h is assumed to be much smaller than the hard scale $Q^2 = -q^2 \geq 0$ ($q = l - l'$) of the SIDIS process, defined by kinematic variables $x = Q^2/2P \cdot q$, $y = P \cdot q/P \cdot l$, $z = P \cdot P_h/P \cdot q$ and $\gamma = 2Mx/Q$. With P_1 and P_2 denoting the hadron momenta, $P_h = P_1 + P_2$ and $R = (P_1 - P_2)/2$ denote the pair total momentum and relative momentum, respectively. Finally, this cross section is integrated over dihadron transverse momentum $P_{h\perp}$, and the angle ϕ_h , defined as the angle between the lepton scattering plane and the plane spanned by P_h and q .

The structure functions on the r.h.s. depend on x , Q^2 , z , $\cos \theta$, and M_h^2 . The angle θ is defined in the center-of-mass of the two hadrons, where the hadron emission occurs back-to-back; it is defined as the angle between the direction of emission and the direction of P_h from the photon-target rest frame. The angle ψ is the azimuthal angle of ℓ' around the lepton beam axis with respect to an arbitrary fixed direction, which in case of a transversely polarized target we choose to be the direction of S . The corresponding relation between ψ and ϕ_S is given in Ref. [50]; in deep inelastic kinematics one has $d\psi \approx d\phi_S$. The first and second subscript of the above structure functions indicate the respective polarization of beam and target, and if there is a third subscript, it specifies the polarization of the virtual photon.

In theoretical models, the target polarization is defined with respect to the virtual photon momentum direction, however this definition is not practical for experiments. In practice, the target polarization is understood with respect to the incoming electron momentum direction, a frame where the virtual photon has a nonzero transverse momentum. The conversion of the target polarization between the two frames is straightforward [50], and it turns out that measurements with longitudinally polarized targets with respect to the beam receive small contributions from the structure functions with transverse polarization with respect to the photon. Single-hadron measurements indicate that this contribution is usually negligible. This issue will be considered with care in our analysis. For the moment, we restrict our attention only to the longitudinal structure functions.

The relevant spin asymmetries can be built as ratios of structure functions. For the longitudinal polarization of the beam or of the target, denoted with LU and UL , one can define the following asymmetries:

$$A_{LU}^{\sin \phi_R \sin \theta}(x, y, z, M_h, Q) = \frac{1}{\lambda_e} \frac{\frac{8}{\pi} \int d\phi_R d\cos \theta \sin \phi_R (d\sigma^+ - d\sigma^-)}{\int d\phi_R d\cos \theta (d\sigma^+ + d\sigma^-)} = \frac{\frac{4}{\pi} \sqrt{2\varepsilon(1-\varepsilon)} \int d\cos \theta F_{LU}^{\sin \phi_R}}{\int d\cos \theta (F_{UU,T} + \epsilon F_{UU,L})},$$

$$A_{UL}^{\sin \phi_R \sin \theta}(x, y, z, M_h, Q) = \frac{1}{S_L} \frac{\frac{8}{\pi} \int d\phi_R d\cos \theta \sin \phi_R (d\sigma^+ - d\sigma^-)}{\int d\phi_R d\cos \theta (d\sigma^+ + d\sigma^-)} = \frac{\frac{4}{\pi} \sqrt{2\varepsilon(1+\varepsilon)} \int d\cos \theta F_{UL}^{\sin \phi_R}}{\int d\cos \theta (F_{UU,T} + \epsilon F_{UU,L})}. \quad (4)$$

² From the theoretical point of view, different definitions for the azimuthal angles may be adopted, as long as they differ by terms of order γ^2 .

In the $M_h^2 \ll Q^2$ limit³ the structure functions can be written in terms of PDF and Dihadron Fragmentation Functions (DiFF) in the following way [41]⁴:

$$F_{UU,T} = x f_1^q(x) D_1^q(z, \cos \theta, M_h), \quad (5)$$

$$F_{UU,L} = 0, \quad (6)$$

$$F_{UU}^{\cos \phi_R} = -x \frac{|\mathbf{R}| \sin \theta}{Q} \frac{1}{z} f_1^q(x) \tilde{D}^{\triangleleft q}(z, \cos \theta, M_h), \quad (7)$$

$$F_{UU}^{\cos 2\phi_R} = 0, \quad (8)$$

$$F_{LU}^{\sin \phi_R} = -x \frac{|\mathbf{R}| \sin \theta}{Q} \left[\frac{M}{M_h} x e^q(x) H_1^{\triangleleft q}(z, \cos \theta, M_h) + \frac{1}{z} f_1^q(x) \tilde{G}^{\triangleleft q}(z, \cos \theta, M_h) \right], \quad (9)$$

$$F_{UL}^{\sin \phi_R} = -x \frac{|\mathbf{R}| \sin \theta}{Q} \left[\frac{M}{M_h} x h_L^q(x) H_1^{\triangleleft q}(z, \cos \theta, M_h) + \frac{1}{z} g_1^q(x) \tilde{G}^{\triangleleft q}(z, \cos \theta, M_h) \right], \quad (10)$$

$$F_{UL}^{\sin 2\phi_R} = 0, \quad (11)$$

$$F_{LL} = x g_1^q(x) D_1^q(z, \cos \theta, M_h), \quad (12)$$

$$F_{LL}^{\cos \phi_R} = -x \frac{|\mathbf{R}| \sin \theta}{Q} \frac{1}{z} g_1^q(x) \tilde{D}^{\triangleleft q}(z, \cos \theta, M_h), \quad (13)$$

174 where

$$|\mathbf{R}| = \frac{1}{2} \sqrt{M_h^2 - 2(M_1^2 + M_2^2) + (M_1^2 - M_2^2)^2 / M_h^2}. \quad (14)$$

175 All the structure functions that vanish can be nonzero at order $\mathcal{O}\left(\frac{M^2}{Q^2}, \frac{M_h^2}{Q^2}\right)$. In the above structure
176 functions, there are essentially three kinds of combinations of PDF and fragmentation functions (FF):⁵
177 leading-twist PDF and FF (e.g., $f_1 D_1$), leading-twist PDF and subleading-twist FF (e.g., $f_1 \tilde{D}^{\triangleleft}$), subleading-
178 twist PDF and leading-twist FF (e.g., $e H_1^{\triangleleft}$).

179 The main interest of the structure functions with leading-twist combinations ($F_{UU,T}$ in particular) is to
180 allow a flavor-dependent analysis of the DiFF D_1 , similarly to what happens for the single-hadron case.

181 The subleading-twist fragmentation functions $\tilde{D}^{\triangleleft}$ and $\tilde{G}^{\triangleleft}$ originate from quark-gluon correlation functions
182 on the fragmentation side. They vanish in the so-called Wandzura–Wilczek approximation [52]. Although
183 this approximation is often used in phenomenological works (see, e.g., [53–56] and references therein) there
184 are no compelling theoretical grounds for supporting its validity [57–60]. At present it is not confirmed
185 nor disproved by experimental data [60]. The measurement of $\cos \phi_R$ modulations in unpolarized or doubly
186 polarized collisions ($F_{UU}^{\cos \phi_R}$ and $F_{LL}^{\cos \phi_R}$) offers a way to address this question directly and represents an
187 example of how dihadron measurements can be useful for the study of quark-gluon correlations in general.

188 The most interesting terms for our purposes are the ones containing the functions e and h_L , multiplied by
189 the interference fragmentation function H_1^{\triangleleft} , occurring in the structure functions $F_{LU}^{\sin \phi_R}$ and $F_{UL}^{\sin \phi_R}$. The
190 extraction of the PDF is made possible by the fact that H_1^{\triangleleft} has been recently extracted [44] from BELLE
191 measurements [61]. Unfortunately, the structure functions contain also another term involving the twist-3
192 fragmentation function $\tilde{G}^{\triangleleft}$, although its magnitude is predicted to be small, except perhaps at low x or high
193 M_h [62]. Measuring the double-spin asymmetry $A_{LL}^{\cos \phi_R}$ as well as evaluating the z and M_h -dependence of
194 the ratio $A_{LU}^{\sin \phi_R} / A_{UL}^{\sin \phi_R}$ can help evaluate the relative magnitude of $\tilde{G}^{\triangleleft}$ [3, 63].

³ For some discussion of the case of larger M_h , see Ref. [51]

⁴ a summation $\sum_q e_q^2$ is understood, and the k_T -integrated T -odd twist-3 distribution functions $h(x)$ and $e_L(x)$ are omitted, which are expected to vanish if the only source of the T -odd behavior is the gauge link

⁵ leading-twist functions are always indicated by a subscript 1

Two other contributions to the structure functions $F_{UU}^{\cos \phi_R}$ and $F_{LL}^{\cos \phi_R}$, included in Ref. [41], contain the collinear T -odd distribution functions h and e_L . They should vanish if the gauge link is the only source of a T -odd behavior. Measuring a nonzero h or e_L would cast doubts on collinear factorization at subleading twist. It would be interesting to experimentally check this feature, even though the problem is complicated by the presence of the standard T -even terms discussed above. The significance of such an observation can be compared to the measurements of a nonzero $\sin \phi_S$ signal in inclusive DIS [64–67], which indicates either a violation of T -reversal invariance or the presence of a significant two-photon exchange contribution [68].

C. Partial-wave analysis

Two-hadron fragmentation functions can be decomposed in partial waves in the following way [40, 41]:

$$D_1 \rightarrow D_{1,ss+pp} + D_{1,sp} \cos \theta + D_{1,pp} \frac{1}{4} (3 \cos^2 \theta - 1), \quad (15)$$

$$G_1^\perp \rightarrow G_{1,sp}^\perp + G_{1,pp}^\perp \cos \theta, \quad (16)$$

$$H_1^\triangleleft \rightarrow H_{1,sp}^\triangleleft + H_{1,pp}^\triangleleft \cos \theta, \quad (17)$$

$$\tilde{D}^\triangleleft \rightarrow \tilde{D}_{sp}^\triangleleft + \tilde{D}_{pp}^\triangleleft \cos \theta, \quad (18)$$

$$\tilde{G}^\triangleleft \rightarrow \tilde{G}_{sp}^\triangleleft + \tilde{G}_{pp}^\triangleleft \cos \theta, \quad (19)$$

where the relative partial waves of each pion pair are put into evidence. For sake of simplicity, we will make the replacement $D_{1,ss+pp} \equiv D_1$ since no ambiguity arises in the following. A thorough study of the cross section with partial-wave analysis has been recently presented in Ref. [47], with a different notation compared to the one adopted here. The functions on the r.h.s. depend on z and M_h . It may be useful to note that a symmetrization $f(\theta) + f(\pi - \theta)$ gets rid of all the $\cos \theta$ terms [69]. In general, those terms will vanish even if the θ acceptance is not complete but still symmetric about $\theta = \pi/2$.

Measuring asymmetry modulations in θ enable the ability to constrain the DiFF partial waves. In the full generalization of [47], the DiFF partial waves are associated with angular momentum eigenvalues $\ell = 0, 1, 2$ and $m = -\ell, \dots, \ell$. Each partial wave term corresponds to a particular interference between two dihadrons which are either in the s -wave or p -wave: a dihadron in the s -wave is unpolarized, whereas one in the p -wave has pseudovector polarization, decomposed into longitudinal and transverse components. The partial wave with $\ell = 0$ corresponds to the interference of two s -wave dihadrons, $\ell = 1$ corresponds to the interference of an s -wave dihadron with a p -wave dihadron, and $\ell = 2$ corresponds to the interference between two p -wave dihadrons. The value of m enumerates the possible relative polarizations of the two dihadrons for each fixed value of ℓ . Consequently, measuring θ -modulations of asymmetries grants access to correlations between the fragmenting quark spin and the angular momentum of the final dihadron state. Understanding such correlations can help shed light on production mechanisms for dihadrons with a specific angular momentum, such as those which originate from the decay of the ρ , a vector meson.

D. Flavor structure

We now discuss the flavor structure of the structure functions. The analysis will be different depending on the kind of target and final-state hadrons. We will consider here $\pi^+\pi^-$, K^+K^- , or $K^+\pi^-$ final-state pairs. Isospin symmetry and charge conjugation suggest the the following relations [44]:

$$D_1^{u \rightarrow \pi^+\pi^-} = D_1^{d \rightarrow \pi^+\pi^-} = D_1^{\bar{u} \rightarrow \pi^+\pi^-} = D_1^{\bar{d} \rightarrow \pi^+\pi^-}, \quad (20)$$

$$D_1^{s \rightarrow \pi^+\pi^-} = D_1^{\bar{s} \rightarrow \pi^+\pi^-}, \quad (21)$$

$$D_1^{c \rightarrow \pi^+\pi^-} = D_1^{\bar{c} \rightarrow \pi^+\pi^-}, \quad (22)$$

$$H_1^{\triangleleft u \rightarrow \pi^+\pi^-} = -H_1^{\triangleleft d \rightarrow \pi^+\pi^-} = -H_1^{\triangleleft \bar{u} \rightarrow \pi^+\pi^-} = H_1^{\triangleleft \bar{d} \rightarrow \pi^+\pi^-}, \quad (23)$$

$$H_1^{\triangleleft s \rightarrow \pi^+\pi^-} = -H_1^{\triangleleft \bar{s} \rightarrow \pi^+\pi^-} = H_1^{\triangleleft c \rightarrow \pi^+\pi^-} = -H_1^{\triangleleft \bar{c} \rightarrow \pi^+\pi^-} = 0. \quad (24)$$

For \tilde{G}^\triangleleft we expect the same relations as for H_1^\triangleleft . In practice, for $\pi^+\pi^-$ and neglecting charm quarks, there are only two independent D_1 functions and one H_1^\triangleleft (and \tilde{G}^\triangleleft).

226 For K^+K^- , similar considerations lead to:

$$D_1^{u \rightarrow K^+K^-} = D_1^{\bar{u} \rightarrow K^+K^-}, \quad (25)$$

$$D_1^{s \rightarrow K^+K^-} = D_1^{\bar{s} \rightarrow K^+K^-}, \quad (26)$$

$$D_1^{d \rightarrow K^+K^-} = D_1^{\bar{d} \rightarrow K^+K^-}, \quad (27)$$

$$D_1^{c \rightarrow K^+K^-} = D_1^{\bar{c} \rightarrow K^+K^-}, \quad (28)$$

$$H_1^{\triangleleft u \rightarrow K^+K^-} = -H_1^{\triangleleft \bar{u} \rightarrow K^+K^-} \quad (29)$$

$$H_1^{\triangleleft s \rightarrow K^+K^-} = -H_1^{\triangleleft \bar{s} \rightarrow K^+K^-}, \quad (30)$$

$$H_1^{\triangleleft d \rightarrow K^+K^-} = -H_1^{\triangleleft \bar{d} \rightarrow K^+K^-} = H_1^{\triangleleft c \rightarrow K^+K^-} = -H_1^{\triangleleft \bar{c} \rightarrow K^+K^-} = 0. \quad (31)$$

227 For K^+K^- and neglecting charm quarks, there are three independent D_1 functions and two H_1^{\triangleleft} .

The flavor structure of $K^+\pi^-$ suggests:

$$D_1^{u \rightarrow K^+\pi^-} = D_1^{\bar{u} \rightarrow K^+\pi^-} \quad (32)$$

$$D_1^{s \rightarrow K^+\pi^-} = D_1^{\bar{s} \rightarrow K^+\pi^-} = D_1^{c \rightarrow K^+\pi^-} = D_1^{\bar{c} \rightarrow K^+\pi^-}, \quad (33)$$

$$H_1^{\triangleleft u \rightarrow K^+\pi^-} = -H_1^{\triangleleft \bar{u} \rightarrow K^+\pi^-} \quad (34)$$

$$H_1^{\triangleleft s \rightarrow K^+\pi^-} = H_1^{\triangleleft \bar{s} \rightarrow K^+\pi^-} = H_1^{\triangleleft c \rightarrow K^+\pi^-} = H_1^{\triangleleft \bar{c} \rightarrow K^+\pi^-} = 0. \quad (35)$$

228 Together with the above functions, we have to consider also $D_1^{d \rightarrow K^+\pi^-}$ and $D_1^{\bar{s} \rightarrow K^+\pi^-}$, for a total of four
 229 independent unpolarized fragmentation functions, and $H_1^{\triangleleft d \rightarrow K^+\pi^-}$ and $H_1^{\triangleleft \bar{s} \rightarrow K^+\pi^-}$, for a total of three
 230 independent interference fragmentation functions.

231 E. Cross sections

Using the expressions of the structure functions (9), and (10), along with the partial-wave expansion of the fragmentation functions in Sec. IIC, we can rewrite the asymmetries of Eqs. (4) as

$$A_{LU}^{\sin \phi_R \sin \theta}(x, y, z, M_h, Q) = -\frac{W(y)}{A(y)} \frac{M}{Q} \frac{|\mathbf{R}|}{M_h} \frac{\sum_q e_q^2 \left[x e_q(x) H_{1,sp}^{\triangleleft,q}(z, M_h) + \frac{M_h}{zM} f_1^q(x) \tilde{G}_{sp}^{\triangleleft,q}(z, M_h) \right]}{\sum_q e_q^2 f_1^q(x) D_1^q(z, M_h)}, \quad (36)$$

$$A_{UL}^{\sin \phi_R \sin \theta}(x, y, z, M_h, Q) = -\frac{V(y)}{A(y)} \frac{M}{Q} \frac{|\mathbf{R}|}{M_h} \frac{\sum_q e_q^2 \left[x h_L^q(x) H_{1,sp}^{\triangleleft,q}(z, M_h) + \frac{M_h}{zM} g_1^q(x) \tilde{G}_{sp}^{\triangleleft,q}(z, M_h) \right]}{\sum_q e_q^2 f_1^q(x) D_1^q(z, M_h)}. \quad (37)$$

For the specific case of the $\pi^+\pi^-$ final state, we can introduce in the flavor sum the assumptions (20)–(24),

and we get

$$A_{LU}^{\sin \phi_R \sin \theta}(x, y, z, M_h, Q) \approx -\frac{W(y)}{A(y)} \frac{M}{Q} \frac{|\mathbf{R}|}{M_h} \times \frac{H_{1,sp}^{\triangleleft,u} [4xe^{u-\bar{u}}(x) - xe^{d-\bar{d}}(x)] + \frac{M_h}{zM} \tilde{G}_{sp}^{\triangleleft,u} [4f_1^{u-\bar{u}}(x) - f_1^{d-\bar{d}}(x)]}{D_1^u [4f_1^{u+\bar{u}}(x) + f_1^{d+\bar{d}}(x)] + D_1^s f_1^{s+\bar{s}}(x)}, \quad (38)$$

$$A_{UL}^{\sin \phi_R \sin \theta}(x, y, z, M_h, Q) \approx -\frac{V(y)}{A(y)} \frac{M}{Q} \frac{|\mathbf{R}|}{M_h} \times \frac{H_{1,sp}^{\triangleleft,u} [4xh_L^{u-\bar{u}}(x) - xh_L^{d-\bar{d}}(x)] + \frac{M_h}{zM} \tilde{G}_{sp}^{\triangleleft,u} [4g_1^{u-\bar{u}}(x) - g_1^{d-\bar{d}}(x)]}{D_1^u [4f_1^{u+\bar{u}}(x) + f_1^{d+\bar{d}}(x)] + D_1^s f_1^{s+\bar{s}}(x)}, \quad (39)$$

where for the PDF we adopt the compact notation $f_1^{q\pm\bar{q}}(x) = f_1^q(x) \pm f_1^{\bar{q}}(x)$, and similarly for the other functions. For neutron targets, assuming isospin symmetry, we can simply interchange the role of u and d quarks in the PDF.

The ratio of beam spin to target spin asymmetries may shed some light on the relative contribution of $\tilde{G}^{\triangleleft}$:

$$\frac{A_{LU}^{\sin \phi_R \sin \theta}}{A_{UL}^{\sin \phi_R \sin \theta}} = \frac{W(y)}{V(y)} \frac{H_{1,sp}^{\triangleleft,u} [4e^{u-\bar{u}}(x) - e^{d-\bar{d}}(x)] + \frac{M_h}{zM} \tilde{G}_{sp}^{\triangleleft,u} [4f_1^{u-\bar{u}}(x) - f_1^{d-\bar{d}}(x)]}{H_{1,sp}^{\triangleleft,u} [4h_L^{u-\bar{u}}(x) - h_L^{d-\bar{d}}(x)] + \frac{M_h}{zM} \tilde{G}_{sp}^{\triangleleft,u} [4g_1^{u-\bar{u}}(x) - g_1^{d-\bar{d}}(x)]}. \quad (40)$$

If $\tilde{G}_{sp}^{\triangleleft,u}$ is negligible, this ratio simplifies to

$$\frac{A_{LU}^{\sin \phi_R \sin \theta}}{A_{UL}^{\sin \phi_R \sin \theta}} = \frac{W(y)}{V(y)} \frac{4e^{u-\bar{u}}(x) - e^{d-\bar{d}}(x)}{4h_L^{u-\bar{u}}(x) - h_L^{d-\bar{d}}(x)}, \quad (41)$$

which is not dependent on z or M_h . Thus if $\tilde{G}_{sp}^{\triangleleft,u}$ is zero, we expect the asymmetry ratio to be constant in z and M_h [63]; while the converse of this claim may not necessarily be true, the observation of z and/or M_h dependence of this ratio could hint at a non-negligible contribution from $\tilde{G}^{\triangleleft}$.

F. Parametrization of the DiFF H_1^{\triangleleft}

The chiral-odd Dihadron Fragmentation Function $H_1^{\triangleleft q}$ [39] describes the correlation between the transverse polarization of the fragmenting quark with flavor q and the azimuthal orientation of the plane containing the momenta of the detected hadron pair. $H_{1,sp}^{\triangleleft q}$ is the component of $H_1^{\triangleleft q}$ that is sensitive to the interference between the fragmentation amplitudes into pion pairs in relative s wave and in relative p wave, from which comes the common name of Interference Fragmentation Functions [37]. For this reason, we expect the function to be sizeable in kinematic regions where s and p waves are present. This is typically true where spin-1 resonances (e.g., ρ or K^*) are present.

Before the Belle measurement of the angular distribution of two pion pairs in e^+e^- annihilation [61], the only estimates of DiFF were based on model calculations [39, 42, 70]. The unpolarized D_1 was tuned to Monte Carlo event generators [42] and the polarized $H_{1,sp}^{\triangleleft}$ compared to HERMES asymmetry data [71].

The recent analysis of the so-called Artru–Collins asymmetry [72] by the Belle collaboration gave rise to new parametrization of both D_1 and $H_{1,sp}^{\triangleleft}$ for the production of $\pi^+\pi^-$.

The former was parameterized to reproduce the two-hadron yields of the PHYTIA event generator, which is known to give a good description of data. Three main decay channels were considered for $\pi^+\pi^-$: (i) ρ resonance decaying into the two pions, (ii) ω resonance decaying into the two pions, plus the fragmentation into a ω resonance decaying into $\pi^+\pi^-\pi^0$ with π^0 unobserved, (iii) the continuum, i.e. the fragmentation into an “incoherent” $\pi^+\pi^-$ pair. Combining the fit of the asymmetry data with the parametrization of its denominator allowed the extraction of the IFF $H_{1,sp}^{\triangleleft}$.

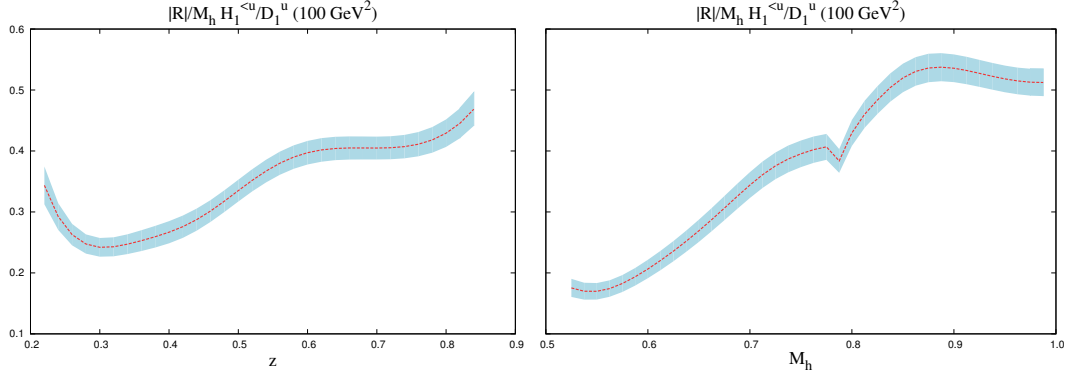


FIG. 2. The ratio $|R|H_{1,sp}^{\triangleleft,u}/M_h D_1^u$ as a function of z and M_h respectively. The error band comes from the calculation of error propagation from the fit.

The ratio $|R|H_{1,sp}^{\triangleleft,u}(z, M_h)/M_h D_1^u(z, M_h)$ at the Belle's scale is depicted in figure 2. It is integrated over M_h or z , respectively. The error band is estimated through the propagation of errors based on the fit's results. The evolution effects, downward to HERMES' scale, have been studied in Ref. [44]. The integrals of the DiFFs over the kinematical ranges for (z, M_h) at both scales lead to the ratios

$$\frac{n_{H_1^{\triangleleft}}^u}{n_{D_1}^u}(\sim 2 \text{ GeV}^2) \Big/ \frac{n_{H_1^{\triangleleft}}^u}{n_{D_1}^u}(100 \text{ GeV}^2) = 92\% \pm 8\%, \quad (42)$$

where n denotes the integral over the DiFF labelled in the subscript. This result indicates that evolution effects are almost negligible at the level of the integrated DiFF. We will not take such a correction into account in this proposal.

There is at the moment no data on interference fragmentation functions for $K\pi$ pairs. In order to have an estimate of the magnitude of the effect, we assume it to have the form:

$$\frac{|R|H_{1,sp}^{\triangleleft}(z, M_h)}{M_h D_1(z, M_h)} \approx 3M_h \frac{|R|\sqrt{D_{1\text{con}}(z, M_h) D_{1K^*}(z, M_h)}}{M_h D_1(z, M_h)}, \quad (43)$$

where with $D_{1\text{con}}$ and D_{1K^*} we mean the components of the fragmentation function that describe the $K\pi$ continuum and the K^* resonance, respectively. We estimate these fragmentation function components using the LEPTO Monte Carlo event generator. The above ansatz is motivated by the fact that the function $H_{1,sp}^{\triangleleft}$ arises from the interference between pairs produced in s wave and p wave (as explained at the beginning of the section). The above ansatz applied to the $\pi^+\pi^-$ system reproduces the size and qualitative feature of the extracted ratio displayed in figure 2. Finally, for $K\pi$ pairs we assume that the fragmentation function is the same for all flavors (the largest component should anyway come from the u quark).

G. Collinear twist-3 parton distribution functions $e(x)$ and $h_L(x)$

The PDFs $e(x)$ and $h_L(x)$ are twist-3 functions which can be written in the following way [48, 73]:

$$xe = x\tilde{e} + \frac{m}{M} f_1, \quad (44)$$

$$xh_L = x\tilde{h}_L + \frac{p_T^2}{M^2} h_{1L}^\perp + \frac{m}{M} g_{1L}. \quad (45)$$

The functions on the l.h.s. can be expressed in terms of quark fields only. This property allows an explicit calculation in quark models [74]. The functions with the tilde on the r.h.s. are related to quark-gluon-quark correlators and are specifically referred to as “pure twist-3” contributions [57]. The rest of each expression on the r.h.s. contains only twist-2 functions and corresponds to its Wandzura–Wilczek part. Neglecting quark

masses, the function $xe(x)$ is entirely determined by pure twist-3 contributions. (Notice that multiplying $e(x)$ by x is necessary to cancel a δ -function-type singularity at $x = 0$, see below.)

The function $e(x)$ has attracted a lot of interest [30] because it is directly related to the soft physics of chiral symmetry breaking [75].

The first Mellin moment of the isoscalar flavor-combination of $e^a(x)$ is related to the pion-nucleon sigma-term:

$$\int_0^1 dx (e^u + e^{\bar{u}} + e^d + e^{\bar{d}})(x) = \frac{\sigma_{\pi N}}{m}, \quad (46)$$

where $m = \frac{1}{2}(m_u + m_d)$ is the average current mass of light quarks, and (small) “double-isospin-breaking” effects proportional to $(m_u - m_d)\langle N | (\bar{\psi}_u \psi_u - \bar{\psi}_d \psi_d) | N \rangle$ are neglected. In the pre-QCD era $\sigma_{\pi N}$ was introduced as the double commutator of the strong interaction Hamiltonian with two axial isovector charges [76]. In QCD it is related to matrix elements of the operators $m_q \bar{\psi}_q \psi_q$ which explicitly break chiral symmetry. In the chiral limit $\sigma_{\pi N} \rightarrow 0$ but $\sigma_{\pi N}/m$ is finite. The pion-nucleon sigma-term is given by the scalar form factor $\sigma(t)$ at zero momentum transfer $t = 0$. This form factor describes the elastic scattering off a spin- $\frac{1}{2}$ target via the exchange of a spin-0 particle (e.g. the Higgs [77]), and has not yet been measured except for its value in the time-like region at the so-called Chen-Dashen point $t = 2m_\pi^2$, with m_π the pion mass, which can be deduced from pion-nucleon scattering data by means of low-energy theorems [78–80]. Chiral perturbation theory and dispersion relation techniques allow one to relate $\sigma(2m_\pi^2)$ to $\sigma(0) \equiv \sigma_{\pi N}$ [81–83]. The phenomenological value of $\sigma_{\pi N} = (50\text{--}70 \text{ MeV})$ [81, 84–86] is sometimes said to be “unexpectedly large” because it implies a large “strangeness content of the nucleon” defined as

$$y_N = \frac{\langle N | \bar{\psi}_s \psi_s | N \rangle}{\frac{1}{2} \langle N | (\bar{\psi}_u \psi_u + \bar{\psi}_d \psi_d) | N \rangle} = 1 - \frac{m}{m_s - m} \frac{M_\Xi + M_\Sigma - 2M_N}{\sigma_{\pi N}} \quad (47)$$

where the second equality is valid in leading order of chiral perturbation theory [87, 88]. Numerically one finds $y_N = 0.2\text{--}0.4$ but this does not imply that (20–40)% of the nucleon mass is due to strangeness (taking also the contributions of the “kinetic” and “potential” energies in QCD into account one deduces a much smaller strangeness contribution to the nucleon mass [89]). Direct lattice studies of $\sigma_{\pi N}$ have been performed [90] but are demanding because of difficulties associated with the renormalization of the operator $m_q \bar{\psi}_q \psi_q$ on the lattice. Another method to deduce $\sigma_{\pi N}$ from lattice calculations makes use of the Feynman-Hellmann theorem [91, 92] which relates $\sigma_{\pi N}$ to the slope of the nucleon mass as function of the pion mass, $\sigma_{\pi N} = m_\pi^2 \frac{\partial M_N}{\partial m_\pi^2}$. Lattice data analysis yield results compatible with the phenomenological $\sigma_{\pi N}$ -determinations [93–95]. Let us also mention the interesting connection of $\sigma_{\pi N}$ to negative Mellin moments of $f_1^a(x)$ discussed in [96]. At first glance, Eq. (46) seems to imply that one could access information on $\sigma_{\pi N}$ from deeply inelastic scattering experiments. But in QCD the contribution of $\sigma_{\pi N}$ to (46) is due to a δ -function-type singularity at $x = 0$, a well-known [97] but rarely emphasized fact [98]. A $\delta(x)$ -contribution was found in a $(1 + 1)$ -dimensional version of the Gross-Neveu model [99], in perturbative approaches [100], and in the chiral quark-soliton model [101–104] (which consistently allows one to calculate $\sigma_{\pi N}$ from $\sigma(t)$, the coefficient of $\delta(x)$ in $e(x)$, and the Feynman-Hellmann theorem [105], see also [106]). In the chiral quark-soliton model the origin of the $\delta(x)$ -contribution in $e(x)$ is of non-perturbative character [101, 102]. In other models of $e(x)$ no $\delta(x)$ -contribution was found [74, 107–109].

Even though one cannot access information on $\sigma_{\pi N}$ from DIS of $e(x)$ [98], the presence of the $\delta(x)$ -singularity in $e(x)$ can be concluded indirectly. Numerically, if the point $x = 0$ was included, the sum rule (46) would give a large number of $\mathcal{O}(10)$ for the first moment of $e(x)$. Experimentally, since the point $x = 0$ cannot be reached, one would observe approximately zero [98]. The possible existence of $\delta(x)$ -contributions in structure functions can be inferred from the analytical properties of the respective forward Compton scattering amplitudes and was debated before QCD [110–112] ($e(x)$ is related to the structure functions $F_4(x)$ and $F_5(x)$ which in principle could be measured in (anti)neutrino-nucleon DIS [111]). More prominent examples of sum rules which could possibly be spoiled in this way are the Burkhardt-Cottingham sum rule [113] and the Gerasimov-Drell-Hearn sum rule [114].

The second moment of $e(x)$ is equally interesting, as it arises from the mass term in (44) suggesting that,

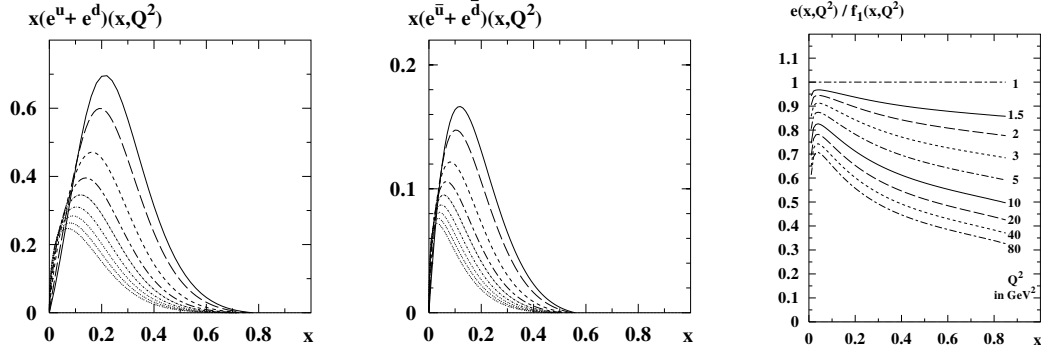


FIG. 3. Evolution effects for the isoscalar flavor combinations (a) $xe^{u+d}(x)$ and (b) $xe^{\bar{u}+\bar{d}}(x)$ from the chiral quark-soliton model in the chiral limit [101]. Solid line: the results at the initial scale of the chiral quark soliton model $\mu_0^2 = (600 \text{ MeV})^2$. The dashed and dotted curves are the results after evolution (in decreasing order) to the scales $Q^2 = 0.5, 1, 2, 4, 8, 16, 32$ and 64 GeV^2 . (c) The scale dependence of the ratio $e(x, Q^2)/f_1(x, Q^2)$ from the “toy model” $e(x, Q_0^2) = f_1(x, Q_0^2)$ at $Q_0^2 = 1 \text{ GeV}^2$. For definiteness: we use the LO parametrization for $f_1(x, Q^2)$ from [120]. The evolution of $e(x)$ is performed in all figures according to [117].

in principle, an “extraction” of current quark masses from SIDIS is possible, namely [74]:

$$\int_0^1 dx x(e^q - e^{\bar{q}})(x) = \frac{m_q}{M_N} N_q, \quad (48)$$

where for flavor q , m_q is the quark mass and N_q is the number of valence quarks. Effects associated with $e(x)$ are power suppressed, however, by M_N/Q , *i.e.*, the contribution of (48) to observables is of $\mathcal{O}(m_q/Q)$ and hence negligible. For the above-discussed reasons, the practical DIS sum rules for $e(x)$ are [98]:

$$\int_\epsilon^1 dx (e^q + e^{\bar{q}})(x) \approx 0, \quad \int_\epsilon^1 dx x(e^q - e^{\bar{q}})(x) \approx 0, \quad (49)$$

where $\epsilon > 0$ represents the smallest x -value accessible in experiments. This situation is analog to the Efremov-Leader-Teryaev sum rule [115]. The pure twist-3 piece in $e^q(x)$ drops out from the first two moments (46, 48) and contributes only to the third Mellin moment. Noteworthy, the matrix element $\int dx x^2 \bar{e}^q(x)$ describes the average transverse force acting on a transversely polarized quark q in an unpolarized target after interaction with the virtual photon [13].

The renormalization scale dependence of $\tilde{e}(x)$ and $\tilde{h}_L(x)$ was studied in Refs. [116–118], see also Refs. [97, 119] for reviews. The evolution of these pure twist-3 functions is characterized by a complicated operator mixing pattern, typical for twist-3 quantities. In the multi-color limit the evolution of $\tilde{e}(x)$ simplifies to a DGLAP-type evolution – as it does for the other two nucleon twist-3 distribution functions $\tilde{h}_L(x)$ and (the flavour non-singlet) $\tilde{g}_T(x)$. Figs. 3a and 3b show respectively the evolution of $e^{u+d}(x, Q^2)$ and $e^{\bar{u}+\bar{d}}(x, Q^2)$ from the chiral quark soliton model [101] from an initial scale $\mu_0^2 = (600 \text{ MeV})^2$ of the chiral quark soliton model to higher scales.

In order to better understand the evolution pattern figure 3c shows the evolution of the “toy model” $e(x, Q_0^2) = f_1(x, Q_0^2)$ at $Q^2 = 1 \text{ GeV}^2$ to higher scales normalized with respect to $f_1(x, Q^2)$ at the respective scales. The LO unpolarized parton distribution functions at the respective scales are taken from [120]. We see that the ratio of $e(x)/f_1(x)$ drops from unity at $Q_0^2 = 1 \text{ GeV}^2$, by about (20–30) % when going to experimentally relevant scales of typically (2–3) GeV^2 at Jefferson Lab. Finally, figure 4 shows the parton distribution functions $e(x)$ and $h_L(x)$ as predicted by the chiral quark soliton model [104, 121] at $Q^2 = 2.5 \text{ GeV}^2$.

These features make $e(x)$ and $h_L(x)$ extremely interesting functions, and having experimental access to them is of great importance.

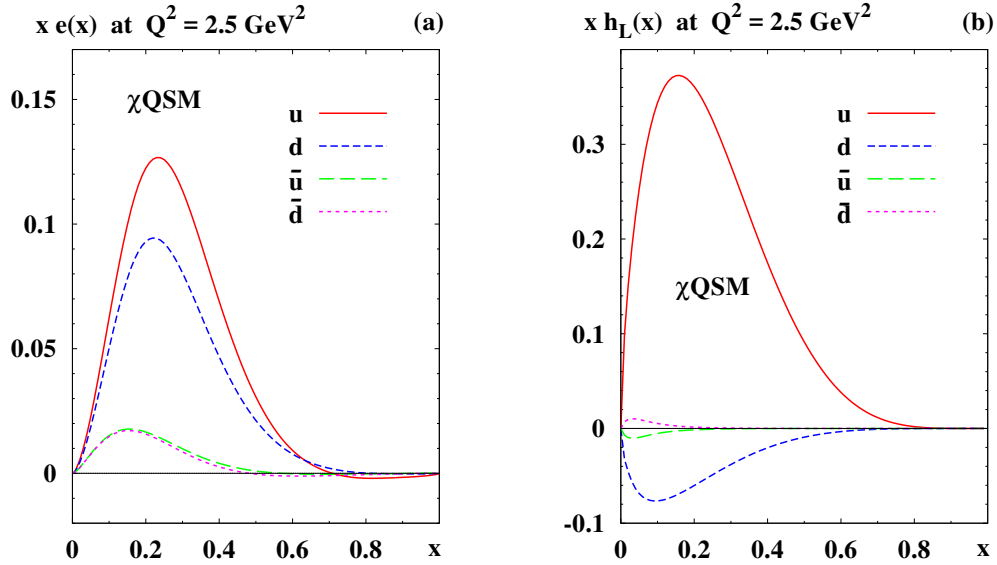


FIG. 4. The parton distribution functions $x e(x)$ and $x h_L(x)$ from the chiral quark soliton model (χ QSM) [104, 121]. All results are LO-evolved to $Q^2 = 2.5 \text{ GeV}^2$.

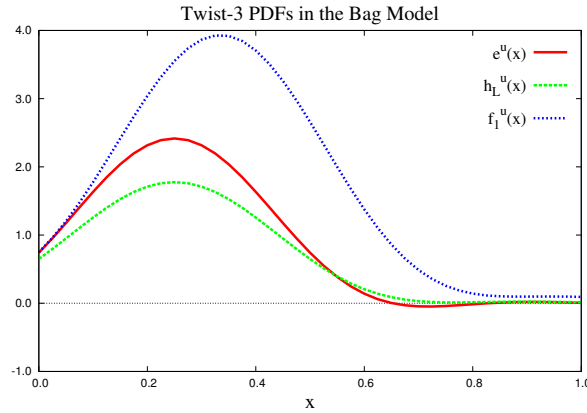


FIG. 5. The functions $e^u(x)$, $h_L^u(x)$, and $f_1^u(x)$ in the bag model [74].

There are few model calculations concerning the twist-3 PDF: MIT bag model [74, 107, 122], diquark spectator model [108], instanton QCD vacuum calculus [123, 124], chiral quark soliton model [101–104, 125], and the perturbative light-cone Hamiltonian approach to $\mathcal{O}(\alpha_S)$ with a quark target [100, 109]. In these calculations there are no contributions from either strange or sea quarks, except for the chiral quark soliton model.

The bag model has given several powerful results and predictions concerning PDF as well as transverse-momentum dependent distributions (TMD). It is a relativistic model where quarks and antiquarks are excitations inside the confined bag. It is generally assumed that the proton wave function is invariant under the $SU(6)$ spin-flavor symmetry. In the case of two-body problems, this symmetry leads to proportionality between the different flavor components. The contribution to $e(x)$ in the bag is entirely due to the bag boundary, and therefore to the quark-gluon-quark correlation. The result of the model calculation of the twist-3 $e^u(x)$, $h_L^u(x)$, as well as of the unpolarized distribution $f_1^u(x)$, is depicted in figure 5. On the other hand, the function $h_L(x)$ contains twist-2 and pure twist-3 contributions. Although it is a popular assumption that pure twist-3 (and mass) terms are small [53–56], this has rarely been justified by theoretical calculations.

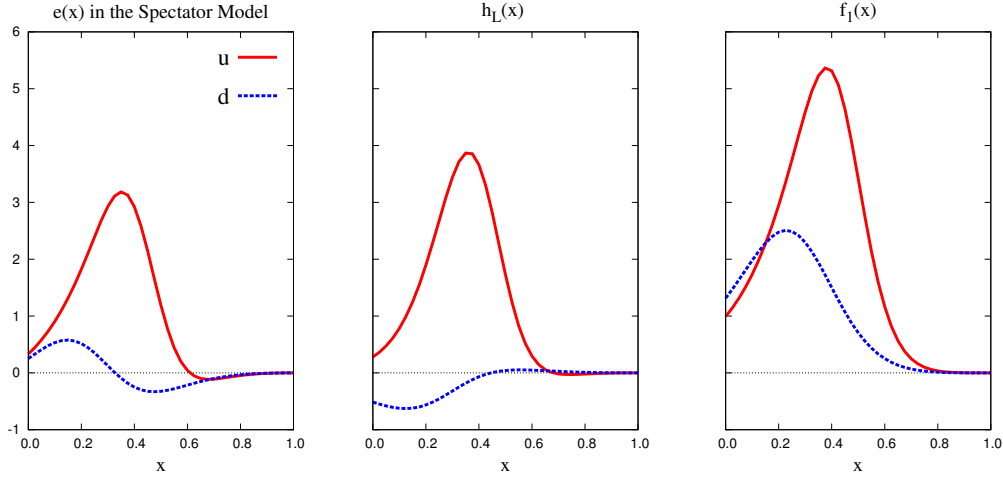


FIG. 6. The function $e^q(x)$, $h_L^q(x)$, $f_1^q(x)$, for $q = u$ (solid red line) and $q = d$ (dotted blue line) in the spectator model of Ref. [108].

In the bag model, assuming for simplicity the Wandzura–Wilczek approximation $\tilde{G}^{\triangleleft} = 0$, the asymmetries (39) become:

$$A_{LU}^{\sin \phi_R \sin \theta}(x, y, z, M_h, Q) = -\frac{W(y)}{A(y)} \frac{M}{Q} \frac{|\mathbf{R}|}{M_h} \frac{(4 - \frac{1}{2}) x e^u(x) H_{1,sp}^{\triangleleft,u}(z, M_h)}{(4 + \frac{1}{2}) f_1^u(x) D_1^u(z, M_h)}, \quad (50)$$

$$A_{UL}^{\sin \phi_R \sin \theta}(x, y, z, M_h, Q) = -\frac{V(y)}{A(y)} \frac{M}{Q} \frac{|\mathbf{R}|}{M_h} \frac{(4 + \frac{1}{4}) x h_L^u(x) H_{1,sp}^{\triangleleft,u}(z, M_h)}{(4 + \frac{1}{2}) f_1^u(x) D_1^u(z, M_h)}. \quad (51)$$

In the spectator model calculation [108], the nucleon states do not strictly follow the $SU(6)$ symmetry and there is no flavor symmetry for a given distribution. Adopting the same approximation as before, in the spectator model the asymmetries (39) become:

$$A_{LU}^{\sin \phi_R \sin \theta}(x, y, z, M_h, Q) = -\frac{W(y)}{A(y)} \frac{M}{Q} \frac{|\mathbf{R}|}{M_h} \frac{x (4 e^u(x) - e^d(x)) H_{1,sp}^{\triangleleft,u}(z, M_h)}{(4 f_1^u(x) + f_1^d(x)) D_1^u(z, M_h)}, \quad (52)$$

$$A_{UL}^{\sin \phi_R \sin \theta}(x, y, z, M_h, Q) = -\frac{V(y)}{A(y)} \frac{M}{Q} \frac{|\mathbf{R}|}{M_h} \frac{x (4 h_L^u(x) - h_L^d(x)) H_{1,sp}^{\triangleleft,u}(z, M_h)}{(4 f_1^u(x) + f_1^d(x)) D_1^u(z, M_h)}. \quad (53)$$

The results for the twist-3 PDF $e(x)$, $h_L(x)$, and the unpolarized $f_1(x)$ in the spectator model of Ref. [108] are depicted in figure 6 for both the u and d flavor.

In all model results above, the model's scale has been used. This scale turns out to be rather low, $Q_0^2 \sim 0.1 \text{ GeV}^2$. We neglect the evolution effects on the PDF part of the asymmetries. However, we expect QCD evolution to affect the distributions in pushing them towards lower x values. The missing QCD evolution of the twist-3 PDF is believed to be the largest source of errors in the predictions.

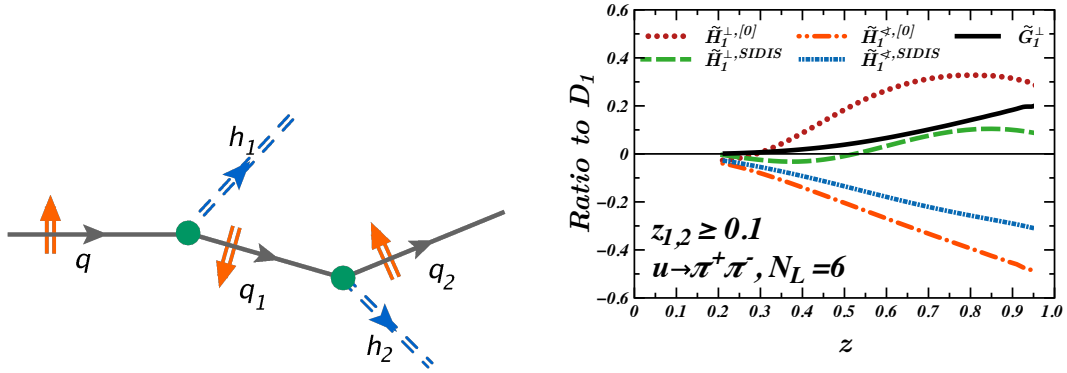


FIG. 7. Hadronization within the quark-jet model including spin (left) and model calculations for the ratios of G_1^\perp and H_1^\less to the unpolarized DiFF D_1 (right). The different definitions for H_1^\less reflect a process dependence in the definitions for this particular model (e^+e^- versus SIDIS). Here, the $\tilde{H}_1^{\less,SIDIS}$ is relevant, where the $\tilde{\cdot}$ denotes that the functions have been integrated over the mass of the dihadron system. Figures taken from [128]

III. Novel spin-orbit correlations in hadronization in TMD DiFFs

As described earlier, having an additional degree of freedom allows the existence of DiFFs that have no correspondence in single-hadron fragmentation. An exciting example is the DiFF G_1^\perp , which describes the azimuthal dependence of an unpolarized hadron pair on the helicity of the outgoing quark [126]. Similar to, e.g., the Boer-Mulders effect, this effect needs intrinsic transverse momentum acquired in the fragmentation process. Fragmentation functions are not accessible on the lattice [2], therefore this channel presents a unique opportunity to extend our knowledge of spin-momentum dynamics in hadronization.

In quark-jet models [127, 128], which describe in the transverse case the observed H_1^\less well, the intrinsic transverse momentum is acquired in the quark-to-quark splitting in the fragmentation process, and through the associated spin transfer the recoiling quarks acquire a non-zero transverse polarization. These polarizations are correlated, leading to an effect which is predicted to be significant, with the magnitude of G_1^\perp about 30% of the magnitude of H_1^\less [127]. This process, along with the model predictions for G_1^\perp compared to H_1^\less , is shown in figure 7. We know that H_1^\less is large, therefore it is reasonable to expect that we should be able to observe effects sensitive to G_1^\perp , which is about one third in magnitude.

Another model prediction is from the spectator model [129]. Figure 8 shows the ratio⁶ of G_1^\perp to the unpolarized DiFF D_1 ; there is a sign change at the ρ resonance (770 MeV). The authors proceed to extract a corresponding prediction of the target spin asymmetry, which is compared to the COMPASS results from [4]. While the relevant asymmetry measured by COMPASS is consistent with zero within the experimental precision, the spectator model predicts a small asymmetry, which is fairly close to the COMPASS result, as shown in figure 9.

Aside from the COMPASS results, in the literature there are no constraints on G_1^\perp from data. In section VIB we show the recent CLAS12 preliminary result on beam spin asymmetries in dihadron production, which shows promise to provide the first significant constraints. While the analysis is not finalized, it does indicate the presence of a sign change of G_1^\perp at the ρ meson mass, consistent with the above spectator model. A longitudinal target would allow for complementary access to G_1^\perp through target spin asymmetries, providing further constraints on any extraction.

A. Access to the helicity DiFF

The differential cross section for dihadron production given in Eq.2 is integrated over ϕ_h and $P_{h\perp}^2$, causing several terms to vanish. Additional modulations are present if this integration is not performed, the most

⁶ lowest-order partial waves

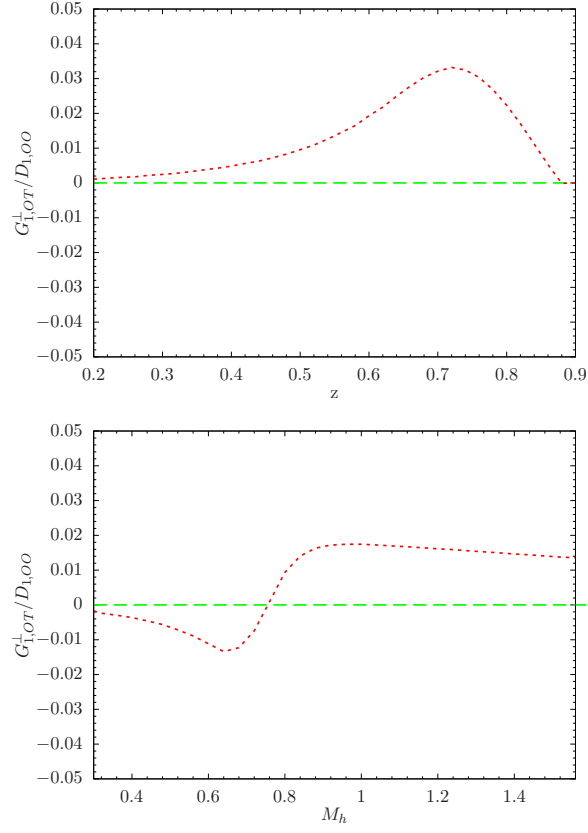


FIG. 8. Spectator model prediction of the ratio $G_{1,OT}^\perp/D_{1,OO}$ for z -dependence (left) and M_h -dependence (right). From [129].

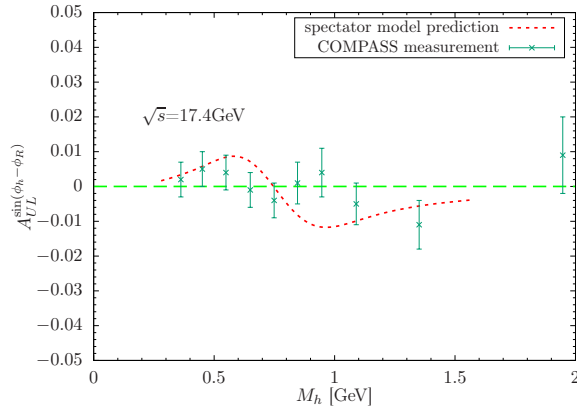


FIG. 9. Spectator model prediction of the target spin asymmetry (dashed curve), compared to the COMPASS result from [4] (points). From [129].

relevant for this proposal being [47]:

$$F_{LU,T}^{P_{\ell,m} \sin(m(\phi_h - \phi_{R\perp}))} = -\mathcal{I} \left[2 \cos(m(\phi_h - \phi_p)) f_1 G_1^{\perp|\ell,m} \right], \quad (54)$$

$$F_{UL}^{P_{\ell,m} \sin(m(\phi_h - \phi_{R\perp}))} = -\mathcal{I} \left[2 \cos(m(\phi_h - \phi_p)) g_{1L} G_1^{\perp|\ell,m} \right], \quad (55)$$

$$F_{UL}^{P_{\ell,m} \sin((2-m)\phi_h + m\phi_{R\perp})} = -\mathcal{I} \left[\frac{|\mathbf{k}_T||\mathbf{p}_T|}{MM_h} \cos((m-2)\phi_h + \phi_k + (1-m)\phi_p) h_{1L}^{\perp} H_1^{\perp|\ell,m} \right], \quad (56)$$

where \mathcal{I} denotes a weighted convolution of the PDF and FF. The notation $|\ell, m\rangle$ denotes a partial wave of the DiFF, parameterized by angular momentum eigenvalues ℓ and m . The modulations are expressed as products of a Fourier sinusoid dependent on ϕ_h , ϕ_R , and m , with an associated Legendre polynomial $P_{\ell,m}$ dependent on θ .

The helicity-dependent DiFF G_1^{\perp} is found in Eqs. 54 and 55, and is experimentally accessible via target-spin and beam-spin asymmetries A_{UL} and A_{LU} . In A_{LU} it couples to the spin averaged PDF $f_1(x)$, whereas in A_{UL} it couples to the helicity distribution $g_1(x)$, both of which have a significant magnitude. Additionally, Eq. 56 shows sensitivity to the wormgear distribution function h_{1L}^{\perp} coupled with the H_1^{\perp} DiFF.

Some of the initial interest in G_1^{\perp} was motivated by its connection to the so-called jet-handedness [126], which in turn might receive contributions from CP-violating QCD vacuum fluctuations [98]. This was one reason for the measurement at Belle [130] which did not find a signal. However, after a revisit of the original calculation by another theory group [131], it became clear this was due to a sign-mistake in the original calculation. For SIDIS, they propose a measurement of dihadron asymmetries with the weight factors [132, 133]:

$$A = \frac{\langle P_{h\perp} \sin(\phi_h - \phi_R)/M_h \rangle}{\langle 1 \rangle} = \frac{\int d_{LU} P_{h\perp} \sin(\phi_h - \phi_R)/M_h}{\int d_{UU}}. \quad (57)$$

This weight breaks up the momentum convolution, and the corresponding target-spin and beam-spin asymmetries are:

$$A_{UL}^{\rightarrow}(x, z, M_h^2) = S_L \frac{\sum_a e_a^2 g_{1L}^a(x) z G_1^{\perp a}(z, M_h^2)}{\sum_a e_a^2 f_1^a(x) D_1^a(z, M_h^2)}, \quad (58)$$

$$A_{LU}^{\rightarrow}(x, y, z, M_h^2) = \lambda_l \frac{C'(y) \sum_a e_a^2 f_1^a(x) z G_1^{\perp a}(z, M_h^2)}{A'(y) \sum_a e_a^2 f_1^a(x) D_1^a(z, M_h^2)}. \quad (59)$$

The aforementioned CLAS12 preliminary result is of this beam spin asymmetry, while the target spin asymmetry is another proposed measurement for the longitudinal target program. A measurement of both is complementary, since each corresponds to a coupling with a different PDF.

This is the first time that a TMD DiFF will be measured, and it can also be accessed in a re-measurement of G_1^{\perp} in e^+e^- annihilation, which is well motivated to test the validity of factorization. A comparison with the SIDIS measurements might be sensitive to parity violating vacuum fluctuations as discussed above.

B. Transverse Momentum Dependent DiFFs

It is interesting to draw analogies between single-hadron TMD FFs, accessible in Λ production, to TMD DiFFs. Table II shows an attempt at a comparison, where the left half is for single-hadron FF and the right half for DiFFs. Dihadron polarization is better understood within the partial wave expansion, however, so it is more correct to expand the matrix to include the interference between relative s and p waves.

To do the expansion, we first enumerate the possible polarization pairings in the interference terms. Truncating the expansion at $\ell = 2$, which limits us to consider only up to a relative p wave difference, the s -state dihadron is unpolarized (denoted U or O), and the p -state dihadron has either transverse (T) or longitudinal (L) polarization; $\ell = 0$ corresponds to the ss terms, $\ell = 1$ to the sp terms, and $\ell = 2$ to the pp terms. We can then rearrange these partial waves into an enhanced table of DiFFs, following the notation given in Eqs. 62-74 of [47]. Table III is the updated table, where rows are grouped by the following classifications:

- unpolarized only, the ss terms

h/q	U	L	T	h/q	U	L	T
U	$D_1^{\Lambda/q}$		$H_1^{\perp,\Lambda/q}$	U	$D_1^{h_1 h_2/q}$		$H_1^{\perp,h_1 h_2/q}$
L		$G_1^{\Lambda/q}$	$H_{1L}^{\Lambda/q\perp}$	L			
T	$D_{1T}^{\perp\Lambda/q}$	$G_{1T}^{\perp\Lambda/q}$	$H_1^{\Lambda/q}, H_{1T}^{\perp\Lambda/q}$	T		$G_1^{\perp h_1 h_2/q}$	$H_1^{\triangleleft h_1 h_2/q}$

TABLE II. TMD FFs for Λ production (left) and dihadrons (right) appearing at leading order in $1/Q^2$ in the SIDIS cross section. The U, L, and T labels of the rows (columns) represent the dependence of the distributions on the polarization (unpolarized, longitudinally, transversely) of the quark (hadron).

- interference with longitudinally polarized dihadron, but not transverse, which contains sp and pp terms with $m = 0$

- interference with transversely polarized dihadron, which contains sp and pp terms with $m = 1, 2$

It is interesting to note that G_1^\perp necessitates the interference with a transversely polarized dihadron, while this DiFF encodes a correlation of fragmenting quark with longitudinal polarization; this correlation of longitudinal quark polarization to transverse dihadron polarization could represent a contribution from a “wormgear-like” splitting.

$h_1 h_2/q$	U	L	T
UU	$D_{1,OO}$		$H_{1,OO}^\perp$
LU	$D_{1,OL}$		$H_{1,OL}^\perp$
LL	$D_{1,LL}$		$H_{1,LL}^\perp$
TU	$D_{1,OT}$	$G_{1,OT}^\perp$	$\begin{cases} H_{1,OT}^\perp & \text{if } m < 0 \\ H_{1,OT}^\triangleleft & \text{if } m > 0 \end{cases}$
TL	$D_{1,LT}$	$G_{1,LT}^\perp$	$\begin{cases} H_{1,LT}^\perp & \text{if } m < 0 \\ H_{1,LT}^\triangleleft & \text{if } m > 0 \end{cases}$
TT	$D_{1,TT}$	$G_{1,TT}^\perp$	$\begin{cases} H_{1,TT}^\perp & \text{if } m < 0 \\ H_{1,TT}^\triangleleft & \text{if } m > 0 \end{cases}$

TABLE III. Table of DiFFs, where the rows are the dihadron polarizations, *i.e.*, interference, and the columns are the fragmenting quark polarization; the DiFFs follow the notation given in [47]

IV. Correlations in hadron production in the current and target fragmentation region

All of the above asymmetries assume the factorization model with the hadron production occurring from the scattered parton, that is, in the Current Fragmentation Region (CFR). It is possible to study hadronization which originates from the target as well, which is called the Target Fragmentation Region (TFR). Correlations between hadrons from the CFR with those from the TFR represent another class of dihadron production which is of interest in this section.

A. SIDIS in the TFR

As it has become clear during the last decades, the study of the three dimensional spin-dependent partonic structure of the nucleon requires excellent understanding of the hadronization process after hard lepton-quark scattering. The unique feature of CLAS12 is the wide coverage of the produced hadron phase space; in contrast to previous SIDIS experiments, we will have access not only to the CFR but also to the TFR. These two regions are defined in the virtual photon - target nucleon center of mass frame, with the z -axis aligned to the virtual photon momentum. The CFR includes hadrons produced in the forward hemisphere (along the virtual photon), whereas the TFR is for hadrons produced in the backward hemisphere.

The QCD description of this process for collinear kinematics includes new nonperturbative objects, the fracture functions, which were first introduced by Trentadue and Veneziano [45]. Recently this approach was generalized by Anselmino, Barone and Kotzinian [46] to the spin and transverse momentum dependent case. The polarized and transverse-momentum dependent fracture functions appear in the expansion of the leading twist projections of the hadronic tensor

$$\begin{aligned} \mathcal{M}^{[\Gamma]}(x, \mathbf{k}, \zeta, \mathbf{P}_h) & \equiv \frac{1}{4\zeta} \int \frac{dk^+ dk^-}{(2\pi)^3} \delta(k^- - xP^-) \text{Tr}(\mathcal{M}\Gamma) \\ & = \frac{1}{4\zeta} \int \frac{d\xi^+ d^2\xi_\perp}{(2\pi)^6} e^{i(xP^- \xi^+ - \mathbf{k} \cdot \xi_\perp)} \sum_X \int \frac{d^3\mathbf{P}_X}{(2\pi)^3 2E_X} \times \\ & \quad \langle P, S | \bar{\psi}(0) \Gamma | P_h, S_h; X \rangle \langle P_h, S_h; X | \psi(\xi^+, 0, \xi_\perp) | P, S \rangle, \end{aligned} \quad (60)$$

where $\Gamma = \gamma^-, \gamma^- \gamma_5, i\sigma^{i-} \gamma_5$.

The fracture functions represent the conditional probabilities to find an unpolarized ($\Gamma = \gamma^-$), a longitudinally polarized ($\Gamma = \gamma^- \gamma_5$) or a transversely polarized ($\Gamma = i\sigma^{i-} \gamma_5$) quark with longitudinal momentum fraction x and transverse momentum \mathbf{k} inside a nucleon, fragmenting into a hadron carrying a fraction $\zeta = P_h^-/P^- \simeq E_h/E$ of the nucleon longitudinal momentum and a transverse momentum \mathbf{P}_h .

The most general parameterization of the traced fracture matrix for the production of a spinless hadron can be written as:

$$\mathcal{M}^{[\gamma^-]} = \hat{f}_1 + \frac{\mathbf{P}_h \times \mathbf{S}_T}{m_h} \hat{f}_{1T}^h + \frac{\mathbf{k} \times \mathbf{S}_T}{m_N} \hat{f}_{1T}^\perp + \frac{S_L (\mathbf{k} \times \mathbf{P}_h)}{m_N m_h} \hat{f}_{1L}^{\perp h}, \quad (61)$$

$$\mathcal{M}^{[\gamma^- \gamma_5]} = S_L \hat{g}_{1L} + \frac{\mathbf{P}_h \cdot \mathbf{S}_T}{m_h} \hat{g}_{1T}^h + \frac{\mathbf{k} \cdot \mathbf{S}_T}{m_N} \hat{g}_{1T}^\perp + \frac{\mathbf{k} \times \mathbf{P}_h}{m_N m_h} \hat{g}_1^{\perp h}, \quad (62)$$

$$\begin{aligned} \mathcal{M}^{[i\sigma^{i-} \gamma_5]} & = S_T^i \hat{h}_{1T} + \frac{S_L P_h^i}{m_h} \hat{h}_{1L}^h + \frac{S_L k^i}{m_N} \hat{h}_{1L}^\perp \\ & \quad + \frac{(\mathbf{P}_h \cdot \mathbf{S}_T) P_h^i}{m_h^2} \hat{h}_{1T}^{hh} + \frac{(\mathbf{k} \cdot \mathbf{S}_T) k^i}{m_N^2} \hat{h}_{1T}^{\perp\perp} \\ & \quad + \frac{(\mathbf{k} \cdot \mathbf{S}_T) P_h^i - (\mathbf{P}_h \cdot \mathbf{S}_T) k^i}{m_N m_h} \hat{h}_{1T}^{\perp h} \\ & \quad + \frac{\epsilon_{\perp ij} P_{h\perp j}}{m_h} \hat{h}_1^h + \frac{\epsilon_{\perp ij} k_{\perp j}}{m_N} \hat{h}_1^\perp, \end{aligned} \quad (63)$$

where by the vector product of the two-dimensional vectors we mean the pseudo-scalar quantity $\mathbf{a}_\perp \times \mathbf{b}_\perp = \epsilon_{\perp ij} a_\perp^i b_\perp^j = |\mathbf{a}_\perp| |\mathbf{b}_\perp| \sin(\phi_b - \phi_a)$. In total there are 16 fracture functions ($\hat{f}, \hat{g}, \hat{h}$) depending on the scalar

variables $x, \mathbf{k}^2, \zeta, \mathbf{P}_h^2, \mathbf{k} \cdot \mathbf{P}_h$. Note, that, in contrast with [46], here for fracture functions we use notations corresponding to Amsterdam notations for DFs.

The general LO cross section expression for SIDIS in the TFR is presented in [46] and gives access only to four quark-transverse-momentum integrated fracture functions. To gain access to all LO fracture functions, one has to “measure” the final quark transverse polarization. The Double SIDIS process, outlined in the next section, allows this by means of the Collins effect for hadrons produced in the CFR. Exploiting the SIDIS in TFR, Double SIDIS will allow us to check the validity of factorization and deepen our understanding the hadronization mechanism.

B. The Double SIDIS (DSIDIS) process

Let us consider the polarized SIDIS process in Eq. (1) with one hadron produced in the current fragmentation region (CFR) and the other in the target fragmentation region (TFR) [134], shown in figure 10. The LO expression for Spin and Transverse Momentum Dependent (STMD) DSIDIS is given as:

$$\frac{d\sigma^{\ell(l,\lambda)+N(P,S)\rightarrow\ell(l')+\bar{h}_1(P_1)+h_2(P_2)+X}}{dx dQ^2 d\phi_S dz d^2P_{T1} d\zeta d^2P_{T2}} = \sum_q \mathcal{M}_{q,s/N,S}^{h_2} \otimes \frac{d\sigma^{\ell(l,\lambda)+q(k,s)\rightarrow\ell(l')+q(k',s')}}{dQ^2} \otimes D_{q,s'}^{h_1}, \quad (64)$$

where $\mathcal{M}_{q,s/N,S}^{h_2}$ are the STMD fracture functions Eqs. (61–63), and $D_{q,s'}^{h_1}$ are the STMD fragmentation functions to a spinless hadron from unpolarized and transversely polarized quarks (see, for example, [48]),

$$D_{q,s'}^{h_1}(z, \mathbf{p}) = D_1(z, p^2) + \frac{\mathbf{p} \times \mathbf{s}'}{m_h} H_1(z, p^2), \quad (65)$$

where \mathbf{p} is a transverse momentum of the hadron, with respect to the fragmenting quark momentum.

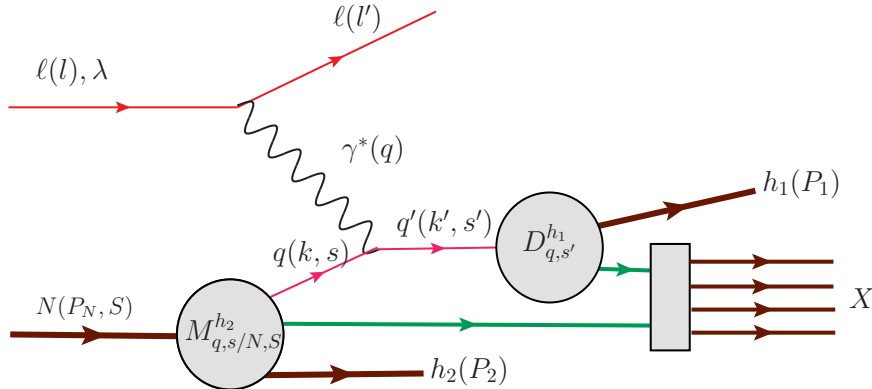


FIG. 10. DSIDIS description with hadronization function. From [134].

1. DSIDIS cross section and asymmetries

The cross section for the DSIDIS from a polarized lepton scattering off a longitudinally polarized nucleon can be written in the form:

$$\frac{d\sigma^{\ell(l,\lambda)+N(P,S)\rightarrow\ell(l')+\bar{h}_1(P_1)+h_2(P_2)+X}}{dx dy d\phi_S dz d^2P_{T1} d\zeta d^2P_{T2}} = \frac{\alpha^2 x}{Q^4 y} (1 + (1 - y)^2) (\sigma_{UU} + S_L \sigma_{UL} + S_T \sigma_{UT} + \lambda D_{U\sigma_{LU}} + \lambda S_L D_{U\sigma_{LL}} + \lambda S_T D_{U\sigma_{LT}}), \quad (66)$$

where

$$Du(y) = \frac{y(2-y)}{1+(1-y)^2}. \quad (67)$$

455 The terms depending on the longitudinal polarization of initial particles are given by [135]:

$$\begin{aligned} \sigma_{UU} = & F_0^{\hat{M} \cdot D_1} - D_{nn} \left[\frac{P_{T1}^2}{m_1 m_N} F_{kp1}^{\hat{h}_1^\perp \cdot H_1} \cos(2\phi_1) \right. \\ & + \frac{P_{T1} P_{T2}}{m_1 m_2} F_{p1}^{\hat{h}_1^h \cdot H_1} \cos(\phi_1 + \phi_2) \\ & \left. + \left(\frac{P_{T2}^2}{m_1 m_N} F_{kp2}^{\hat{h}_1^\perp \cdot H_1} + \frac{P_{T2}^2}{m_1 m_2} F_{p2}^{\hat{h}_1^h \cdot H_1} \right) \cos(2\phi_2) \right]. \end{aligned} \quad (68)$$

$$\begin{aligned} \sigma_{UL} = & -\frac{P_{T1} P_{T2}}{m_2 m_N} F_{k1}^{\hat{M}_L^{\perp h} \cdot D_1} \sin(\phi_1 - \phi_2) \\ & + D_{nn} \left[\frac{P_{T1}^2}{m_1 m_N} F_{kp1}^{\hat{h}_{1L}^\perp \cdot H_1} \sin(2\phi_1) \right. \\ & + \frac{P_{T1} P_{T2}}{m_1 m_2} F_{p1}^{\hat{h}_{1L}^h \cdot H_1} \sin(\phi_1 + \phi_2) \\ & \left. + \left(\frac{P_{T2}^2}{m_1 m_N} F_{kp2}^{\hat{h}_{1L}^\perp \cdot H_1} + \frac{P_{T2}^2}{m_1 m_2} F_{p2}^{\hat{h}_{1L}^h \cdot H_1} \right) \sin(2\phi_2) \right]. \end{aligned} \quad (69)$$

$$\sigma_{LU} = -\frac{P_{T1} P_{T2}}{m_2 m_N} F_{k1}^{\hat{g}_1^{\perp h} \cdot D_1} \sin(\phi_1 - \phi_2). \quad (70)$$

$$\sigma_{LL} = F_0^{\hat{g}_{1L} \cdot D_1}, \quad (71)$$

where

$$D_{nn}(y) = \frac{(1-y)}{1+(1-y)^2}. \quad (72)$$

456 The structure functions $F_0^{\Delta \hat{M}_L \cdot D_1}$, $F_{k1}^{\Delta \hat{M}_L^{\perp h} \cdot D_1}$, *etc.* are convolutions of the fracture function M and frag-
457 mentation function D (see appendix B). The fracture functions which depend on quark polarization have
458 the notation \hat{g} for longitudinally polarized quarks and \hat{h} for transversely polarized quarks; the motivation
459 for this notation will become apparent in the next section.

460 Equations 68-71 indicate the various fracture functions that azimuthal modulations of DSIDIS spin asym-
461 metries are sensitive to. Beam spin asymmetries give access only to \hat{g}_1 , the fracture function of longitudinally
462 polarized quarks in an unpolarized nucleon. With the addition of target polarization, several other fracture
463 functions become accessible in modulations of the target spin and double spin asymmetries:

- 464 • \hat{M}_L : unpolarized quark in a longitudinally polarized nucleon
- 465 • \hat{h}_{1L} : transversely polarized quark in a longitudinally polarized nucleon (note there are two types for
466 this case: \hat{h}_{1L}^h which includes a factor of $P_{h\perp}$ and \hat{h}_{1L}^\perp which includes a factor of k_\perp).
- 467 • \hat{g}_{1L} : longitudinally polarized quark in a longitudinally polarized nucleon; this one is accessible in the
468 double spin asymmetry

469 Significant SSAs have been measured by CLAS for azimuthal correlations of hadrons in the target and current
470 fragmentation regions, providing direct access to underlying fracture functions [136]. Figure 11 shows that
471 A_{LU} is very significant at large x , which is the main focus of our proposal.

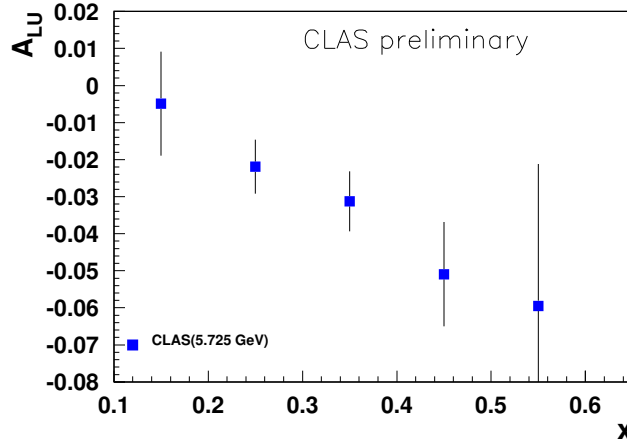


FIG. 11. $A_{LU}^{\sin(\phi_2 - \phi_1)}$ dependence on x for $0.4 < z < 0.7$, for the process $ep \rightarrow e'\pi^+X$ with pion $x_F > 0$ and proton $x_F < 0$.

2. Integrated cross sections

To compare with observables in single hadron production in target or current fragmentation regions, one can integrate the cross section over the transverse momentum of the TFR hadron. In this case the Eq. (66) will contain the integrated fracture functions:

$$\int d^2 P_{T2} \mathcal{M}^{[\gamma^-]} = \check{f}_1(x, \zeta, \mathbf{k}^2) - \frac{\mathbf{k} \times \mathbf{S}_T}{m_N} \check{f}_{1T}^\perp(x, \zeta, \mathbf{k}^2), \quad (73)$$

$$\int d^2 P_{T2} \mathcal{M}^{[\gamma^- \gamma^5]} = S_L \check{g}_{1L}(x, \zeta, \mathbf{k}^2) + \frac{\mathbf{k} \cdot \mathbf{S}_T}{m_N} \check{g}_{1T}(x, \zeta, \mathbf{k}^2), \quad (74)$$

$$\begin{aligned} \int d^2 P_{T2} \mathcal{M}^{[i\sigma^{+-}\gamma^5]} &= S_T^i \check{h}_1(x, \zeta, \mathbf{k}^2) + \frac{S_L k^i}{m_N} \check{h}_{1L}^\perp(x, \zeta, \mathbf{k}^2) \\ &+ \frac{(\mathbf{k} \cdot \mathbf{S}_T) k^i - \frac{1}{2} \mathbf{k}^2 S_T^i}{m_N^2} \check{h}_{1T}^\perp(x, \zeta, \mathbf{k}^2) + \frac{\epsilon_{\perp}^{ij} k_j}{m_N} \check{h}_1^\perp(x, \zeta, \mathbf{k}^2), \end{aligned} \quad (75)$$

where

$$\check{f}_1(x, \zeta, \mathbf{k}^2) = \int d^2 \mathbf{P}_h \hat{f}_1, \quad (76)$$

$$\check{f}_{1T}^\perp(x, \zeta, \mathbf{k}^2) = - \int d^2 \mathbf{P}_h \left(\hat{f}_{1T}^\perp + \frac{m_N}{m_h} \frac{\mathbf{k} \cdot \mathbf{P}_h}{\mathbf{k}^2} \hat{f}_{1T}^h \right), \quad (77)$$

$$\check{g}_{1L}(x, \zeta, \mathbf{k}^2) = \int d^2 \mathbf{P}_h \hat{g}_{1L}, \quad (78)$$

$$\check{g}_{1T}(x, \zeta, \mathbf{k}^2) = \int d^2 \mathbf{P}_h \left(\hat{g}_{1T}^\perp + \frac{m_N}{m_h} \frac{\mathbf{k} \cdot \mathbf{P}_h}{\mathbf{k}^2} \hat{g}_{1T}^h \right), \quad (79)$$

$$\check{h}_{1L}^\perp(x, \zeta, \mathbf{k}^2) = \int d^2 \mathbf{P}_h \left(\hat{h}_{1L}^\perp + \frac{m_N}{m_h} \frac{\mathbf{k} \cdot \mathbf{P}_h}{\mathbf{k}^2} \hat{h}_{1L}^h \right), \quad (80)$$

$$\check{h}_1^\perp(x, \zeta, \mathbf{k}^2) = - \int d^2 \mathbf{P}_h \left(\hat{h}_1^\perp + \frac{m_N}{m_h} \frac{\mathbf{k} \cdot \mathbf{P}_h}{\mathbf{k}^2} \hat{h}_1^h \right), \quad (81)$$

$$\check{h}_{1T}^\perp(x, \zeta, \mathbf{k}^2) = \int d^2 \mathbf{P}_h \left(\hat{h}_{1T}^{\perp\perp} + \frac{m_N^2}{m_h^2} \frac{2(\mathbf{k} \cdot \mathbf{P}_h)^2 - \mathbf{k}^2 \mathbf{P}_h^2}{(\mathbf{k}^2)^2} \hat{h}_{1T}^{hh} \right), \quad (82)$$

$$\check{h}_1(x, \zeta, \mathbf{k}^2) = \int d^2 \mathbf{P}_h \left(\hat{h}_{1T} + \frac{\mathbf{k}^2}{2m_N^2} \hat{h}_{1T}^{\perp\perp} + \frac{\mathbf{P}_h^2}{2m_h^2} \hat{h}_{1T}^{hh} \right). \quad (83)$$

Note, that the combinations of fracture functions in the r.h.s. enter also in the momentum sum rules derived in [46].

Now, looking at Eqs. (73–75) one immediately can see that they exactly reproduce the structures entering in the decomposition of quark correlators for ordinary TMD PDFs. This means that the LO cross section expression for the DSIDIS process will exactly coincide with the LO expression for the SIDIS cross section in the CFR [48], with the replacement of the PDFs by corresponding fracture functions. The result is:

$$\frac{d\sigma^{\ell(l,\lambda)+N(P,S)\rightarrow\ell(l')+h_1(P_1)+h_2(P_2)+X}}{dx dQ^2 d\phi_S dz d^2 P_{1T} d\zeta} = \frac{\alpha^2 x}{y Q^2} (1 + (1-y)^2) \times \\ \times \left[F_{UU} + D_{nn}(y) F_{UU}^{\cos 2\phi_1} \cos(2\phi_1) + S_L D_{nn}(y) F_{UL}^{\sin 2\phi_1} \sin(2\phi_1) + \lambda S_L D_u(y) F_{LL} \right], \quad (84)$$

with

$$F_{UU} = \mathcal{C}[\check{f}_1 D_1], \quad (85)$$

$$F_{UU}^{\cos 2\phi_1} = \mathcal{C}\left[-\frac{2(\hat{\mathbf{h}} \cdot \mathbf{k}_T)(\hat{\mathbf{h}} \cdot \mathbf{p}_T) - \mathbf{k}_T \cdot \mathbf{p}_T}{MM_h} \check{h}_1^\perp H_1^\perp\right], \quad (86)$$

$$F_{UL}^{\sin 2\phi_1} = \mathcal{C}\left[-\frac{2(\hat{\mathbf{h}} \cdot \mathbf{k}_T)(\hat{\mathbf{h}} \cdot \mathbf{p}_T) - \mathbf{k}_T \cdot \mathbf{p}_T}{MM_h} \check{h}_{1L}^\perp H_1^\perp\right], \quad (87)$$

$$F_{LL} = \mathcal{C}[\check{g}_{1L} D_1], \quad (88)$$

where the standard notation

$$\mathcal{C}[w f D] = x \sum_a e_a^2 \int d^2 \mathbf{k} d^2 \mathbf{p} \delta^{(2)}(\mathbf{k} - \mathbf{p} - \mathbf{P}_{h\perp}/z) w(\mathbf{k}, \mathbf{p}) f^a(x, \zeta, \mathbf{k}^2) D^a(z, \mathbf{p}^2) \quad (89)$$

was used and the unit vector $\hat{\mathbf{h}} = \mathbf{P}_{h\perp}/|\mathbf{P}_{h\perp}|$.

One could instead integrate the DSIDIS cross section over the CFR hadron transverse momentum. The LO expression Eq. (66) will contain the following integrations:

$$\int d^2 \mathbf{p} \int d^2 \mathbf{k} \int d^2 \mathbf{P}_1 \delta^2(\mathbf{P}_1 - \mathbf{p} - z\mathbf{k}) \mathcal{M}(x, \zeta, \mathbf{k}^2, \mathbf{P}_2) \mathcal{D}(z, \mathbf{p}_1) = \\ \int d^2 \mathbf{p} \int d^2 \mathbf{k} \hat{\mathcal{M}}(x, \zeta, \mathbf{k}, \mathbf{P}_2) \mathcal{D}(z, \mathbf{p}_\perp) = M(x, \zeta, \mathbf{P}_2) D_1(z). \quad (90)$$

One can see that in this case we do not access transversely polarized quark fracture functions and the LO cross section expression can be obtained as in the case of one hadron production in the TFR [46]:

$$\frac{d\sigma^{\text{TFR}}}{dx dy d\zeta d^2 \mathbf{P}_h d\phi_S dz} = \frac{2\alpha_{\text{em}}^2}{Q^2 y} \left\{ \left(1 - y + \frac{y^2}{2} \right) \right. \\ \left. \times \sum_a e_a^2 \left[\check{f}_1(x, \zeta, \mathbf{P}_h^2) + D_u(y) S_L \check{g}_{1L}(x, \zeta, \mathbf{P}_h^2) \right] D_1(z) \right\}, \quad (91)$$

with

$$\check{f}_1(x, \zeta, \mathbf{P}_h^2) = \int d^2 \mathbf{k} \hat{M}(x, \mathbf{k}^2, \zeta, \mathbf{P}_h^2, \mathbf{k} \cdot \mathbf{P}_h) \quad (92)$$

$$\check{g}_{1L}(x, \zeta, \mathbf{P}_h^2) = \int d^2 \mathbf{k} \hat{g}_{1L}(x, \mathbf{k}^2, \zeta, \mathbf{P}_h^2, \mathbf{k} \cdot \mathbf{P}_h). \quad (93)$$

The DSIDIS cross section LO expressions can be, therefore, studied for three different cases: (i) integrated over TFR hadron transverse momentum, (ii) over CFR hadron transverse momentum and (iii) unintegrated over transverse momenta. The expressions are rather simple for (i) and (ii), but experimental measurements of azimuthal asymmetries in these cases will be more difficult since azimuthal acceptance corrections will be needed. In (iii), the three-dimensional (in azimuths) analysis will allow to avoid this problem and will give access to all TMD fracture functions. Measured single and double leading twist asymmetries for pion and kaon pairs in a large range of kinematic variables (x , Q^2 , z , $P_{h\perp}$, and ϕ) with longitudinally polarized targets, will thus provide a first glimpse into the fracture functions.

V. Experimental details

A. CLAS12

The proposed experiment will run in similar conditions to an already approved CLAS12 proposal for semi-inclusive DIS studies with CLAS12 [7–10] for longitudinally polarized proton and deuteron targets. We will use the upgraded CLAS12 spectrometer [137] with part of the low threshold Cherenkov counter replaced by the ring-imaging Cherenkov detectors, which will help allow for kaon identification. We will run at the standard magnetic field configurations. The central tracker will also be used for coincident detection of protons, pions and kaons both in target and current fragmentation regions. The solenoid for the central tracker is also used simultaneously to provide the magnetic field for the polarized target.

B. CLAS12 Particle Identification

In the baseline design of CLAS12 [137, 138], particle identification (PID) in the forward detector is obtained by using the high threshold Cerenkov counter (HTCC) [139], the low threshold Cerenkov counter (LTCC) [140] and the time-of-flight scintillator arrays (TOF) [141, 142]. In the $\sim 2.5 - 5 \text{ GeV}/c$ momentum region, the π/K separation relies only on the LTCC performance. Moreover, in the $4.7 - 8 \text{ GeV}/c$ momentum region it is not possible to separate protons from kaons, unless we make use of the Ring Imaging Cherenkov (RICH) detector [143]; one RICH sector (out of 6) is currently installed, and a second one is planned to be ready by the time of the proposed run period.

In general this PID system matches the requirements of the physics program at 12 GeV, however there are some physics reactions of high interest, such as the ones covered by this proposal, that cannot be accessed without a better PID, especially for charged kaon detection. At 12 GeV for semi-inclusive processes, the K/π ratio is of the order of 10 – 15% (see figure 12) thus the required rejection factor for pions is around 1 : 500 (corresponding to 4σ pion-kaon separation) while with the present configuration, assuming a pion detection inefficiency for the LTCC of 10%, the π/K contamination is 1 : 1. Currently, one of the CLAS sectors is covered by a new RICH detector which has been installed in place of the low threshold Cerenkov counter. For the measurements proposed here, a second RICH sector, currently under construction, might be in place. Together, these will provide the capabilities needed to detect $\pi - K$ and $K - K$ pairs, where the kaon has high momentum. Note, that since in the dihadron channel the momentum is shared between the outgoing hadrons, one of the hadrons usually has a low enough momentum to be within the CLAS12 PID acceptance without the RICH.

C. The polarized target

The target configuration will be the same as for already approved proposals using the polarized target [7–10]. Further information on the target design can be found in references including [144–146]. It will be polarized via the method of Dynamic Nuclear Polarization (DNP) which is a well established technique that has been used extensively in nuclear and particle physics experiments, including the ones performed in Hall B of Jefferson Lab. Dynamically polarized target systems consist of a hydrogenated (polarized protons) or deuterated (polarized neutrons) compound containing paramagnetic centers, such as unpaired electrons, placed in a high magnetic field and cooled to low temperatures, with a B/T ratio of the order of 5 Tesla/Kelvin. In these conditions, the free electron spins can approach polarization of 100%. The high polarization of unpaired electrons is then transferred dynamically to the nucleons by irradiating the target material at frequency near that of electron spin resonance. This technique typically achieves a proton polarization of 80-90%, and a deuteron polarization of 30-40%. The nucleons in the target will be polarized either parallel or anti-parallel to the electron beam direction.

The main systems required to realize DNP are the superconducting magnet to provide a strong (5 T) field, a ^4He evaporation refrigerator to maintain the target material at 1 K, a target insert, which will house the target material and some additional instrumentation, a microwave system to transfer the polarization to the nucleon spins, and a Nuclear Magnetic Resonance (NMR) system to determine the state of polarization.

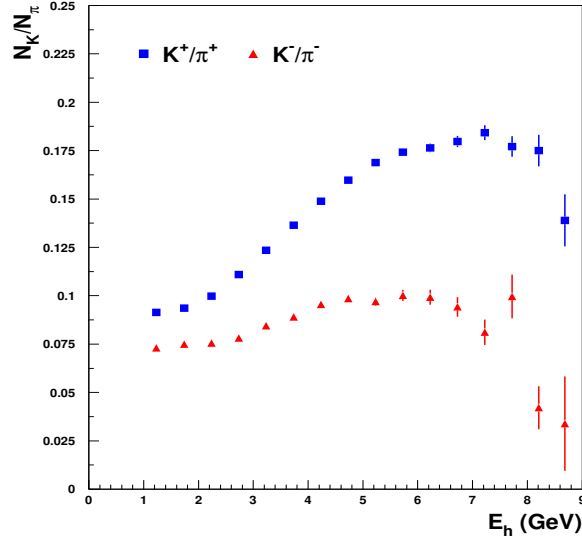


FIG. 12. Semi-Inclusive kaon versus pion yield ratio.

In CLAS12 the polarizing magnetic field will be provided by the superconducting solenoid of the central detector. Ammonia and deuterated ammonia will be used as target material with the electron beam and CLAS12. In order to determine the dilution factor (fraction of events originating from polarized target materials) for each process with sufficiently high accuracy, about 20% of the running time will be devoted to measurements with carbon, nitrogen, and helium. To determine the proton to deuteron and deuteron to carbon cross section ratios, we will need a few days of running with the same magnetic fields and target position as the present experiment, but with gas or liquid hydrogen and deuterium targets. We anticipate that this can be scheduled in conjunction with other planned experiments with CLAS12.

For measurements on polarized deuterium, while we plan to use the ND_3 target, we could also make use of the ^3He target, which is also proposed to this year's PAC [147] (see also [148]). The ^3He target has similar dilution, but a higher polarization of 50%. With a higher polarization statistical uncertainties will be lower; moreover, having two different targets could lead to a better understanding of systematics. It would be most advantageous to make use of data from both targets for a full analysis with polarized deuterium.

The target polarization will be monitored during the run via the NMR system, in the field of the solenoid magnet [149]. The calibration of the proton NMR can be done by measurements of polarization in thermal equilibrium, taken with the polarizing magnet. The experiment will run with a beam of about 10 nA on a 5 cm long ammonia target, resulting in a luminosity of $10^{35}/\text{cm}^2\text{s}$. The beam will be rastered over the diameter of the polarized target to minimize the dose density (we will need at most one anneal every other day under these conditions).

D. The data set and analysis

The expected kinematical coverage in the DIS region from the proposed experiment with 11 GeV beam and CLAS12 is shown in figure 13. This will constitute a substantial increase over the existing Jefferson Lab data in both x and Q^2 (maximum Q^2 of 5 GeV^2 and x between 0.2 and 0.6), while the precision of the expected data in the valence region will be far superior to existing DIS experiments from other labs.

Realistic MC simulations are crucial for separation of different contributions to azimuthal moments arising from higher twists, both kinematical [150] and dynamical [151–154], radiative corrections [155, 156] and in particular from the detector acceptance. The CLAS12 FAST-MC program was used to simulate the physics events and study the extraction of azimuthal moments and acceptance corrections. The large acceptance of CLAS12 allows detection of final state hadrons produced both in target and current fragmentation regions.

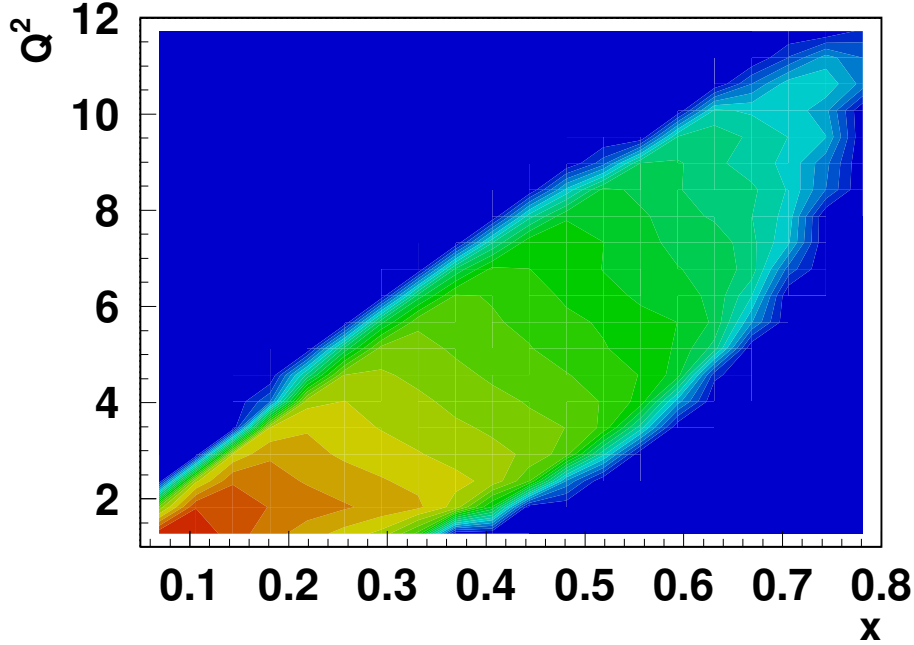


FIG. 13. Kinematical coverage in the SIDIS region of the proposed experiment for ehX events.

The 2D x_F -distributions are shown on figure 14. By selecting different kinematical regions, one can measure azimuthal asymmetries in those regions and extract underlying non-perturbative functions.

Figure 15 shows the typical mass distribution for $\pi^+\pi^-$ dihadron production, along with contributions from various meson decay channels. The CLAS12 data occupy the same region shown on the figure. In particular there is a large contribution from ρ -mesons, which can be selected by a cut on M_h and additionally on the angular momentum from a partial wave analysis. Because such a large fraction of pions can originate from a ρ decay, understanding the ρ production mechanism from the perspective of dihadrons can help clarify single pion production.

In projected results we assume a beam polarization of 0.8, which has been routinely achieved in recent experiments running at Jefferson Lab. The beam helicity will be flipped in a pseudo-random pattern every 33 ms. We will use the standard Hall B beam devices to monitor and stabilize the beam intensity and position. In particular, we will reduce any helicity-correlated beam asymmetries to less than 10^{-3} .

The data will consist of the number of counts for beam electron or target proton helicity parallel (N^+) and anti-parallel (N^-) states, each normalized to the dead-time corrected integrated beam charge; details of the trigger system are found at [157]. We will subtract from these rates the backgrounds from misidentified kaons/pions (which can be obtained from fits to the distribution of photo-electrons in the high-threshold Cerenkov counter and the measured ratio of visible energy deposited in the electromagnetic calorimeter to the measured momentum) and from electrons coming from pair-symmetric decays (e.g., $\pi^0 \rightarrow e^+e^-$ or $\pi^0 \rightarrow \gamma e^+e^-$ as well as $\gamma \rightarrow e^+e^-$ conversions). From the corrected counts, we will form the ratio $A^{raw} = (N^+ - N^-)/(N^+ + N^-)$. This ratio has to be divided by the beam or target polarization and the additional dilution factor for the polarized target case (the fraction of counts coming from the polarized nuclei in the target to the total).

For the polarized target configuration, following the procedure developed for the single-hadron case [10], the dilution factor can be calculated from a detailed model of the target content. The only ingredient needed is the packing fraction (the fraction of the cell volume occupied by the ammonia beads), which can be extracted by comparing the rate from ammonia to that from an auxiliary carbon target. Additional

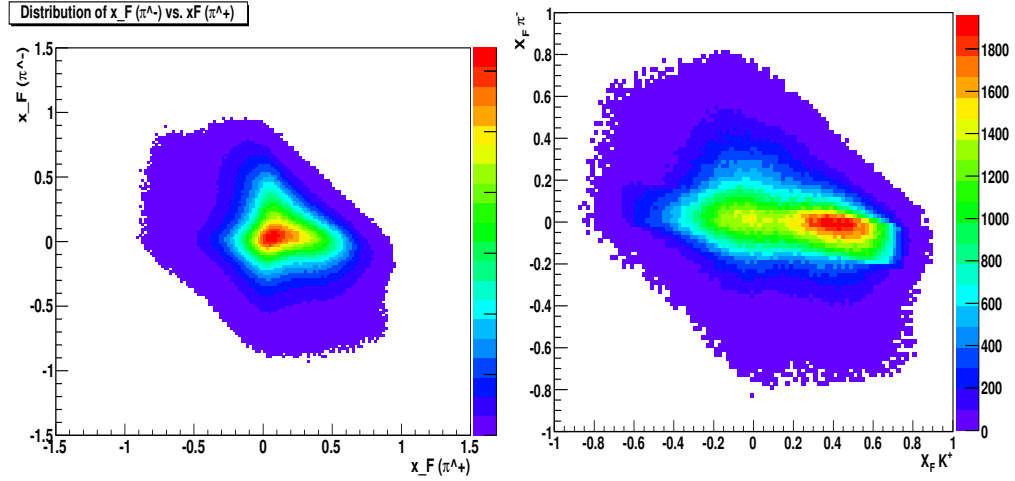


FIG. 14. Distribution over x_F for pion-pion and pion-kaon pairs from FASTMC

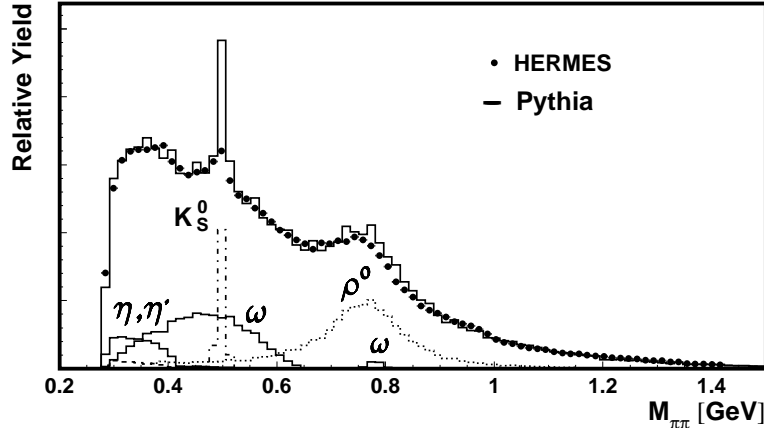


FIG. 15. Typical mass distribution for $\pi^+\pi^-$ dihadrons, including contributions from decays. From [69].

measurements on empty and liquid-helium only targets will also be needed. Past experience with the EG1 experiment in Hall B has shown that a typical error of 3% on the dilution factor can be achieved [158]. An additional correction for the small polarization in ^{15}N and contamination by ^{14}N and, in the case of the deuterated ammonia, H, will be applied as well. Section VI C includes some plots that show the dependence of dilution factors on kinematic variables.

The beam (P_B) and target (P_T) polarization will be independently measured using Möller scattering and NMR, respectively. The target polarization, however, can be extracted from the product of $P_B * P_T$ with higher precision directly from our data, by measuring the asymmetry of elastic (quasi-elastic) scattering $\vec{p}(\vec{e}, e'p)$ ($\vec{d}(\vec{e}, e'p)$) from our NH_3 (ND_3) targets, respectively. We did a full simulation of this method, including radiative effects, CLAS12 acceptance, and expected beam parameters. We found that the uncertainty on P_T for the proton will be about 3% and on the deuteron about 5%.

1. Event Selection Criteria

We focus the analysis on inclusive dihadron production. For each event, we build a list of dihadrons, where each dihadron is a permutation of 2 hadrons from the event, along with the coincident scattered electron. We plan to use particle identification provided by the CLAS12 event builder [138], along with any refinements,

to select on the dihadron channel of interest as well as the scattered electron. The electron momentum determines the following variables, which are listed here along with criteria for analysis:

- Virtual photon momentum-squared: $Q^2 > 1 \text{ GeV}^2$, to be in the scaling regime
- Invariant mass of proton + photon: $W > 2 \text{ GeV}$, which is above the resonance region
- Fraction of beam energy carried by photon: $y < 0.8$, since radiative effects are more severe at high y

For the dihadron, denoted $h_1 h_2$, we require

- Fragmentation fraction: $z_{h_1 h_2} < 0.95$, to avoid exclusive region
- Missing mass: $M_X > 1.5 \text{ GeV}$, to get above exclusive events and resonances
- Feynman- x : $x_F > 0$ for each hadron, so both are produced in the current fragmentation region
- Hadron momentum: $p_{h_{1,2}} > 1.25 \text{ GeV}$, for track reconstruction efficiency

While these cuts are still being refined, their aim is to provide a clean sample of inclusive dihadrons with minimal systematic uncertainties and maximal statistics. These cuts are similar to those used for the CLAS6 analysis on dihadron beam spin asymmetries [159], as well as the recent CLAS12 preliminary results described in section VIB.

Finally, it is worth noting that these cuts can be further tuned for different analyses. For example, while these cuts are well studied for the $\pi\pi$ channel, there may be some alterations or further cuts necessary for πK or KK channels. For the case of DSIDIS, a cut requiring x_F of one hadron to be positive and that of the other hadron to be negative is necessary; however, this may not be sufficient enough to separate the target and current fragmentation regions, requiring further cut refinement.

2. Asymmetry Measurement

There are many techniques to extract the asymmetry from data. Because there are multiple modulations of the dihadron cross section, including partial wave expansions, we employ an unbinned extended maximum likelihood method (MLM).

Let h_b and h_t respectively denote the electron beam helicity and the target helicity. The ratio of the cross section for a particular combination of helicities to the total cross section can be written in terms of the spin asymmetries:

$$\frac{d\sigma_{h_b h_t}}{d\sigma} = \frac{1}{4} (1 + h_b A_{LU} + h_t A_{UL} + h_b h_t A_{LL}), \quad (94)$$

Without loss of generality, we will proceed with focus on the target spin asymmetry; the same procedure is applicable to beam spin and double spin asymmetries. Defining $d\sigma_{\pm} = d\sigma_{++} + d\sigma_{-+}$, we have

$$\frac{d\sigma_{\pm}}{d\sigma} = \frac{1}{2} (1 \pm A_{UL}). \quad (95)$$

The asymmetry A_{UL} is written in terms of cross sections for each helicity, which can be converted into yields N , divided by luminosity L and acceptance Ω . This is the experimentally measured asymmetry, which represents a fraction fP of the true asymmetry, where f is the dilution factor and P is the target polarization. In other words:

$$A_{UL} = \frac{d\sigma_{+} - d\sigma_{-}}{d\sigma} \implies fPA_{UL} = \frac{N_{+}/L_{+}\Omega_{+} - N_{-}/L_{-}\Omega_{-}}{N/L\Omega} \quad (96)$$

We can then define the following probability distributions

$$p_{\pm} = \frac{N_{\pm}}{N} = \mu_{\pm} (1 \pm fPA_{LU}), \quad (97)$$

where $\mu_{\pm} = L_{\pm}\Omega_{\pm}/2L\Omega$ represents a normalization factor.

Both the numerator and denominator of A_{UL} expand in terms of structure functions, each modulated by functions of ϕ_h , ϕ_R , and θ , and scaled by depolarization factors $k(\varepsilon, y)$. For the unpolarized differential cross section in the denominator, in practice one integrates it to obtain the total cross section; this assumes that the modulations of the unpolarized cross section are linearly independent from a constant, which is not necessarily true, however we will return to this concern later when discussing systematics. The total unpolarized cross section is then the product of the depolarization factor $k_{UU}^{\text{const}} = A(y)$ (see Appendix A) and structure function F_{UU}^{const} , which is $F_{UU,T}$ from equation 5.

Expanding the numerator in terms of modulations $\psi_i(\phi_h, \phi_R, \theta)$, we have

$$A_{UL} = \sum_i \frac{k_{UL}^{\psi_i} F_{UL}^{\psi_i}}{k_{UU}^{\text{const}} F_{UU}^{\text{const}}} \psi_i = \sum_i A_{UL}^{\psi_i} \psi_i, \quad (98)$$

where we have defined

$$A_{UL}^{\psi_i} = K_{UL}^{\psi_i} \frac{F_{UL}^{\psi_i}}{F_{UU}}, \quad (99)$$

with $K_{UL}^{\psi_i} = k_{UL}^{\psi_i}/k_{UU}^{\text{const}}$, the ratio of depolarization factors. $A_{UL}^{\psi_i}$ is the amplitude of the ψ_i modulation of A_{UL} , and it is proportional to a ratio of structure functions.

To isolate the ψ_i modulation amplitude, one can take the ψ_i moment of the numerator and all terms will vanish except for $A_{UL}^{\psi_i}$. In practice however, the modulations ψ_i may not be completely linearly independent; it is therefore more appropriate to implement a simultaneous determination of several modulation amplitudes. We have chosen to perform the simultaneous determination using an unbinned extended MLM fit, based on the probability distributions

$$p_{\pm} = \frac{N_{\pm}}{N} = \mu_{\pm} \left(1 \pm fP \sum_i A_{UL}^{\psi_i} \psi_i \right). \quad (100)$$

From here, we can proceed with an extended unbinned MLM fit, which is a standard procedure (see [160], for example). These two probability distributions, one for each target helicity, are used simultaneously to build an extended likelihood function, which depends on the asymmetry amplitudes and kinematics (independent variables), as well as the normalization. The set of asymmetry amplitudes which maximizes the likelihood function is the result of the fit. In practice, this is a minimization problem since it is computationally favorable to minimize the negative logarithm of the likelihood.

The data over which the likelihood is minimized consist of the yields for each target helicity. This is a discrete dataset, and therefore must be binned discretely in the full phase space; however, in the *unbinned* limit, the bins are taken to be small enough such that only 0 or 1 event is present in each bin. Finally, the independent normalizations of the two probability densities are allowed to float, which can compensate for any difference in the luminosities from the two target helicities; for this reason, the likelihood fit is called *extended*.

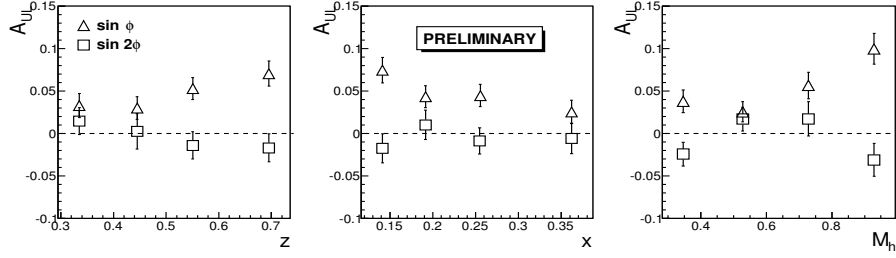


FIG. 16. CLAS6 preliminary target spin asymmetries [3].

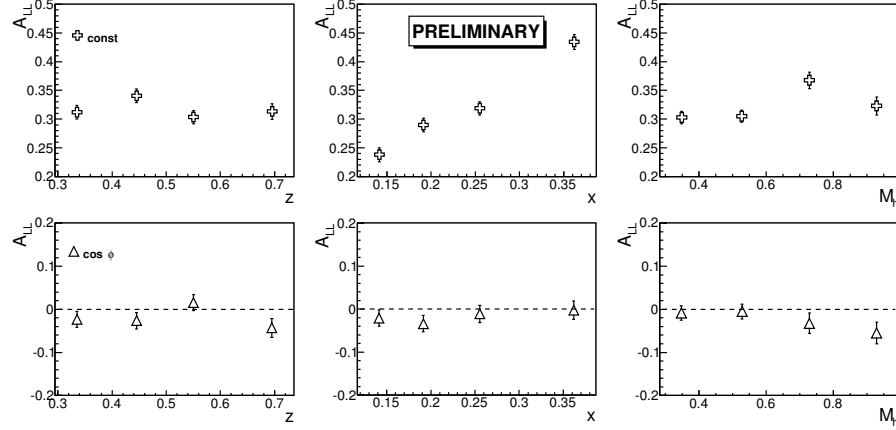


FIG. 17. CLAS6 preliminary double spin asymmetries [3].

VI. Expected results

Before discussing the expected results and projections, it is useful to review the current data on SIDIS dihadron spin asymmetries.

A. Existing data on target spin and double spin asymmetries

Preliminary data from CLAS [3] at 6 GeV indicate large azimuthal $\sin \phi_R$ moments both for unpolarized and polarized targets; the target spin asymmetry shown in figure 16, the open-triangle points, is sensitive to the collinear twist-3 PDF $h_L(x)$. An additional moment, $\sin(2\phi_R)$, is included in the figure and is consistent with zero; this modulation is of the twist-2 structure function, which includes a convolution of the wormgear distribution h_{1L}^\perp and the IFF $H_{1,TT}^\perp$. Figure 17 shows the double spin asymmetries, where the constant modulation is sensitive to $g_1 D_1$ and the $\cos \phi_R$ modulation is sensitive to $g_1 \tilde{D}$, where \tilde{D} is a twist-3 DiFF; these results indicate that \tilde{D} is at least an order of magnitude smaller than D_1 .

COMPASS also measured various modulations of the target spin and double spin asymmetries in dihadron production from inelastic scattering of muons on a polarized solid ammonia target [4]. Figure 18 shows the average asymmetry amplitudes for a variety of modulations. The $\sin(\phi_h - \phi_R)$ amplitude of the target spin asymmetry, sensitive to the helicity distribution convolved with G_1^\perp , is consistent with zero even when binned in M_h , although with these uncertainties it is not inconsistent with the spectator model prediction from [129] that was shown in figure 9. The amplitude $A_{UL}^{\sin \phi_R}$ shows a slight rise as a function of x and of z , up to about 1%; this is at a lower x range than what was shown from CLAS6 in figure 16. The other target spin asymmetries correspond to structure functions which involve the wormgear distribution, or higher order partial waves, and are all consistent with or close to zero, as are the double spin asymmetries.

HERMES measured transverse target spin asymmetries [69], sensitive to the transversity $h_1(x)$ and the IFF H_1^\perp , and with measurements by Belle [61], can be used to extract the transversity distribution from

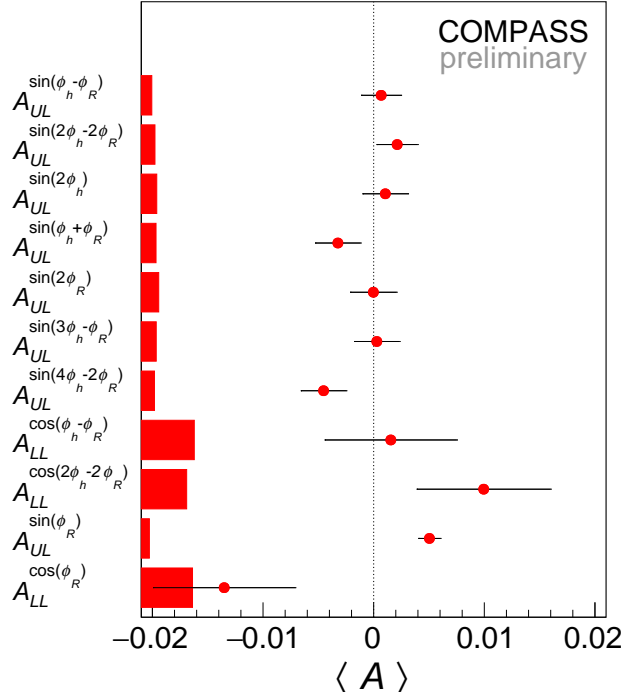


FIG. 18. COMPASS preliminary target spin and double spin asymmetries [4]

680 SIDIS data. Significant asymmetries were observed, and a future program with a transversely polarized
 681 target at CLAS12 as well as the EIC can help improve and extend these measurements.

682 B. Preliminary CLAS12 dihadron beam spin asymmetries

683 CLAS12 recently released a preliminary measurement of the dihadron beam spin asymmetries, shown in
 684 figure 19 [161, 162]. The blue triangles show the $\sin \phi_R$ amplitude which is sensitive to the collinear twist-3
 685 PDF $e(x)$ and shows a rise in M_h to about 4%. The $\sin(\phi_h - \phi_R)$ modulation is sensitive to the helicity
 686 DiFF G_1^\perp , convolved with the unpolarized PDF $f_1(x)$, and exhibits a clear sign change near the ρ -meson
 687 mass, somewhat similar to the spectator model from figure 9. The spectator model prediction [129] was
 688 for the target spin asymmetry, which involves the helicity distribution instead of $f_1(x)$; since $g(x) < f_1(x)$,
 689 it is natural to assume their prediction for the beam spin asymmetry is larger in magnitude, and possibly
 690 consistent with these preliminary results. Finally, the $\sin \phi_h$ modulation is included as well, because it turns
 691 out that all three amplitudes are linearly dependent and must be fit altogether simultaneously.

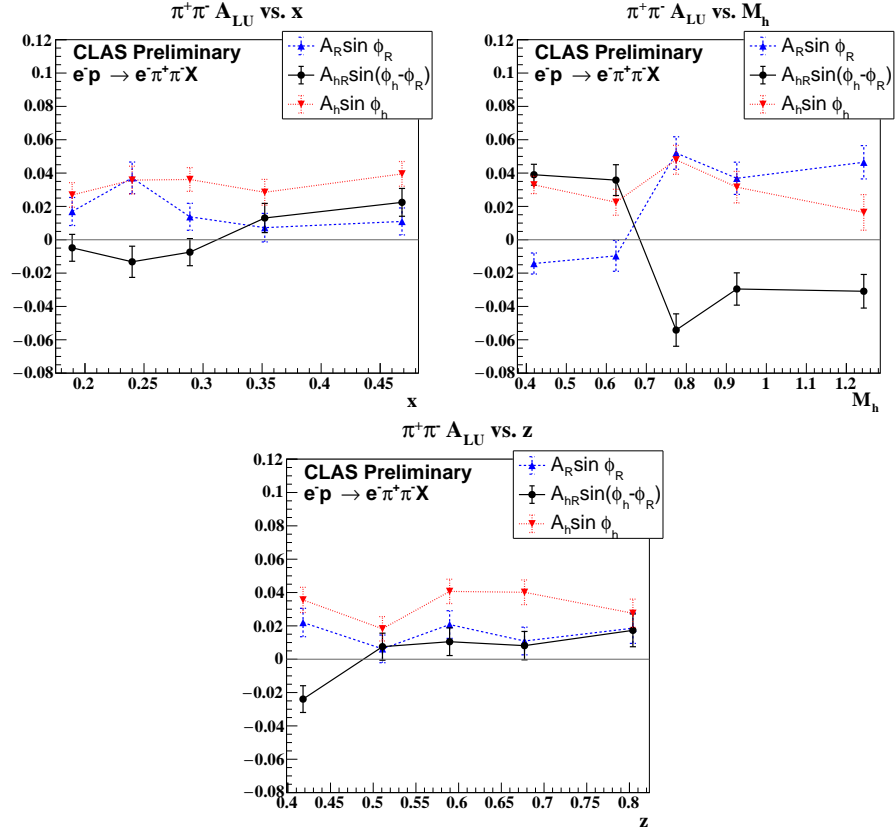


FIG. 19. CLAS12 preliminary results for the beam spin asymmetry. From [161].

C. Statistical projections for this proposal

Table IV shows a summary of beam spin, target spin, and double spin asymmetries, along with the primary physics goal, which is a PDF or a DiFF. Shown additionally are the corresponding kinematic depolarization ratios $K(y, \varepsilon)$, which depend on y and ε from equation 3 (see appendix A for definitions), along with their average values based on present CLAS12 data, taken by Run Group A. In the following statistical projections of target spin and double spin asymmetries, we base our predicted statistical uncertainty on the assumption of running on NH_3 and ND_3 targets [163] with 50% efficiency; however, more days on ND_3 than NH_3 would ensure that both have the same statistical error at large P_T and optimizes the error on extracted $h_L^{u,d}$. We also include projections for a ^3He target, which is also part of a proposal to PAC48.

Asymmetry	Modulation	Physics Goal	Depolarization Ratio $K(\varepsilon, y)$	$\langle K(\varepsilon, y) \rangle$
A_{LU}	$\sin(\phi_R)$	$e(x)$	W/A	0.7
	$\sin(\phi_h - \phi_R)$	G_1^\perp	C/A	0.8
A_{UL}	$\sin(\phi_R)$	$h_L(x)$	V/A	1.3
	$\sin(\phi_h - \phi_R)$	G_1^\perp	A/A	1
	$\sin(\phi_h + \phi_R)$	h_{1L}^\perp	B/A	0.6
A_{LL}	$\cos(m\phi_h - m\phi_R)$	$D_1^{\langle \ell, m \rangle}$	C/A	0.8
	$\cos(\phi_h + \phi_R)$	\tilde{D}	W/A	0.7

TABLE IV. Table of beam spin, target spin, and double spin asymmetries, and corresponding physics goals

The presented estimated statistical projections are based on effectively running 60, 90, and 120 days, assuming 50% efficiency of running. In principle one could use the fast Monte Carlo to extrapolate asymmetry projections (see appendix C), however given that we have plenty of data from Run Group A, it is simpler and more accurate to extrapolate dihadron yields from the data rate. By counting the number of dihadrons which pass all event selection criteria and a selection of Run Group A data with minimal downtime, we estimate a rate of 5.1 Hz for dihadron acquisition.

In addition to the extrapolated dihadron yield, the polarization and dilution factors are also needed. Table V shows the targets along with mean dilution and polarization factors. Dilution factors for each target, estimated with the Monte Carlo, are shown in figures 20-22. While there is some mild kinematic dependence, we have elected to use the average values of the dilution factors in table V for the statistical projections shown below. Lastly, for projections of the double spin asymmetries, a beam polarization of 0.8 is assumed.

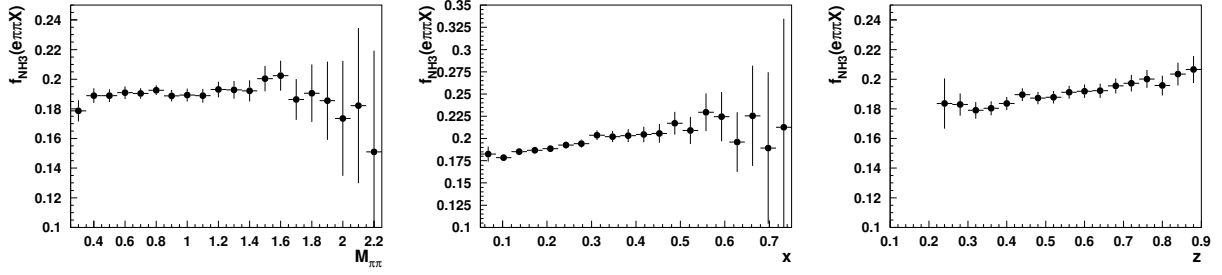
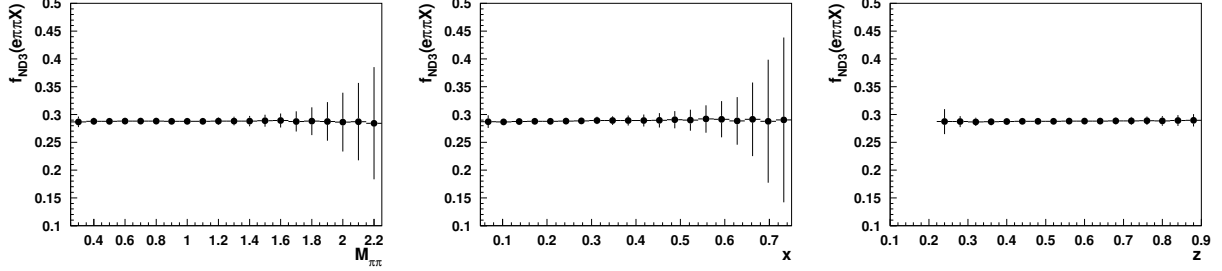
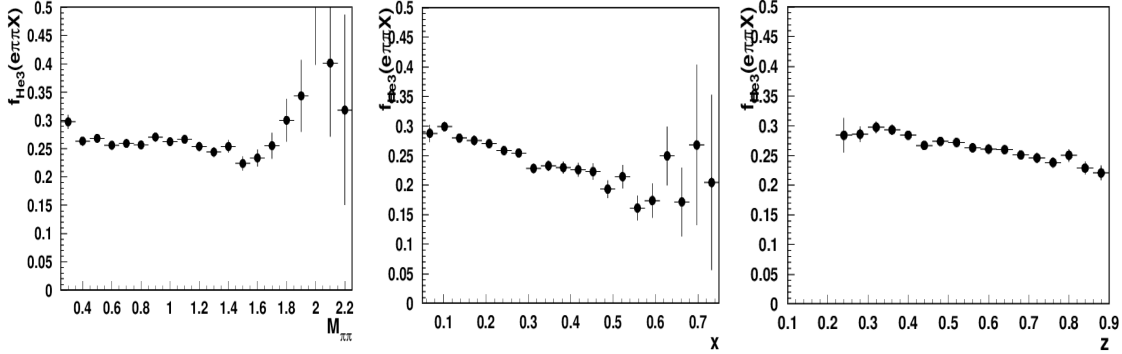
Target	Dilution f	Polarization P
NH_3	0.2	0.85
ND_3	0.285	0.35
^3He	0.27	0.5

TABLE V. Targets along with estimated averages of dilution and polarization.

The ^3He target from [147], also submitted to PAC48, is included as well. Since the goals of measuring dihadrons from the ND_3 target match those from the ^3He target, we include additional statistical projections for ^3He here for convenient comparison.

In order to estimate the magnitudes of the expected target spin asymmetries, we make use of the CLAS12 preliminary results on the beam spin asymmetries from a proton (p) target, denoted A_{LU}^p , and mean kinematic depolarization factors from the data. Note that while it is possible to measure a beam spin asymmetry in the proposed experimental configuration, it is not the priority. Nonetheless, it may be interesting to at least take a preliminary look at the beam spin asymmetry for the different targets.

First we discuss $A_{UL}^{\sin \phi_R}$, which is sensitive to $h_L(x)$. We first assume that for the unpolarized PDFs, $f^d(x) = 0.4f^u(x)$. Since some models claim $h_L^u(x)$ will be a bit larger than $e^u(x)$, whereas others claim the opposite, we make the assumption that $h_L^u(x) \approx e^u(x)$. We also make the assumption that $e^d(x)$ can range between 0 and $e^u(x)$, which is motivated by the existing models. The remaining freedom is in the ratio $R := h_L^d(x)/h_L^u(x)$. Models suggest that R is likely small, and the asymmetries with the smallest

FIG. 20. NH_3 dilution factors versus M_h , x , and z FIG. 21. ND_3 dilution factors versus M_h , x , and z FIG. 22. ^3He dilution factors versus M_h , x , and z

magnitudes occur when $|R| < 0.25$, so we will consider this range for our projections. For a proton target, the value of A_{UL}^p is approximately twice the value of A_{LU}^p , for all values of R in the range. For neutrons (n), however, A_{UL}^n is zero for $R = 0.25$, approximately equal to A_{LU}^p for $R = 0$, and approximately twice A_{LU}^p for $R = -0.25$; if $R > 0.25$, then A_{UL}^n will have the opposite sign as A_{LU}^p . We therefore have chosen to plot the projections along a polynomial curve which fits the CLAS12 preliminary data on $k \cdot A_{LU}^p$, where $k = 2$ for the A_{UL}^p projection and $k = 1$ for A_{UL}^n . Figure 23 shows the resulting projections.

For the other primary target spin asymmetry modulation, $A_{UL}^{\sin(\phi_h - \phi_R)}$, the ratio of $A_{UL}^{p,n}$ to A_{LU}^p depends on the ratio of the helicity PDF to the unpolarized PDF. We find that, for approximate values of these PDFs taken at $x \sim 0.3$, $A_{UL}^p \approx 0.4A_{LU}^p$ and $A_{UL}^n \approx -0.05A_{LU}^p$. The smaller target spin asymmetry, relative to the beam spin asymmetry, is compatible with the recent spectator model predictions [129], so we have therefore decided to draw the prediction for A_{UL}^p along a curve which approximates the spectator model prediction. On the other hand, the prediction for A_{UL}^n will likely be too small to be statistically discernible from zero, so its projection is omitted.

Fig 24 shows the projection for $A_{UL}^{\sin(\phi_h - \phi_R)}$ with a proton target. The data points are positioned along

a curve which approximately follows the spectator model prediction [129]⁷. The run time with 30 days is shown in the left panel, but with an expected maximum amplitude of 1%, the signal will not be sufficiently significant; the right panel shows a comparison for 90 days of running with no downtime.

Figure 25 shows A_{LL} for the $\cos\phi_R$ modulation, which is sensitive to the twist-3 TMD PDF e_L convolved with the IFF H_1^Δ , summed with the helicity $g_1(x)$ convolved with the twist-3 DiFF \tilde{D} . Since e_L is not collinear, it will vanish under an integral over the quark transverse momentum, thus a measurement of this asymmetry can constrain the twist-3 DiFF \tilde{D} . Measurements of the collinear twist-3 PDFs $e(x)$ and $h_L(x)$ include an additional term involving the twist-3 DiFF \tilde{G} , which is thought to be smaller than \tilde{D} . Thus a constraint on \tilde{D} can in turn help further constrain $e(x)$ and $h_L(x)$. COMPASS and CLAS6 measurements of this asymmetry were consistent with zero, so the projected points are also set to zero [3, 4].

The numerical values for these projections are given in tables VI-XII. The first and second columns give the bins in which the asymmetries are shown, written as the bin range and mean. In all projections, the bin boundaries are chosen as quantiles. The third column is the value of the asymmetry, and the remaining columns give its projected statistical uncertainty, assuming 60, 90, and 120 days, with 50% efficiency of running.

Although we have not prepared projections for the DSIDIS process, we again remark that careful studies of the separation of the current and target fragmentation regions are needed. As a first step toward this separation, we can compare the ratio of the number of dihadrons where one hadron has $x_F < 0$ with the other having $x_F > 0$, to the number of current fragmentation region dihadrons, where both hadrons have $x_F > 0$. In Run Group A data the ratio is approximately 15% or 5% for $\pi^+\pi^-$ dihadrons, and it depends on which hadron is associated with which x_F cut. Thus the estimated statistical uncertainty of DSIDIS asymmetries may be a factor of 2–4 times larger than those presented in figures 23–25. If the asymmetries are not large, then at least a measurement of DSIDIS asymmetries could provide upper bounds and still constrain the fracture functions.

⁷ Although these predictions are for COMPASS and EIC energies, the dependence of the model on \sqrt{s} appears to be negligible.

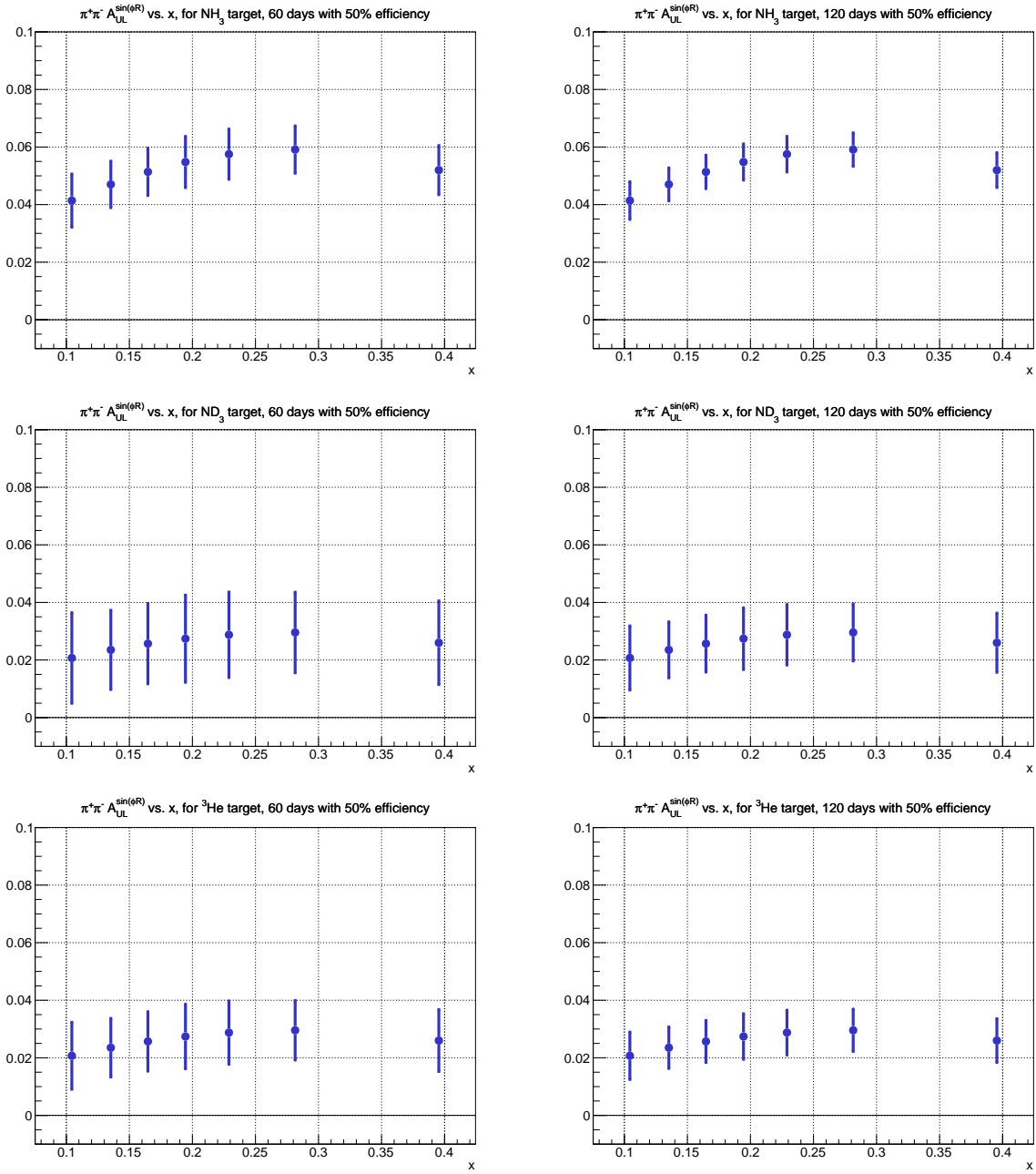


FIG. 23. Projection of the $\sin \phi_R$ modulation of A_{UL} , versus x , for 60 days (left column) and for 120 days (right column). Three targets are shown: NH₃ (top row), ND₃ (middle row), and ³He (bottom row). See text for details.

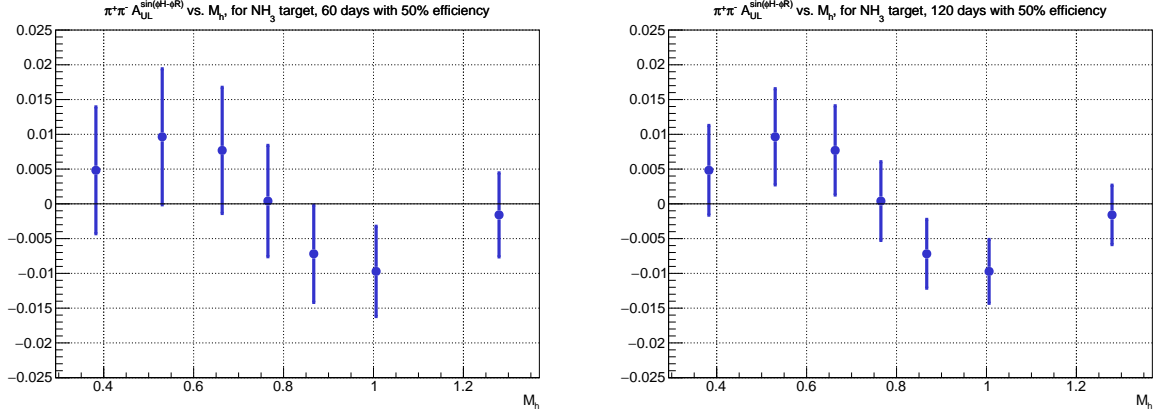


FIG. 24. Projection of the $\sin(\phi_h - \phi_R)$ modulation of A_{UL} with the NH_3 target, versus x , for 60 days (left) and for 120 days (right). See text for details.

x range	$\langle x \rangle$	A_{UL}	60 days σ	90 days σ	120 days σ
[0.00, 0.12)	0.1	0.041	0.0092	0.0075	0.0065
[0.12, 0.15)	0.14	0.047	0.0081	0.0066	0.0057
[0.15, 0.18)	0.16	0.051	0.0082	0.0067	0.0058
[0.18, 0.21)	0.19	0.055	0.0089	0.0072	0.0063
[0.21, 0.25)	0.23	0.058	0.0087	0.0071	0.0062
[0.25, 0.32)	0.28	0.059	0.0082	0.0067	0.0058
[0.32, 1.00)	0.4	0.052	0.0085	0.007	0.006

TABLE VI. Data table for projection of $A_{UL}^{\sin \phi_R}$ in bins of x , for the NH_3 target. See figure 23, top row.

x range	$\langle x \rangle$	A_{UL}	60 days σ	90 days σ	120 days σ
[0.00, 0.12)	0.1	0.021	0.016	0.013	0.011
[0.12, 0.15)	0.14	0.024	0.014	0.011	0.0097
[0.15, 0.18)	0.16	0.026	0.014	0.011	0.0099
[0.18, 0.21)	0.19	0.027	0.015	0.012	0.011
[0.21, 0.25)	0.23	0.029	0.015	0.012	0.01
[0.25, 0.32)	0.28	0.03	0.014	0.011	0.0099
[0.32, 1.00)	0.4	0.026	0.015	0.012	0.01

TABLE VII. Data table for projection of $A_{UL}^{\sin \phi_R}$ in bins of x , for the ND_3 target. See figure 23, middle row.

x range	$\langle x \rangle$	A_{UL}	60 days σ	90 days σ	120 days σ
[0.00, 0.12)	0.1	0.021	0.012	0.0095	0.0082
[0.12, 0.15)	0.14	0.024	0.01	0.0083	0.0072
[0.15, 0.18)	0.16	0.026	0.01	0.0084	0.0073
[0.18, 0.21)	0.19	0.027	0.011	0.0091	0.0079
[0.21, 0.25)	0.23	0.029	0.011	0.0089	0.0077
[0.25, 0.32)	0.28	0.03	0.01	0.0084	0.0073
[0.32, 1.00)	0.4	0.026	0.011	0.0088	0.0076

TABLE VIII. Data table for projection of $A_{UL}^{\sin \phi_R}$ in bins of x , for the ^3He target. See figure 23, bottom row.

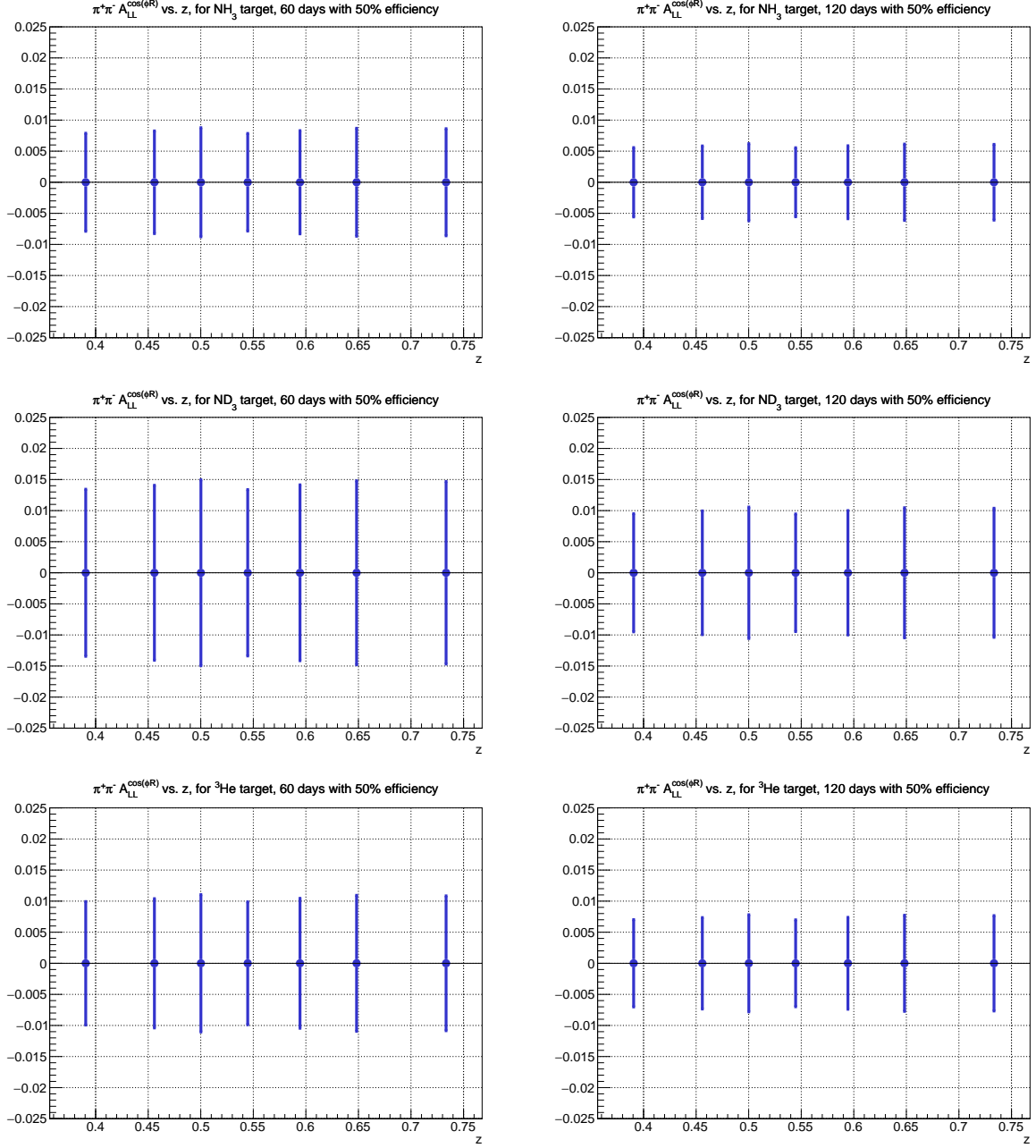


FIG. 25. Projection of the $\cos \phi_R$ modulation of A_{LL} , versus z , for 60 days (left column) and for 120 days (right column). Three targets are shown: NH_3 (top row), ND_3 (middle row), and ^3He (bottom row). See text for details.

M_h range	$\langle M_h \rangle$	A_{UL}	60 days σ	90 days σ	120 days σ
[0.00, 0.46)	0.38	0.0048	0.0091	0.0074	0.0064
[0.46, 0.60)	0.53	0.0096	0.0098	0.008	0.0069
[0.60, 0.72)	0.66	0.0077	0.0091	0.0074	0.0064
[0.72, 0.81)	0.77	0.0004	0.008	0.0065	0.0057
[0.81, 0.93)	0.87	-0.0072	0.007	0.0057	0.0049
[0.93, 1.10)	1	-0.0097	0.0065	0.0053	0.0046
[1.10, 3.00)	1.3	-0.0016	0.006	0.0049	0.0043

TABLE IX. Data table for projection of $A_{UL}^{\sin(\phi_h - \phi_R)}$ in bins of M_h , for the NH_3 target. See figure 24.

z range	$\langle z \rangle$	A_{LL}	60 days σ	90 days σ	120 days σ
[0.00, 0.43)	0.39	0	0.0079	0.0064	0.0056
[0.43, 0.48)	0.46	0	0.0083	0.0067	0.0058
[0.48, 0.52)	0.5	0	0.0088	0.0072	0.0062
[0.52, 0.57)	0.54	0	0.0079	0.0064	0.0056
[0.57, 0.62)	0.59	0	0.0083	0.0068	0.0059
[0.62, 0.68)	0.65	0	0.0087	0.0071	0.0061
[0.68, 1.00)	0.73	0	0.0086	0.007	0.0061

TABLE X. Data table for projection of $A_{LL}^{\cos \phi_R}$ in bins of z , for the NH_3 target. See figure 25, top row.

z range	$\langle z \rangle$	A_{LL}	60 days σ	90 days σ	120 days σ
[0.00, 0.43)	0.39	0	0.013	0.011	0.0095
[0.43, 0.48)	0.46	0	0.014	0.011	0.01
[0.48, 0.52)	0.5	0	0.015	0.012	0.011
[0.52, 0.57)	0.54	0	0.013	0.011	0.0095
[0.57, 0.62)	0.59	0	0.014	0.012	0.01
[0.62, 0.68)	0.65	0	0.015	0.012	0.01
[0.68, 1.00)	0.73	0	0.015	0.012	0.01

TABLE XI. Data table for projection of $A_{LL}^{\cos \phi_R}$ in bins of z , for the ND_3 target. See figure 25, middle row.

z range	$\langle z \rangle$	A_{LL}	60 days σ	90 days σ	120 days σ
[0.00, 0.43)	0.39	0	0.0099	0.0081	0.007
[0.43, 0.48)	0.46	0	0.01	0.0085	0.0074
[0.48, 0.52)	0.5	0	0.011	0.009	0.0078
[0.52, 0.57)	0.54	0	0.0099	0.0081	0.007
[0.57, 0.62)	0.59	0	0.01	0.0085	0.0074
[0.62, 0.68)	0.65	0	0.011	0.0089	0.0077
[0.68, 1.00)	0.73	0	0.011	0.0089	0.0077

TABLE XII. Data table for projection of $A_{LL}^{\cos \phi_R}$ in bins of z , for the ^3He target. See figure 25, bottom row.

Systematic Uncertainty Contributor	A_{LU}	A_{UL}	A_{LL}
beam polarization	3%	-	3%
target polarization	-	3%	3%
dilution factor	-	4%	4%
transverse (to γ^*) spin effects	-	3%	3%
radiative corrections	3%	3%	3%
acceptance	20%	20%	20%
baryonic resonances	14%	14%	14%
higher order partial waves of σ_{UU}	10%	10%	10%

TABLE XIII. Uncertainties for asymmetry measurements.

D. Systematic Uncertainty

The proposed spin asymmetry measurements are rather insensitive to uncertainties in acceptances and charge normalization, since those are independent of helicity and cancel in a ratio of cross sections. There are systematic uncertainty contributions that do impact the asymmetry magnitude, however, as listed in Table XIII. The numbers listed are rough estimates, based on past measurements and experience such as HERMES [69], and on present experience with CLAS6 and CLAS12 beam spin asymmetries; for a more accurate determination of a systematic uncertainty, careful analysis of the dataset is needed.

The uncertainty on the target polarization contributes to a systematic uncertainty on the scale of target spin asymmetries, and double spin asymmetries receive an additional systematic uncertainty contribution from the beam polarization uncertainty. The uncertainty on the dilution factor also contributes, along with the ratio of the longitudinal to transverse photo-absorption cross section. The other uncertainties require more thorough study to understand, and many require the data to be acquired. We attempted to estimate each, based on current studies on CLAS6 [159] and CLAS12 beam spin asymmetries and on studies from other similar previous experiments, such as HERMES [69]; however, these numbers only serve as an illustration of what the overall uncertainty might be.

Uncertainty from radiative corrections originate from correcting for QED effects. The acceptance contribution can be obtained by comparisons of data and Monte Carlo. Some dihadrons can come from baryonic resonances, which if one chooses to subtract them out of the asymmetry as a background contribution, can result in an asymmetry with a different scale. Lastly, dihadrons from vector meson decays can in-turn contribute to higher order partial waves of the unpolarized dihadron fragmentation function.

With these estimates, the quadrature sum gives a total systematic uncertainty on the asymmetry scale of about 27% (if we exclude the contribution from baryonic resonances, the total is 23%). For an asymmetry of 0.02, the systematic uncertainty is ± 0.005 ; the binning used in the above projections gives statistical uncertainties of $\sim 1\%$, which is still larger than the systematic uncertainty, but does present itself as approaching a limit to how finely the measurement can be binned, either one-dimensionally or multi-dimensionally.

VII. Summary and Request

Detailed measurements of target spin and double spin asymmetries as a function of relevant kinematical variables in different bins in x, z, Q^2 combined with measurements of single-pion and single-kaon measurements [8, 10] will allow study of the underlying distributions and fragmentation processes. The use of different polarized targets, such as NH_3 and ND_3 , will provide access to flavor dependence, while kaon identification provided by the RICH will allow detection of pion-kaon pairs, allowing for studies of the effect of strange and non-strange sea on the flavor and spin structure of the nucleon.

In recent years, significant experimental and theoretical efforts have been made to understand QCD beyond twist-2. Twist-3 functions, describing multiparton correlations corresponding to the interference of higher Fock components in the hadron wave functions, offer fascinating insights into the nucleon structure. In particular, they describe effects of the transverse color force on quarks, along with correlations between the color magnetic field and the spin of the nucleon [13, 14].

The main goal of the proposal is to extract information on the twist-3 collinear PDFs $e(x)$ and $h_L(x)$, using the recent progress in understanding of dihadron fragmentation functions (DiFFs) and their extraction from e^+e^- data. The formalism of DiFFs is based on collinear factorization with well defined evolution equations. The plan is to gather a data set on hadron pairs produced from SIDIS in the region $0.1 \leq x \leq 0.8$, $0.5 \leq M_h \leq 1.2$, and $0.2 \leq z \leq 0.8$. Global analysis of the data will provide fits to higher twist distribution functions $e(x)$ and $h_L(x)$. Furthermore, double spin asymmetries can help establish limits on the twist-3 dihadron fragmentation functions, which in turn help with the extractions of $e(x)$ and $h_L(x)$.

The proposed experiment will provide data on subleading twist asymmetries, which offer valuable insights toward understanding why subleading twist effects appear to be larger than leading twist effects ($A_{UU}^{\cos \phi}$ was larger than $A_{UU}^{\cos 2\phi}$ [164], $A_{UL}^{\sin \phi}$ was larger than $A_{UL}^{\sin 2\phi}$ [15]). Precise data on the production of dihadrons would have an important impact, and motivate further theoretical studies. Ultimately, through a global study of all of these observables, one could simultaneously obtain better knowledge of twist-3 collinear functions and twist-2 TMDs, and at the same time test the validity of the formalism.

These data will also help constrain the helicity-dependent dihadron fragmentation function G_1^\perp , along with its partial waves. G_1^\perp is sensitive to spin-momentum correlations in hadronization, and may require the interference with a transversely polarized dihadron. Preliminary measurements of beam spin asymmetries at CLAS12 provide the first experimental evidence of a sizeable G_1^\perp , and additionally, indication of a possible sign change of G_1^\perp above and below the ρ -resonance mass. The proposed target spin asymmetry measurements will serve to complement the beam spin asymmetry, helping constrain G_1^\perp . Furthermore, the selection of different partial waves can also help pin down production mechanisms of dihadrons with a particular angular momentum, such as those from ρ -meson decays. In particular, partial waves of the unpolarized dihadron fragmentation function are also accessible, via double spin asymmetry measurements.

Another interesting topic of exploration is dihadrons with one hadron produced in the current fragmentation region and the other in the target fragmentation region. This process is known as Double SIDIS [134], and is sensitive to the fracture functions, which describe the probability of the production of a hadron in the target fragmentation region, on the condition that a quark in the target was struck and later fragments into additional hadrons. The large acceptance at CLAS allows for the unique opportunity for this measurement.

The proposed set of measurements with longitudinally polarized proton and deuteron targets will yield a comprehensive set of azimuthal moments in spin-dependent and independent SIDIS, providing access to corresponding distribution and fragmentation functions in a wide range of x, Q^2, z , and M_h . Our data, combined with the data from HERMES, COMPASS, and Belle, will provide independent (complementary to e^+/e^-) measurements of polarized pion and kaon DiFFs and will allow a study of leading twist distributions complementary to single hadron SIDIS analyses.

To achieve this goal we request to run as a Run Group C addition, with a total of 208 days of beam time with an 11 GeV, highly polarized electron beam in Hall B with luminosity of $10^{35} \text{cm}^{-2} \text{sec}^{-1}$; the breakdown of this beam time is shown in Table XIV. Note that the PAC has approved 120 days for NH_3 and 60 days for ND_3 , however, it would be nice to have more beam time for a deuteron target, to compensate for its lower polarization. The proposed ^3He target, also submitted to PAC48, offers an additional target option for measurements with polarized neutrons; data from a ^3He target could be combined with data from ND_3 , which would greatly improve the statistical precision of asymmetries from a polarized neutron target. All of the proposed measurements in this document can be performed with a ^3He target as well. We conclude by noting that while the measurements in this proposal require a substantial commitment of beam time, we

Time	Activity
3 days	Commissioning: Beam raster set up, trigger optimization, low energy calibration runs
120 days	Production data taking on NH_3
60 days	Production data taking on ND_3
3 days (1 1/2 hours every other day)	Target anneals and/or target changes
15 days (intermittent with production data)	Calibration runs on ^{12}C and empty target
5 days	Production runs on ^{15}N
2 day (1 hour every other day – concurrent with anneals)	Möller polarimeter runs

TABLE XIV. Requested beam time broken down by activity.

843 will simultaneously take data with already approved Run Group C experiments [7–10].

Appendices

A. Depolarization Factors

The depolarization factors from Eq.2 can be written as

$$\frac{y^2}{2(1-\varepsilon)} = \frac{1}{1+\gamma^2} \left(1 - y + \frac{1}{2}y^2 + \frac{1}{4}\gamma^2 y^2\right) \approx \left(1 - y + \frac{1}{2}y^2\right) \equiv A(y), \quad (101)$$

$$\frac{y^2}{2(1-\varepsilon)} \varepsilon = \frac{1}{1+\gamma^2} \left(1 - y - \frac{1}{4}\gamma^2 y^2\right) \approx (1 - y) \equiv B(y), \quad (102)$$

$$\frac{y^2}{2(1-\varepsilon)} \sqrt{2\varepsilon(1+\varepsilon)} = \frac{1}{1+\gamma^2} (2 - y) \sqrt{1 - y - \frac{1}{4}\gamma^2 y^2} \approx (2 - y) \sqrt{1 - y} \equiv V(y), \quad (103)$$

$$\frac{y^2}{2(1-\varepsilon)} \sqrt{2\varepsilon(1-\varepsilon)} = \frac{1}{\sqrt{1+\gamma^2}} y \sqrt{1 - y - \frac{1}{4}\gamma^2 y^2} \approx y \sqrt{1 - y} \equiv W(y), \quad (104)$$

$$\frac{y^2}{2(1-\varepsilon)} \sqrt{1-\varepsilon^2} = \frac{1}{\sqrt{1+\gamma^2}} y \left(1 - \frac{1}{2}y\right) \approx y \left(1 - \frac{1}{2}y\right) \equiv C(y). \quad (105)$$

B. Convolutions

For an arbitrary function $w(\mathbf{k}, \mathbf{p})$ we introduce the notation

$$C[\hat{M} \cdot D w] = \sum_a e_a^2 \int d^2 \mathbf{k} d^2 \mathbf{p} \delta^{(2)}(z\mathbf{k} + \mathbf{p} - \mathbf{P}_{T1}) \hat{M}_a(x, \zeta, \mathbf{k}^2, \mathbf{P}_{T2}^2, \mathbf{k} \cdot \mathbf{P}_{T2}) D_a(z, \mathbf{p}^2) w, \quad (106)$$

where $\mathbf{k}, \mathbf{P}_{T1}$ and \mathbf{P}_{T2} are the two-dimensional transverse momenta of quark, hadrons 1 and 2 with respect to virtual photon momentum and \mathbf{p} is a hadron 1 transverse momentum with respect to fragmenting quark momentum. Then, using the identity for Kronecker delta-function in two-dimensional vectors space

$$(\mathbf{P}_{T1}^2 \mathbf{P}_{T2}^2 - (\mathbf{P}_{T1} \cdot \mathbf{P}_{T2})^2) \delta^{ij} = \mathbf{P}_{T2}^2 P_{T1}^i P_{T1}^j + \mathbf{P}_{T1}^2 P_{T2}^i P_{T2}^j - (\mathbf{P}_{T1} \cdot \mathbf{P}_{T2}) (P_{T1}^i P_{T2}^j + P_{T1}^j P_{T2}^i), \quad (107)$$

we have the following general tensorial decomposition over independent structures:

$$\begin{aligned} C[\hat{M} \cdot D] &= F_0^{\hat{M} \cdot D}, \\ C[\hat{M} \cdot D k^i] &= P_{T1}^i F_{k1}^{\hat{M} \cdot D} + P_{T2}^i F_{k2}^{\hat{M} \cdot D}, \\ C[\hat{M} \cdot D p^i] &= P_{T1}^i F_{p1}^{\hat{M} \cdot D} + P_{T2}^i F_{p2}^{\hat{M} \cdot D}, \\ C[\hat{M} \cdot D k^i k^j] &= P_{T1}^i P_{T1}^j F_{kk1}^{\hat{M} \cdot D} + P_{T2}^i P_{T2}^j F_{kk2}^{\hat{M} \cdot D} + \delta^{ij} F_{kk3}^{\hat{M} \cdot D}, \\ C[\hat{M} \cdot D k^i p^j] &= P_{T1}^i P_{T1}^j F_{kp1}^{\hat{M} \cdot D} + P_{T2}^i P_{T2}^j F_{kp2}^{\hat{M} \cdot D} + (P_{T1}^i P_{T2}^j - P_{T1}^j P_{T2}^i) F_{kp3}^{\hat{M} \cdot D} + \delta^{ij} F_{kp4}^{\hat{M} \cdot D}, \\ C[\hat{M} \cdot D k^i k^j p^k] &= P_{T1}^i P_{T1}^j P_{T1}^k F_{kkp1}^{\hat{M} \cdot D} + P_{T1}^i P_{T1}^j P_{T2}^k F_{kkp2}^{\hat{M} \cdot D} + P_{T2}^i P_{T2}^j P_{T2}^k F_{kkp3}^{\hat{M} \cdot D} + P_{T2}^i P_{T2}^j P_{T1}^k F_{kkp4}^{\hat{M} \cdot D} \\ &\quad + P_{T1}^k \delta^{ij} F_{kkp5}^{\hat{M} \cdot D} + P_{T2}^k \delta^{ij} F_{kkp6}^{\hat{M} \cdot D}. \end{aligned} \quad (108)$$

Note, that the functions in the r.h.s. of above equations depend on $x, z, \zeta, \mathbf{P}_{T1}^2, \mathbf{P}_{T2}^2, \mathbf{P}_{T1} \cdot \mathbf{P}_{T2}$.

From Eq.(108), after contracting by appropriate tensorial combinations, constructed from components of \mathbf{P}_{T1} and \mathbf{P}_{T2} and δ^{ij} , we can easily obtain

$$\begin{aligned} F_{k1}^{\hat{M} \cdot D} &= C \left[\hat{M} \cdot D \frac{(\mathbf{P}_{T1} \cdot \mathbf{P}_{T2})(\mathbf{P}_{T2} \cdot \mathbf{k}) - (\mathbf{P}_{T1} \cdot \mathbf{k})\mathbf{P}_{T2}^2}{(\mathbf{P}_{T1} \cdot \mathbf{P}_{T2})^2 - \mathbf{P}_{T1}^2 \mathbf{P}_{T2}^2} \right], \\ F_{k2}^{\hat{M} \cdot D} &= C \left[\hat{M} \cdot D \frac{(\mathbf{P}_{T1} \cdot \mathbf{k})(\mathbf{P}_{T1} \cdot \mathbf{P}_{T2}) - (\mathbf{P}_{T2} \cdot \mathbf{k})\mathbf{P}_{T1}^2}{(\mathbf{P}_{T1} \cdot \mathbf{P}_{T2})^2 - \mathbf{P}_{T1}^2 \mathbf{P}_{T2}^2} \right]. \end{aligned} \quad (109)$$

$$\begin{aligned}
F_{p1}^{\hat{M}\cdot D} &= C \left[\hat{M} \cdot D \frac{(\mathbf{P}_{T1} \cdot \mathbf{P}_{T2})(\mathbf{P}_{T2} \cdot \mathbf{p}) - (\mathbf{P}_{T1} \cdot \mathbf{p})\mathbf{P}_{T2}^2}{(\mathbf{P}_{T1} \cdot \mathbf{P}_{T2})^2 - \mathbf{P}_{T1}^2 \mathbf{P}_{T2}^2} \right], \\
F_{p2}^{\hat{M}\cdot D} &= C \left[\hat{M} \cdot D \frac{(\mathbf{P}_{T1} \cdot \mathbf{p})(\mathbf{P}_{T1} \cdot \mathbf{P}_{T2}) - (\mathbf{P}_{T2} \cdot \mathbf{p})\mathbf{P}_{T1}^2}{(\mathbf{P}_{T1} \cdot \mathbf{P}_{T2})^2 - \mathbf{P}_{T1}^2 \mathbf{P}_{T2}^2} \right]. \tag{110}
\end{aligned}$$

$$\begin{aligned}
F_{kk1}^{\hat{M}\cdot D} &= C \left[\hat{M} \cdot D \frac{\left(-2(\mathbf{P}_{T1} \cdot \mathbf{k})^2 + \mathbf{k}^2 \mathbf{P}_{T1}^2\right) \mathbf{P}_{T2}^4 + \left(2(\mathbf{P}_{T2} \cdot \mathbf{k})^2 - \mathbf{k}^2 \mathbf{P}_{T2}^2\right) \left(2(\mathbf{P}_{T1} \cdot \mathbf{P}_{T2})^2 - \mathbf{P}_{T1}^2 \mathbf{P}_{T2}^2\right)}{4(\mathbf{P}_{T1} \cdot \mathbf{P}_{T2})^2 \left((\mathbf{P}_{T1} \cdot \mathbf{P}_{T2})^2 - \mathbf{P}_{T1}^2 \mathbf{P}_{T2}^2\right)} \right], \\
F_{kk2}^{\hat{M}\cdot D} &= C \left[\hat{M} \cdot D \frac{\left(2(\mathbf{P}_{T1} \cdot \mathbf{P}_{T2})^2 - \mathbf{P}_{T1}^2 \mathbf{P}_{T2}^2\right) (\mathbf{P}_{T1} \cdot \mathbf{k})^2 + \mathbf{P}_{T1}^2 \left(\mathbf{P}_{T1}^2 \mathbf{P}_{T2}^2 - (\mathbf{P}_{T1} \cdot \mathbf{P}_{T2})^2\right) \mathbf{k}^2 - (\mathbf{P}_{T2} \cdot \mathbf{k})^2 \mathbf{P}_{T1}^4}{2(\mathbf{P}_{T1} \cdot \mathbf{P}_{T2})^2 \left((\mathbf{P}_{T1} \cdot \mathbf{P}_{T2})^2 - \mathbf{P}_{T1}^2 \mathbf{P}_{T2}^2\right)} \right], \\
F_{kk3}^{\hat{M}\cdot D} &= C \left[\hat{M} \cdot D \frac{\left((\mathbf{P}_{T1} \cdot \mathbf{P}_{T2})^2 + \mathbf{P}_{T1}^2 \mathbf{P}_{T2}^2\right) \mathbf{k}^2 - (\mathbf{P}_{T2} \cdot \mathbf{k})^2 \mathbf{P}_{T1}^2 - (\mathbf{P}_{T1} \cdot \mathbf{k})^2 \mathbf{P}_{T2}^2}{2(\mathbf{P}_{T1} \cdot \mathbf{P}_{T2})^2} \right]. \tag{111}
\end{aligned}$$

$$\begin{aligned}
F_{kp1}^{\hat{M}\cdot D} &= C \left[\hat{M} \cdot D \left(\frac{(-2(\mathbf{P}_{T1} \cdot \mathbf{k})(\mathbf{P}_{T1} \cdot \mathbf{p}) + (\mathbf{k} \cdot \mathbf{p})\mathbf{P}_{T1}^2) \mathbf{P}_{T2}^4}{4(\mathbf{P}_{T1} \cdot \mathbf{P}_{T2})^2 \left((\mathbf{P}_{T1} \cdot \mathbf{P}_{T2})^4 - \mathbf{P}_{T1}^2 \mathbf{P}_{T2}^2\right)} + \right. \\
&\quad \left. \frac{(2(\mathbf{P}_{T2} \cdot \mathbf{k})(\mathbf{P}_{T2} \cdot \mathbf{p}) - (\mathbf{k} \cdot \mathbf{p})\mathbf{P}_{T2}^2) \left(2(\mathbf{P}_{T1} \cdot \mathbf{P}_{T2})^2 - \mathbf{P}_{T1}^2 \mathbf{P}_{T2}^2\right)}{4(\mathbf{P}_{T1} \cdot \mathbf{P}_{T2})^2 \left((\mathbf{P}_{T1} \cdot \mathbf{P}_{T2})^4 - \mathbf{P}_{T1}^2 \mathbf{P}_{T2}^2\right)} \right), \\
F_{kp2}^{\hat{M}\cdot D} &= C \left[\hat{M} \cdot D \left(\frac{(\mathbf{P}_{T1} \cdot \mathbf{k})(\mathbf{P}_{T1} \cdot \mathbf{p}) \left(2(\mathbf{P}_{T1} \cdot \mathbf{P}_{T2})^2 - \mathbf{P}_{T1}^2 \mathbf{P}_{T2}^2\right)}{2(\mathbf{P}_{T1} \cdot \mathbf{P}_{T2})^2 \left((\mathbf{P}_{T1} \cdot \mathbf{P}_{T2})^2 - \mathbf{P}_{T1}^2 \mathbf{P}_{T2}^2\right)} - \right. \\
&\quad \left. \frac{(\mathbf{P}_{T2} \cdot \mathbf{k})(\mathbf{P}_{T2} \cdot \mathbf{p}) \mathbf{P}_{T1}^4 + (\mathbf{k} \cdot \mathbf{p}) \mathbf{P}_{T1}^2 \left(\mathbf{P}_{T1}^2 \mathbf{P}_{T2}^2 - (\mathbf{P}_{T1} \cdot \mathbf{P}_{T2})^2\right)}{2(\mathbf{P}_{T1} \cdot \mathbf{P}_{T2})^2 \left((\mathbf{P}_{T1} \cdot \mathbf{P}_{T2})^2 - \mathbf{P}_{T1}^2 \mathbf{P}_{T2}^2\right)} \right), \\
F_{kp3}^{\hat{M}\cdot D} &= C \left[\hat{M} \cdot D \frac{(\mathbf{P}_{T1} \cdot \mathbf{k})(\mathbf{P}_{T2} \cdot \mathbf{p}) - (\mathbf{P}_{T1} \cdot \mathbf{p})(\mathbf{P}_{T2} \cdot \mathbf{k})}{2 \left(\mathbf{P}_{T1}^2 \mathbf{P}_{T2}^2 - (\mathbf{P}_{T1} \cdot \mathbf{P}_{T2})^2\right)} \right], \\
F_{kp4}^{\hat{M}\cdot D} &= C \left[\hat{M} \cdot D \frac{(\mathbf{k} \cdot \mathbf{p}) \left((\mathbf{P}_{T1} \cdot \mathbf{P}_{T2})^2 + \mathbf{P}_{T1}^2 \mathbf{P}_{T2}^2\right) - (\mathbf{P}_{T2} \cdot \mathbf{k})(\mathbf{P}_{T2} \cdot \mathbf{p}) \mathbf{P}_{T1}^2 - (\mathbf{P}_{T1} \cdot \mathbf{k})(\mathbf{P}_{T1} \cdot \mathbf{p}) \mathbf{P}_{T2}^2}{2(\mathbf{P}_{T1} \cdot \mathbf{P}_{T2})^2} \right] \tag{112}
\end{aligned}$$

C. Simulation

The CLAS12 FAST-MC program was used to simulate the physics events and study the extraction of azimuthal moments and acceptance corrections. Events were generated with the clas12DIS generator [165], which is basically an implementation of the LUND Monte Carlo package called PEPSI (Polarized Electron-Proton Scattering Interactions) [166]. It is based on polarized and unpolarized parton distribution functions and the LUND string model for hadronization (both in target and current fragmentation region), and has been tested successfully against several low- Q^2 experiments with 5.7 GeV beam at Jefferson Lab.

A fast Monte Carlo simulation program has been used to define the acceptance and resolution of the CLAS12 detector with all of the standard (base) equipment in place. The kaons were assumed identified 100% in sectors covered by CLAS12-RICH, and also at energies above 5 GeV, where the pions start to fire

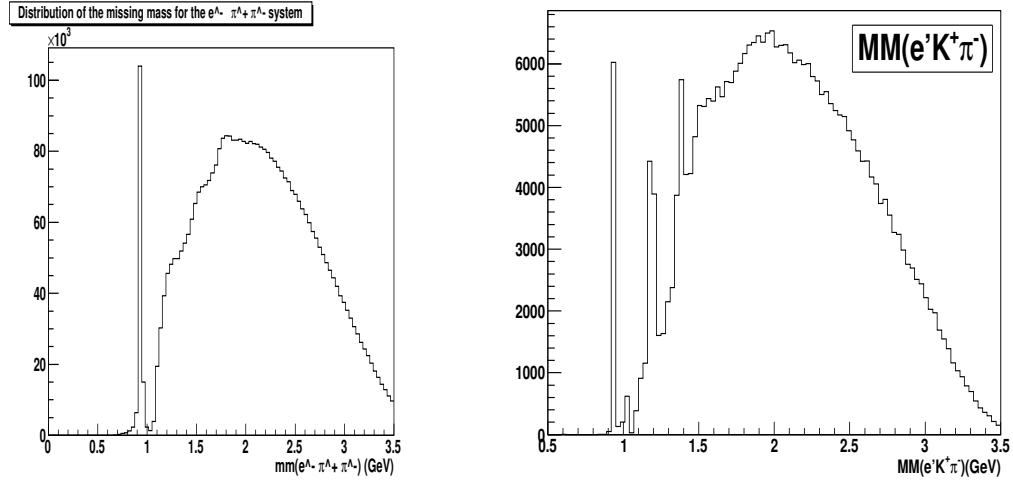


FIG. 26. Missing mass distributions for kaons and pion pairs from PEPSI MC for ehX events.

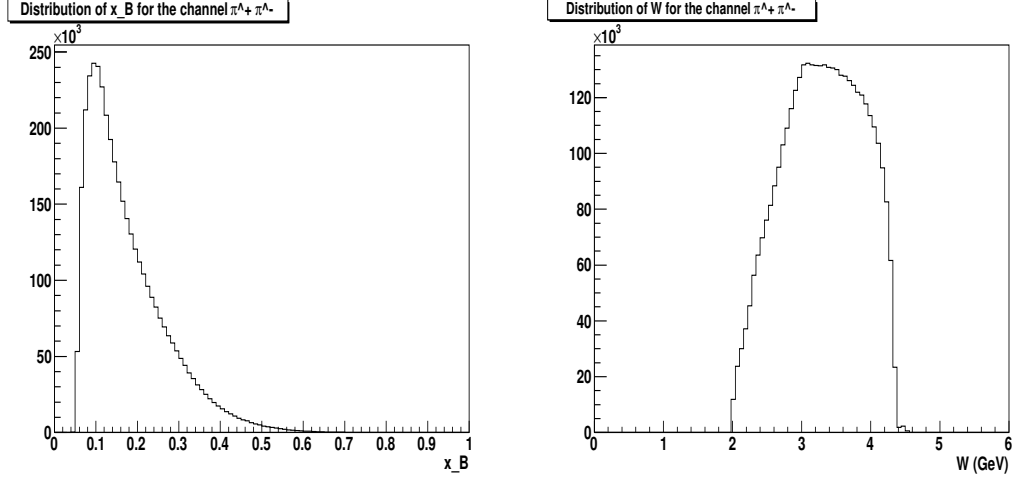
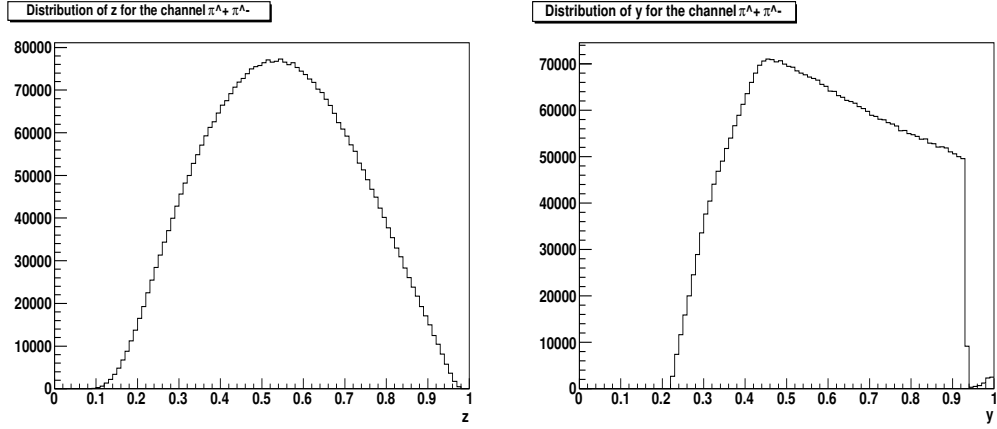
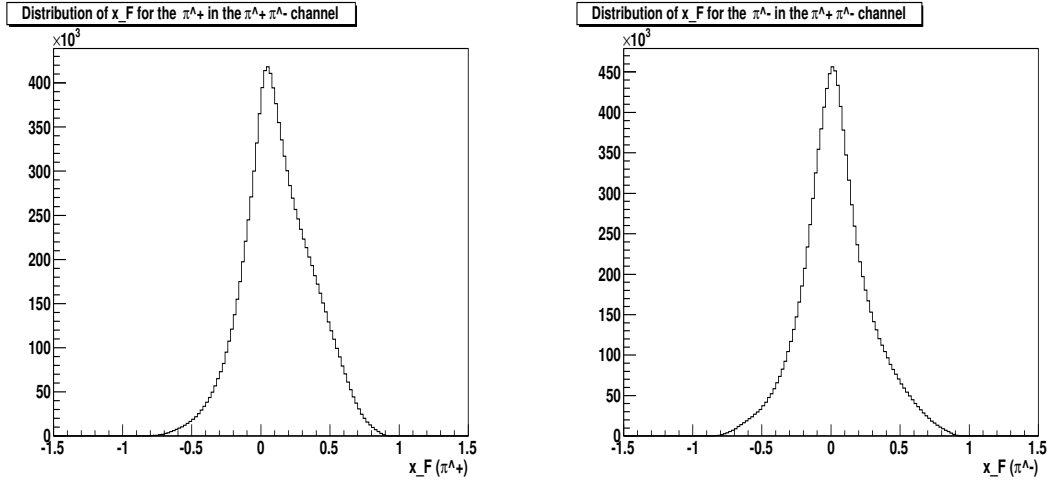
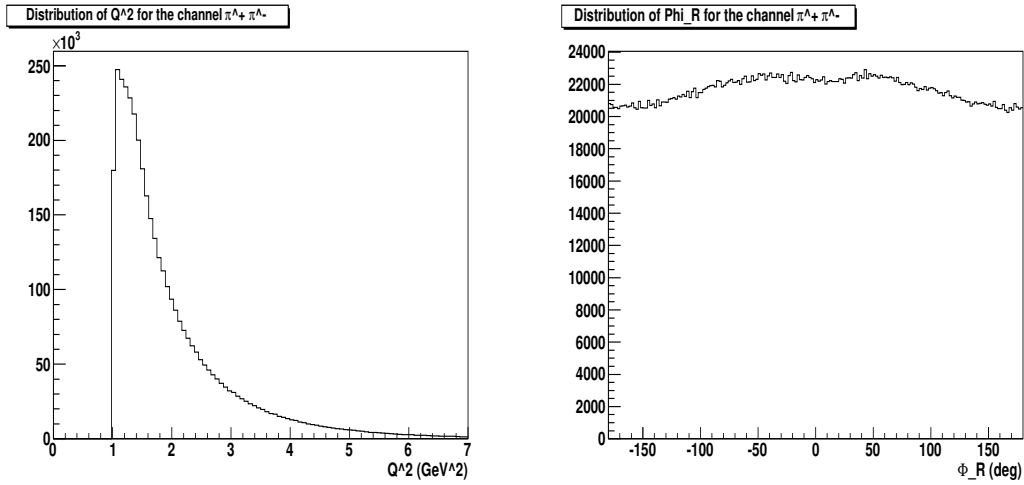


FIG. 27. x and W -distribution of pion pairs.

the High Threshold Cherekov Counter (HTCC). The events generated by clas12DIS are used as input and all particles are followed through all detector elements.

The resolution of the detector is simulated by a simple smearing function which modifies a particle's track by a random amount in momentum and angles according to a Gaussian distribution of the appropriate width. The amount of smearing follows the design specifications of the CLAS12 detector. The resolution in x varies between $0.01 < \sigma_x < 0.035$ and is therefore finer than our planned x bin size of 0.05 in all cases. Figures 26–33 show various kinematic distributions from this simulation.

A full Monte Carlo simulation (GEANT-based) of CLAS12 with all resolution effects will be used to determine the effective mean x (and Q^2) for each x -bin we will use to bin our data so we can accurately extract the x -dependence of the measured asymmetries.

FIG. 28. z and y -distributions of pion pairs.FIG. 29. x_F -distributions of π^+ (left) and π^- (right) of pion pairs.FIG. 30. The Q^2 -distribution of pion pairs (left) and the ϕ_R -distribution of the pair (right).

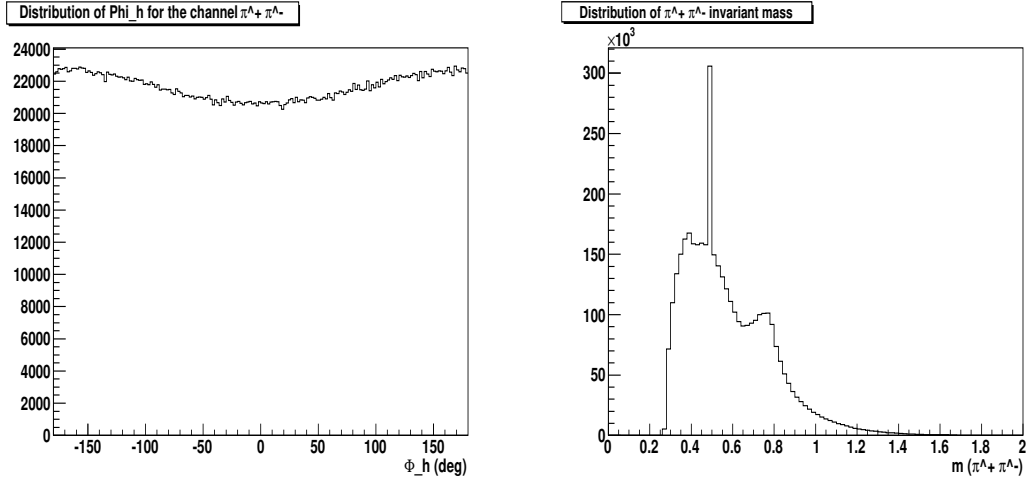


FIG. 31. The ϕ_h distribution (left) and invariant mass distributions of the pair (right).

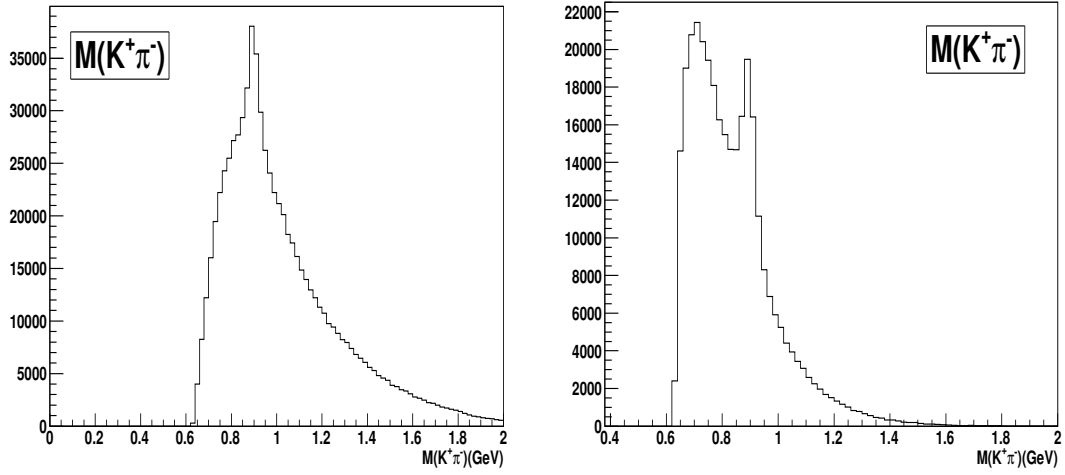


FIG. 32. Invariant masses for Kaon-pion pairs for tfr-cfr and cfr-cfr combinations

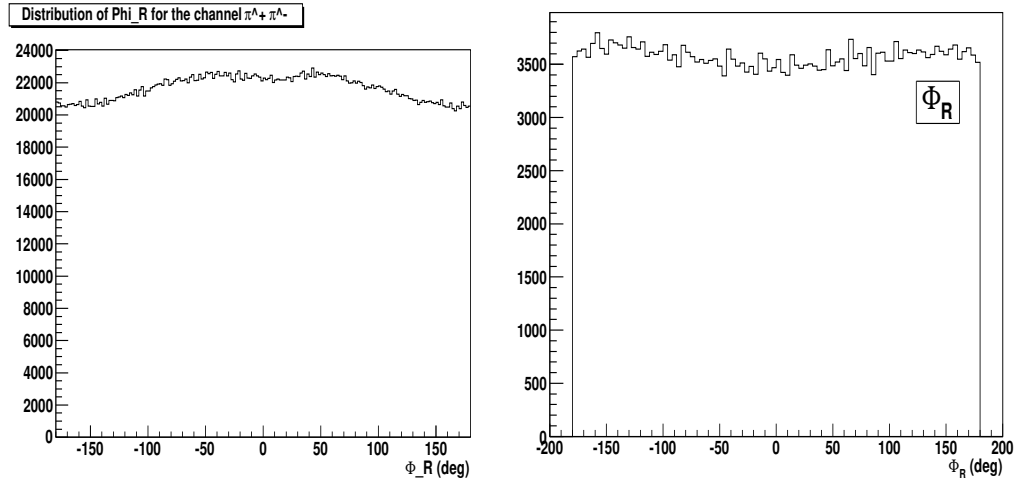


FIG. 33. Distribution over ϕ_R for pion-pion and pion-kaon pairs from FASTMC

-
- [1] C. A. Aidala, S. D. Bass, D. Hasch, and G. K. Mallot, *Rev. Mod. Phys.* **85**, 655 (2013).
- [2] A. Metz and A. Vossen, *Prog. Part. Nucl. Phys.* **91**, 136 (2016).
- [3] S. A. Pereira (CLAS), *Proceedings, 22nd International Workshop on Deep-Inelastic Scattering and Related Subjects (DIS 2014): Warsaw, Poland, April 28-May 2, 2014*, PoS **DIS2014**, 231 (2014).
- [4] S. Sirtl, in *22nd International Symposium on Spin Physics (SPIN 2016) Urbana, IL, USA, September 25-30, 2016* (2017) arXiv:1702.07317 [hep-ex].
- [5] M. Boglione, J. Collins, L. Gamberg, J. O. Gonzalez-Hernandez, T. C. Rogers, and N. Sato, *Phys. Lett.* **B766**, 245 (2017), arXiv:1611.10329 [hep-ph].
- [6] H. Avakian *et al.* (Jefferson Lab Hall B), PAC38 Proposal PR12-11-109 (2011).
- [7] S. Kuhn *et al.*, JLab Experiment E12-06-109 (2006).
- [8] H. Avakian *et al.*, JLab Experiment E12-07-107 (2007).
- [9] K. Hafidi *et al.*, JLab Experiment E12-09-007 (2009).
- [10] H. Avakian *et al.*, JLab Experiment E12-09-009 (2009).
- [11] K. Kanazawa, Y. Koike, A. Metz, D. Pitonyak, and M. Schlegel, *Phys. Rev. D* **93**, 054024 (2016), arXiv:1512.07233 [hep-ph].
- [12] R. L. Jaffe, *Comments Nucl. Part. Phys.* **19**, 239 (1990).
- [13] M. Burkardt, *Phys. Rev. D* **88**, 114502 (2013), arXiv:0810.3589 [hep-ph].
- [14] M. Abdallah and M. Burkardt, *Phys. Rev. D* **94**, 094040 (2016), arXiv:1610.01166 [hep-ph].
- [15] A. Airapetian *et al.* (HERMES), *Phys. Rev. Lett.* **84**, 4047 (2000), hep-ex/9910062.
- [16] A. Airapetian *et al.* (HERMES), *Phys. Rev.* **D64**, 097101 (2001), hep-ex/0104005.
- [17] A. Airapetian *et al.* (HERMES), *Phys. Lett.* **B622**, 14 (2005), arXiv:hep-ex/0505042.
- [18] H. Avakian *et al.* (The CLAS), *Phys. Rev. Lett.* **105**, 262002 (2010), arXiv:hep-ex/1003.4549 [hep-ex].
- [19] M. G. Alekseev *et al.*, *Eur. Phys. J.* **C70**, 39 (2010), arXiv:1007.1562 [hep-ex].
- [20] M. Anselmino and F. Murgia, *Phys. Lett.* **B483**, 74 (2000), arXiv:hep-ph/0002120.
- [21] E. De Sanctis, W. D. Nowak, and K. A. Oganessian, *Phys. Lett.* **B483**, 69 (2000), arXiv:hep-ph/0002091.
- [22] A. V. Efremov, K. Goeke, M. V. Polyakov, and D. Urbano, *Phys. Lett.* **B478**, 94 (2000), arXiv:hep-ph/0001119.
- [23] K. A. Oganessian, N. Bianchi, E. De Sanctis, and W. D. Nowak, *Nucl. Phys.* **A689**, 784 (2001), arXiv:hep-ph/0010261.
- [24] A. V. Efremov, K. Goeke, and P. Schweitzer, *Phys. Lett.* **B522**, 37 (2001), arXiv:hep-ph/0108213.
- [25] A. V. Efremov, K. Goeke, and P. Schweitzer, *Eur. Phys. J.* **C24**, 407 (2002), arXiv:hep-ph/0112166.
- [26] A. V. Efremov, K. Goeke, and P. Schweitzer, *Eur. Phys. J.* **C32**, 337 (2003), arXiv:hep-ph/0309209.
- [27] P. Schweitzer and A. Bacchetta, *Nucl. Phys.* **A732**, 106 (2004), arXiv:hep-ph/0310318.
- [28] A. V. Efremov, K. Goeke, and P. Schweitzer, *Phys. Lett.* **B568**, 63 (2003), arXiv:hep-ph/0303062.
- [29] B.-Q. Ma, I. Schmidt, and J.-J. Yang, *Phys. Rev.* **D65**, 034010 (2002), arXiv:hep-ph/0110324.
- [30] A. V. Efremov, K. Goeke, and P. Schweitzer, *Phys. Rev.* **D67**, 114014 (2003), hep-ph/0208124.
- [31] U. D'Alesio and F. Murgia, *Phys. Rev.* **D70**, 074009 (2004), arXiv:hep-ph/0408092 [hep-ph].
- [32] F. Yuan, *Phys. Lett.* **B589**, 28 (2004), hep-ph/0310279.
- [33] A. Afanasev and C. Carlson, in *8th Conference on the Intersections of Particle and Nuclear Physics* (2003) arXiv:hep-ph/0308163.
- [34] A. Bacchetta, P. J. Mulders, and F. Pijlman, *Phys. Lett.* **B595**, 309 (2004), arXiv:hep-ph/0405154.
- [35] L. P. Gamberg, D. S. Hwang, A. Metz, and M. Schlegel, *Phys. Lett.* **B639**, 508 (2006), arXiv:hep-ph/0604022.
- [36] A. Bacchetta, D. Boer, M. Diehl, and P. J. Mulders, *JHEP* **08**, 023 (2008), arXiv:hep-ph/0803.0227 [hep-ph].
- [37] R. L. Jaffe, X.-m. Jin, and J. Tang, *Phys. Rev. Lett.* **80**, 1166 (1998), arXiv:hep-ph/9709322.
- [38] A. Bianconi, S. Boffi, R. Jakob, and M. Radici, *Phys. Rev.* **D62**, 034008 (2000), arXiv:hep-ph/9907475.
- [39] M. Radici, R. Jakob, and A. Bianconi, *Phys. Rev.* **D65**, 074031 (2002), arXiv:hep-ph/0110252.
- [40] A. Bacchetta and M. Radici, *Phys. Rev.* **D67**, 094002 (2003), arXiv:hep-ph/0212300.
- [41] A. Bacchetta and M. Radici, *Phys. Rev.* **D69**, 074026 (2004), arXiv:hep-ph/0311173.
- [42] A. Bacchetta and M. Radici, *Phys. Rev.* **D74**, 114007 (2006), arXiv:hep-ph/0608037.
- [43] F. A. Ceccopieri, M. Radici, and A. Bacchetta, *Phys. Lett.* **B650**, 81 (2007), arXiv:hep-ph/0703265.
- [44] A. Bacchetta, A. Courtoy, and M. Radici, *Phys. Rev. Lett.* **107**, 012001 (2011), arXiv:1104.3855 [hep-ph].
- [45] L. Trentadue and G. Veneziano, *Phys. Lett.* **B323**, 201 (1994).
- [46] M. Anselmino, V. Barone, and A. Kotzinian, *Phys. Lett.* **B699**, 108 (2011), arXiv:1102.4214 [hep-ph].
- [47] S. Gliske, A. Bacchetta, and M. Radici, *Phys. Rev.* **D90**, 114027 (2014), [Erratum: *Phys. Rev. D* **91**, no. 1, 019902 (2015)], arXiv:1408.5721 [hep-ph].
- [48] A. Bacchetta *et al.*, *JHEP* **02**, 093 (2007), arXiv:hep-ph/0611265.
- [49] A. Bacchetta, U. D'Alesio, M. Diehl, and C. A. Miller, *Phys. Rev.* **D70**, 117504 (2004), arXiv:hep-ph/0410050.
- [50] M. Diehl and S. Sapeta, *Eur. Phys. J.* **C41**, 515 (2005), arXiv:hep-ph/0503023.
- [51] J. Zhou and A. Metz, *Phys. Rev. Lett.* **106**, 172001 (2011), arXiv:1101.3273 [hep-ph].
- [52] S. Wandzura and F. Wilczek, *Phys. Lett.* **B72**, 195 (1977).

- [53] R. Tangerman and P. Mulders, (1994), arXiv:hep-ph/9408305.
- [54] P. J. Mulders and R. D. Tangerman, Nucl. Phys. **B461**, 197 (1996), hep-ph/9510301.
- [55] H. Avakian *et al.*, Phys. Rev. **D77**, 014023 (2008), arXiv:hep-ph/0709.3253 [hep-ph].
- [56] A. Metz, P. Schweitzer, and T. Teckentrup, Phys. Lett. B **680**, 141 (2009), arXiv:0810.5212 [hep-ph].
- [57] R. L. Jaffe and X.-D. Ji, Phys. Rev. **D43**, 724 (1991).
- [58] A. Harindranath and W.-M. Zhang, Phys. Lett. **B408**, 347 (1997), arXiv:hep-ph/9706419.
- [59] R. Kundu and A. Metz, Phys. Rev. **D65**, 014009 (2002), arXiv:hep-ph/0107073.
- [60] A. Accardi, A. Bacchetta, W. Melnitchouk, and M. Schlegel, JHEP **11**, 093 (2009), arXiv:0907.2942 [hep-ph].
- [61] A. Vossen *et al.* (BELLE Collaboration), Phys.Rev.Lett. (2011), arXiv:1104.2425 [hep-ex].
- [62] W. Yang, X. Wang, Y. Yang, and Z. Lu, Phys. Rev. **D99**, 054003 (2019), arXiv:1902.07889 [hep-ph].
- [63] S. Pisano and M. Radici, Eur. Phys. J. **A52**, 155 (2016), arXiv:1511.03220 [hep-ph].
- [64] N. Christ and T. D. Lee, Phys. Rev. **143**, 1310 (1966).
- [65] J. R. Chen *et al.*, Phys. Rev. Lett. **21**, 1279 (1968).
- [66] S. Rock *et al.*, Phys. Rev. Lett. **24**, 748 (1970).
- [67] J. A. Appel *et al.*, Phys. Rev. **D1**, 1285 (1970).
- [68] M. Schlegel and A. Metz, AIP Conf. Proc. **1149**, 543 (2009), arXiv:0902.0781 [hep-ph].
- [69] A. Airapetian *et al.* (HERMES), JHEP **06**, 017 (2008), arXiv:0803.2367 [hep-ex].
- [70] A. Bianconi, S. Boffi, R. Jakob, and M. Radici, Phys. Rev. **D62**, 034009 (2000), arXiv:hep-ph/9907488.
- [71] A. Bacchetta, F. A. Ceccopieri, A. Mukherjee, and M. Radici, Phys. Rev. **D79**, 034029 (2009), arXiv:0812.0611 [hep-ph].
- [72] X. Artru and J. C. Collins, Z. Phys. **C69**, 277 (1996), arXiv:hep-ph/9504220.
- [73] P. Mulders and J. Rodrigues, in *3rd International Workshop on Diquarks and other Models of Compositeness (DIQUARKS III)* (1996) pp. 208–217, arXiv:hep-ph/9702280.
- [74] R. L. Jaffe and X.-D. Ji, Nucl. Phys. **B375**, 527 (1992).
- [75] R. L. Jaffe and X.-D. Ji, Phys. Rev. Lett. **67**, 552 (1991).
- [76] R. L. Jaffe, Phys. Rev. **D21**, 3215 (1980).
- [77] T. P. Cheng, Phys. Rev. **D38**, 2869 (1988).
- [78] S. Weinberg, Phys. Rev. Lett. **17**, 616 (1966).
- [79] T. P. Cheng and W.-K. Tung, Phys. Rev. **D3**, 733 (1971).
- [80] L. S. Brown, W. J. Pardee, and R. D. Peccei, Phys. Rev. **D4**, 2801 (1971).
- [81] J. Gasser, H. Leutwyler, and M. E. Sainio, Phys. Lett. **B253**, 252 (1991).
- [82] J. Gasser, H. Leutwyler, and M. E. Sainio, Phys. Lett. **B253**, 260 (1991).
- [83] T. Becher and H. Leutwyler, Eur. Phys. J. **C9**, 643 (1999), arXiv:hep-ph/9901384.
- [84] J. Gasser, H. Leutwyler, and M. Sainio, in *Pion-Nucleon Physics and the Structure of the Nucleon* (1991) pp. 56–57.
- [85] M. M. Pavan, I. I. Strakovsky, R. L. Workman, and R. A. Arndt, PiN Newslett. **16**, 110 (2002), arXiv:hep-ph/0111066.
- [86] M. G. Olsson and W. B. Kaufmann, PiN Newslett. **16**, 382 (2002).
- [87] J. Gasser, Ann. Phys. **136**, 62 (1981).
- [88] J. Gasser and H. Leutwyler, Phys. Rept. **87**, 77 (1982).
- [89] X.-D. Ji, Phys. Rev. Lett. **74**, 1071 (1995), arXiv:hep-ph/9410274.
- [90] S. J. Dong, J. F. Lagae, and K. F. Liu, Phys. Rev. **D54**, 5496 (1996), arXiv:hep-ph/9602259.
- [91] H. Hellmann, *Einführung in die Quantenchemie* (1937).
- [92] R. P. Feynman, Phys. Rev. **56** (1939).
- [93] D. B. Leinweber, A. W. Thomas, and S. V. Wright, Phys. Lett. **B482**, 109 (2000), arXiv:hep-lat/0001007.
- [94] D. B. Leinweber, A. W. Thomas, and R. D. Young, Phys. Rev. Lett. **92**, 242002 (2004), arXiv:hep-lat/0302020.
- [95] R. D. Young and A. W. Thomas, Phys. Rev. **D81**, 014503 (2010), arXiv:0901.3310 [hep-lat].
- [96] S. J. Brodsky, F. J. Llanes-Estrada, and A. P. Szczepaniak, eConf **C070910**, 149 (2007), arXiv:0710.0981 [nucl-th].
- [97] J. Kodaira and K. Tanaka, Prog. Theor. Phys. **101**, 191 (1999), arXiv:hep-ph/9812449.
- [98] A. V. Efremov and P. Schweitzer, JHEP **08**, 006 (2003), arXiv:hep-ph/0212044.
- [99] M. Burkardt, Phys. Rev. **D52**, 3841 (1995), arXiv:hep-ph/9505226.
- [100] M. Burkardt and Y. Koike, Nucl. Phys. **B632**, 311 (2002), arXiv:hep-ph/0111343.
- [101] P. Schweitzer, Phys. Rev. **D67**, 114010 (2003), arXiv:hep-ph/0303011.
- [102] M. Wakamatsu and Y. Ohnishi, Phys. Rev. **D67**, 114011 (2003), arXiv:hep-ph/0303007.
- [103] Y. Ohnishi and M. Wakamatsu, Phys. Rev. **D69**, 114002 (2004), arXiv:hep-ph/0312044.
- [104] C. Cebulla, J. Ossmann, P. Schweitzer, and D. Urbano, Acta Phys. Polon. **B39**, 609 (2008), arXiv:0710.3103 [hep-ph].
- [105] P. Schweitzer, Phys. Rev. **D69**, 034003 (2004), arXiv:hep-ph/0307336.
- [106] M. Wakamatsu and H. Tsujimoto, (2009), arXiv:0910.5762 [hep-ph].
- [107] A. I. Signal, Nucl. Phys. **B497**, 415 (1997), arXiv:hep-ph/9610480.

- [108] R. Jakob, P. J. Mulders, and J. Rodrigues, Nucl. Phys. **A626**, 937 (1997), hep-ph/9704335.
- [109] A. Mukherjee, Phys. Lett. **B687**, 180 (2010), arXiv:0912.1446 [hep-ph].
- [110] S. J. Brodsky, F. E. Close, and J. F. Gunion, Phys. Rev. **D5**, 1384 (1972).
- [111] R. L. Jaffe and C. H. Llewellyn Smith, Phys. Rev. **D7**, 2506 (1973).
- [112] D. J. Broadhurst, J. F. Gunion, and R. L. Jaffe, Ann. Phys. **81**, 88 (1973).
- [113] H. Burkhardt and W. N. Cottingham, Annals Phys. **56**, 453 (1970).
- [114] S. D. Drell and A. C. Hearn, Phys. Rev. Lett. **16**, 908 (1966).
- [115] A. V. Efremov, O. V. Teryaev, and E. Leader, Phys. Rev. **D55**, 4307 (1997), arXiv:hep-ph/9607217.
- [116] I. I. Balitsky, V. M. Braun, Y. Koike, and K. Tanaka, Phys. Rev. Lett. **77**, 3078 (1996), arXiv:hep-ph/9605439.
- [117] A. V. Belitsky and D. Mueller, Nucl. Phys. **B503**, 279 (1997), arXiv:hep-ph/9702354.
- [118] Y. Koike and N. Nishiyama, Phys. Rev. **D55**, 3068 (1997), arXiv:hep-ph/9609207.
- [119] A. V. Belitsky, Int. J. Mod. Phys. A **32**, 1730018 (2017), arXiv:hep-ph/9703432.
- [120] M. Gluck, E. Reya, and A. Vogt, Z. Phys. **C67**, 433 (1995).
- [121] P. Schweitzer *et al.*, Phys. Rev. **D64**, 034013 (2001), arXiv:hep-ph/0101300.
- [122] H. Avakian, A. V. Efremov, P. Schweitzer, and F. Yuan, Phys. Rev. **D81**, 074035 (2010), arXiv:hep-ph/1001.5467 [hep-ph].
- [123] J. Balla, M. V. Polyakov, and C. Weiss, Nucl. Phys. **B510**, 327 (1998), arXiv:hep-ph/9707515.
- [124] B. Dressler and M. V. Polyakov, Phys. Rev. **D61**, 097501 (2000), arXiv:hep-ph/9912376.
- [125] M. Wakamatsu, Phys. Lett. **B509**, 59 (2001), arXiv:hep-ph/0012331.
- [126] D. Boer, R. Jakob, and M. Radici, Phys. Rev. **D67**, 094003 (2003), arXiv:hep-ph/0302232.
- [127] H. H. Matevosyan, A. Kotzinian, and A. W. Thomas, Phys. Rev. **D96**, 074010 (2017), arXiv:1707.04999 [hep-ph].
- [128] H. H. Matevosyan, A. Kotzinian, and A. W. Thomas, Phys. Rev. **D97**, 014019 (2018), arXiv:1709.08643 [hep-ph].
- [129] X. Luo, H. Sun, and Y.-L. Xie, Phys. Rev. **D101**, 054020 (2020), arXiv:2003.03770 [hep-ph].
- [130] A. Abdesselam *et al.* (Belle), (2015), arXiv:1505.08020 [hep-ex].
- [131] H. H. Matevosyan, A. Bacchetta, D. Boer, A. Courtoy, A. Kotzinian, M. Radici, and A. W. Thomas, Phys. Rev. D **97**, 074019 (2018), arXiv:1802.01578 [hep-ph].
- [132] H. Matevosyan, PoS **DIS2018**, 150 (2018), arXiv:1807.11485 [hep-ph].
- [133] H. H. Matevosyan, A. Kotzinian, and A. W. Thomas, Phys. Rev. Lett. **120**, 252001 (2018), arXiv:1712.06384 [hep-ph].
- [134] A. Kotzinian, M. Anselmino, and V. Barone, Nuovo Cim. C **036**, 127 (2013), arXiv:1303.2461 [hep-ph].
- [135] A. Kotzinian, M. Anselmino, and V. Barone, in *19th International Workshop on Deep-Inelastic Scattering and Related Subjects* (2011) arXiv:1107.2292 [hep-ph].
- [136] H. Avakian and S. Pisano, PoS **DIS2016**, 214 (2016).
- [137] V. Burkert *et al.*, Nucl. Instrum. Meth. A **959**, 163419 (2020).
- [138] V. Ziegler *et al.*, Nucl. Instrum. Meth. A **959**, 163472 (2020).
- [139] Y. Sharabian *et al.*, Nucl. Instrum. Meth. A **968**, 163824 (2020).
- [140] M. Ungaro *et al.*, Nucl. Instrum. Meth. A **957**, 163420 (2020).
- [141] D. Carman *et al.*, Nucl. Instrum. Meth. A **960**, 163629 (2020).
- [142] D. Carman, G. Asryan, V. Baturin, L. Clark, R. De Vita, W. Kim, B. Miller, and C. Wiggins, Nucl. Instrum. Meth. A **960**, 163626 (2020).
- [143] M. Contalbrigo *et al.*, Nucl. Instrum. Meth. A **964**, 163791 (2020).
- [144] J. Brock, PoS **SPIN2018**, 101 (2018).
- [145] C. Keith, PoS **PSTP2017**, 008 (2017).
- [146] C. D. Keith *et al.*, Nucl. Instrum. Meth. A **501**, 327 (2003).
- [147] R. Milner *et al.*, PAC48 Proposal (2020).
- [148] J. Maxwell and R. Milner, (2019), arXiv:1911.06650 [physics.ins-det].
- [149] J. Maxwell, PoS **SPIN2018**, 102 (2018).
- [150] R. N. Cahn, Phys. Lett. **B78**, 269 (1978).
- [151] E. L. Berger, Z. Phys. **C4**, 289 (1980).
- [152] A. Brandenburg, V. V. Khoze, and D. Mueller, Phys. Lett. **B347**, 413 (1995), arXiv:hep-ph/9410327.
- [153] A. Afanasev, C. E. Carlson, and C. Wahlquist, Phys. Lett. **B398**, 393 (1997), hep-ph/9701215.
- [154] S. J. Brodsky, M. Diehl, P. Hoyer, and S. Peigne, Phys. Lett. **B449**, 306 (1999), arXiv:hep-ph/9812277.
- [155] I. Akushevich, N. Shumeiko, and A. Soroko, Eur. Phys. J. **C10**, 681 (1999), arXiv:hep-ph/9903325.
- [156] I. Akushevich, A. Ilyichev, and M. Osipenko, Phys. Lett. B **672**, 35 (2009), arXiv:0711.4789 [hep-ph].
- [157] B. Raydo, S. Boyarinov, A. Celentano, C. Cuevas, R. de Vita, V. Kubarovsky, B. Moffit, S. Niccolai, R. Paremuzyan, and C. Smith, Nucl. Instrum. Meth. A **960**, 163529 (2020).
- [158] K. V. Dharmawardane *et al.* (CLAS), Phys. Lett. **B641**, 11 (2006), nucl-ex/0605028.
- [159] M. Mirazita, H. Avakian, A. Courtoy, and S. Pisano (CLAS), (2020), in preparation.
- [160] R. J. Barlow, Nucl. Instrum. Meth. A **297**, 496 (1990).

- 1052 [161] C. Dilks (Presented at APS DNP2019, 2019).
- 1053 [162] T. Hayward (Presented at APS DNP2019, 2019).
- 1054 [163] G. Gilfoil *et al.*, JLab Experiment E12-07-104 (2007).
- 1055 [164] M. Arneodo *et al.* (European Muon), Z. Phys. **C34**, 277 (1987).
- 1056 [165] H. Avakian and P. Bosted., (2006).
- 1057 [166] L. Mankiewicz, A. Schafer, and M. Veltri, Comput. Phys. Commun. **71**, 305 (1992).